THE BEHAVIOUR OF SMALL CLUSTERS OF BODIES FALLING IN A VISCOUS FLUID

by

KORUWAGE OSWALD LAKSHMAN FERNANDO JAYAWEERA

Department of Physics

Imperial College of Science and Technology

A thesis submitted for the

Degree of Doctor of Philosophy at the

University of London

June 1965

"You are accustomed to have set before you the latest triumphs of mind over matter, ..., however, after you have seen what I shall endeavour to show you, I think you will readily admit that for once the case is reversed, and that the triumph rests with nature, in having for so long concealed what has been so eagerly sought, and what is at last found to have been so thinly covered ".

Osborne Reynolds.

From the proceedings of the Royal Institution of Great Britain.

Read 2nd February 1877.

ABSTRACT

The terminal velocities, drag coefficients, orientations and the flow patterns of single spheres, cylinders and discs falling in a viscous liquid are determined experimentally for Reynolds numbers ranging from 0.007 to 10^3. Detailed investigations are carried out for the orientations of cones and capped cylinders, where the geometry of the body is very important. The transition from steady to unsteady motion for discs and cylinders is discussed in terms of the geometry and the ratio of the densities of the body and the liquid. Shedding of vortex rings give rise to unsteady motion. At Reynolds numbers greater than about 500, discs and spheres fall in a helix, while smooth cones with $Re > 800$, tumble.

Collision occurs between two equal bodies falling directly one behind the other. After collision, discs stay together, initially non-parallel cylinders slide along each other until they bisect at right angles,and spheres and parallel cylinders rotate and separate horizontally at a decreasing rate.

Clusters of bodies fall faster than a single body. Behaviour of 3 or more spheres depends on the Reynolds number. When $0.06 < Re < 0.16$, three similar equally spaced spheres dropped in a horizontal line interchange positions but do not

separate. If unequally spaced, one sphere is left behind, which sphere depends on the initial spacing. 3to 6 spheres initially in a compact cluster form into a regular polygon which expands at a decreasing rate in a horizontal plane, when $0.06 < Re < 7$. If $Re > 7$ or the cluster contains 7 or more equal spheres, no polygon is formed. For this behaviour the sphere and liquid densities have to be comparable, so that the spheres move in response to changes in fluid motion. 3 or more equal discs cluster on a stable " butterfly " configuration formed by three discs, while cylinders form into stable pairs crossed at right angles and into triplets of symmetric form ⊢⊣.

The behaviour of discs and cylinders loaded with spheres depends only on the position of the sphere and the ratio of their weights in the liquid.

CONTENTS

ILLUSTRATIONS

Page

Page

ACKNOWLEDGEMENTS

The research work incorporated in this thesis was carried out in the laboratories of the Cloud Physics department, Imperial College, under the supervision of Professor B.J. Mason F.R.S. whose help and encouragement is most sincerely acknowledged.

Grateful thanks are due, to my colleagues in the department for many fruitful discussions, and to the technical and office staff for their ever-willing cooperation which contributed greatly to the completion of this work.

I am particularly indebted to the " Lobitos Oilfields Ltd, Cheshire, for supplying the liquid paraffin.

Thanks are due, finally, to the British Commonwealth Scholarship Commission for awarding me ~~with~~ a scholarship and to the University of Ceylon for granting me leave, which made this research possible.

PUBLICATIONS

Part of the work described in this thesis has been published in the following papers.

1. " The behaviour of clusters of spheres falling in a viscous fluid."

   Journal of Fluid Mechanics, 20, 121, 1964.

2. " The behaviour of freely-falling cylinders and cones in a viscous fluid."

   Journal of Fluid Mechanics, (in press).

A copy of the first paper is included at the end of the thesis.

CHAPTER 1

INTRODUCTION

1.1 STATEMENT OF THE PROBLEM AND OUTLINE OF THE THESIS

The latter stages of the growth of a precipitating particle is almost entirely governed by the hydrodynamic interactions of the individual particles. This process is studied in the following cases.

(1) A single drop collecting small droplets in its path.

(2) Snow crystals growing into hailpellets by accretion of supercoolcd water drops. And

(3) snow orystals adhering with each other to form snowflakes.

But in all these cases, the calculations so far carried out by cloud physicists have been based only on the interactions of two neighbouring particles. The more complicated problem of the interactions between many particles has not been attempted.

It may soon be necessary to consider the multi-particle problem, owing to the improvements that should take place in our knowledge of cloud models. A serious gap would then be the lack of theoretical or experimental data on the fall behaviour of small clusters of these particles.

The basic forms of most of these precipitating particles fall into few elementary types of bodies of revolution.

For example, cloud droplets and spherical hailstones could be represented by spheres, snow crystals by either discs or cylinders, and conical hailstones by capped cones.

As a primary step towards the understanding of the multi-particle problem, it was decided to make an experimental investigation in the laboratory of how models of these particles behave when falling in close proximity to each other. The treatment was further limited to only small numbers of similar types of particles in a cluster.

The question, however, arises as to the conditions that have to be satisfied to apply the results of these model experiments to the case of precipitating particles falling in air. The usual conditions of matching the geometry and the Reynolds numbers could be seriously challenged. The other requirements and their limitations are discussed in detail in section 1.3.

The work described in this thesis, in addition to the behaviour of small clusters of simple bodies, also deals with the orientation during free fall of more complex models of naturally-occuring snow crystals. The types treated are capped columns, rimed plates and needles. The reason for this study lies in the explanations of the spectacular optical phenomena observed in the sky, when a thin cirrus cloud obscures the sun or the moon. The nature of these depend among other things, on the type and the orientations of ice crystals present in the

cloud (Humphreys 1929). For simple crystals like plates and needles, the orientations during free fall is known, at least in the extreme cases. However, little is known of the orientation during free fall of the more complex crystals. Model experiments, provide an easy means, to investigate this behaviour.

Outline of the thesis

In the subsequent sections of this chapter, previous work on the behaviour and flow round single bodies is discussed. The discussion is mainly on the theoretical work in these fields. The last section deals with the merits and demerits of model experiments.

The present experimental investigations on the behaviour of spheres and cylinders are discussed in chapters 2 and 3 repectively, while chapter 4 includes the work on both discs and cones. These results are compared with the experimental results of earlier workers wherever possible.

1.2 FLOW PAST A SINGLE BODY

A Exact equations for the flow field

The behaviour of more than two bodies falling close to each other is undoubtedly, determined by the interactions of the flow fields around each body. The bodies will move in response to these modified flow fields. Hence the knowledge of

the flow round an individual body, falling unaffected by any other external source, is an extremely important step in the solution of the multi-particle problem.

The uniform motion of a single body through a fluid has been thoroughly investigated, ever since time of Sir Isacc Newton. When a body moves through a fluid it experiences a resistance or drag in the opposite direction to its motion, due to the fluid displaced. Newton postulated the first law for this drag, purely from a momentum theorem. He assumed that the fluid through which the body moves, consists of a large number of particles, which has only mass dimensions, and exert no influence on each other. The body imparts a velocity, proportional to its own velocity, to all the particles in its path. The rate of change of momentum thus imparted being the drag on the body, thus the drag

$$D = f A \rho_f V^2 \qquad \text{.....(1.2.1).}$$

where 'A' is the cross-sectional area normal to the flow, 'ρ_f' the density of the fluid, 'V' the velocity of the body and 'f' a constant of proportionality.

Even though Newton's assumptions give an incorrect value for 'f', this law still holds, with little modification, for the case where the drag is mainly due to inertia.

In the modern conceptions, the entire shape of the body is taken into consideration, and not just the front of the

body as Newton assumed. Also the individuality of the fluid particles is discarded, with the result that each fluid element exerts an influence on its neighbours. This is attributed to the property of the fluid called " Viscosity ". Paradoxically the concept of viscosity was also introduced by Newton. The law of viscosity is named after him.

The viscosity of a fluid alone causes the resistance to the motion of a body, primarily due to the forces necessary to deform the various fluid elements. ~~Prandlt & Tietjens~~ D' Alemberts* (~~1957, p105~~), showed that the drag experienced by a body in a fluid without any viscosity is zero. Hence ~~only~~ inertial forces alone cannot produce a drag, and the viscosity forces however small they may be, are necessary to cause a drag on a moving body. However, the total drag is determined by the importance of the viscous forces compared to the inertial forces. The ratio of inertial to viscous forces is represented by a non-dimensional parameter termed the Reynolds number, and is expressed as

$$Re = \frac{V\,l}{\nu} ,$$

where 'ν' is the kinematic viscosity of the fluid and 'l' a representative length of the body.

Newton's quadratic expression could be modified to include the Reynolds number, and written as

$$D = f(Re)\ A\ \rho_f \frac{V^2}{2} \qquad \text{.....(1.2.2)}$$

The function f(Re) is termed the drag coefficient C_D, and takes care of the complications that arise from the various effects of viscosity.

For geometrically similar bodies, the law of dynamic similarity states that C_D is a unique function of Re. Hence the knowledge of C_D as a function of Re will provide the drag of a particular shape for all fluids, all velocities and all body dimensions (Prandlt & Tietjens 1957, p93).

Theoretical determinations of the drag coefficient and the flow patterns as a function of the Reynolds number, involve the solution of the Navier-Stokes equations under specific boundary conditions.

When a body moves steadily through an incompressible fluid, or when the fluid flows steadily past a stationary body, the velocity of the fluid $\bar{V}$ at any point should satisfy the modified Navier-Stokes equation

$$\bar{V}.\nabla\bar{V} = -\frac{1}{\rho_f}\nabla p + \nu\nabla^2\bar{V}$$

and $$\nabla.\bar{V} = 0 \qquad \text{.....(1.2.3)}$$

where 'p' is the pressure.

No exact solution to this equation has yet been obtained. The mathematical difficulties of this equation are two fold.

(1) The presence of the quadratic term $\bar{V}.\nabla\bar{V}$, and

(2) the term with 'ν' is of a higher order.

Also the correct solution should satisfy the boundary condition which, for a body moving in a stationary fluid, are

(1) the velocity at infinity should be zero, and

(2) the fluid in contact with the body should have the same velocity as the body, so that there is no slipping at the surface of the body. However, solutions have been obtained in special cases.

B Potential Flow

Neglect of the viscous term, $\nu\nabla^2\bar{V}$, gives the potential solution. This solution, even though it satisfies the equation, the necessary boundary condition that both the tangential and normal components of the velocity, at the surface of the body, should be equal to the corresponding velocities of the body, cannot be satisfied. The flow distribution corresponding to this solution is shown in fig 1.1.

As stated earlier, the drag for a frictionless fluid past a body is zero, and the necessity of even a slight amount of viscosity to cause a drag, was emphasised. The no slip boundary condition is another way of stating that viscosity however small, cannot be neglected near the surface of the body. In a layer close to the body and extending behind the body,

Fig. 1.1 POTENTIAL FLOW ROUND A SPHERE.

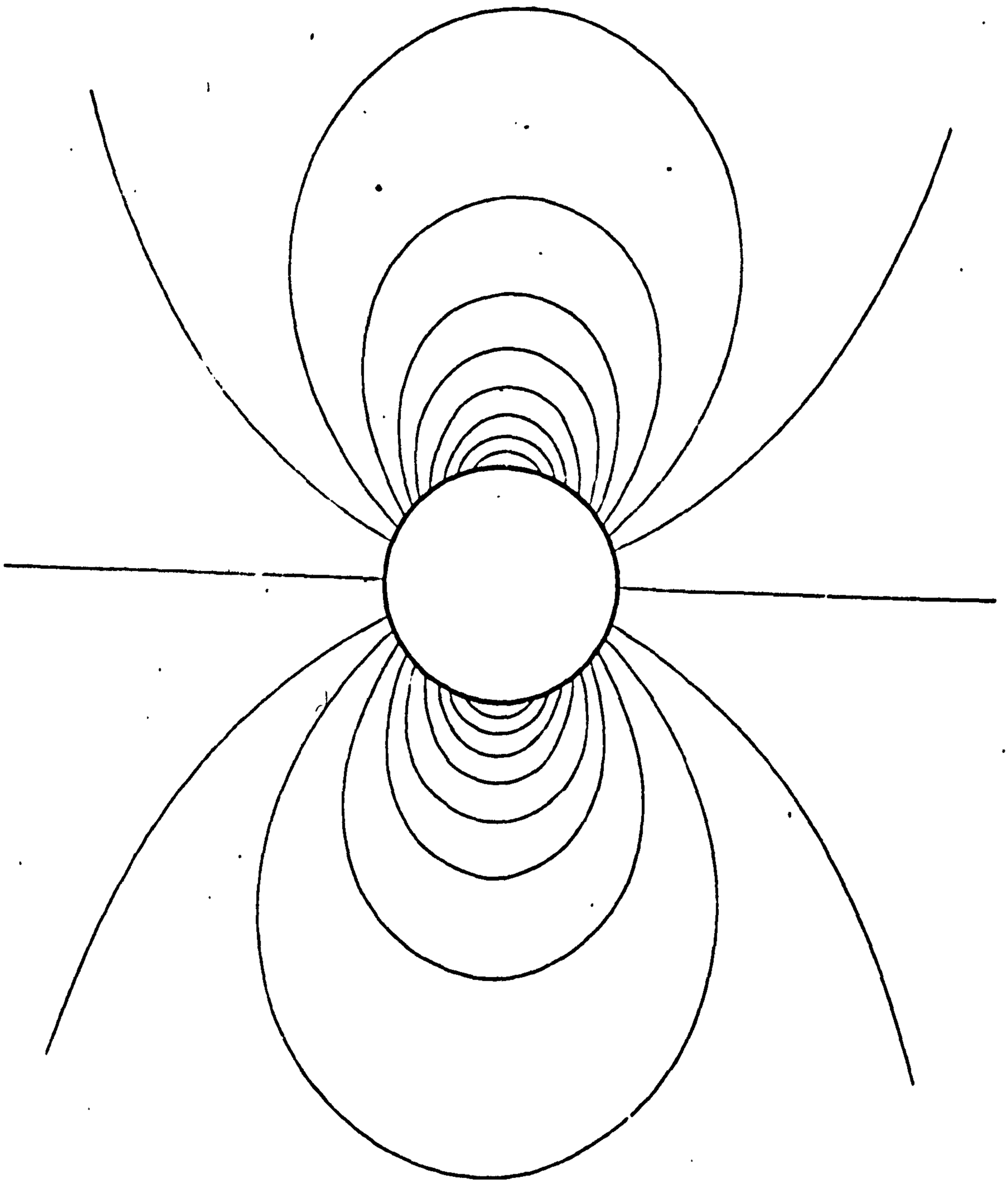

viscous forces cause the whole picture of the flow pattern to be different. Instead of the symmetrical flow lines (fig 1.1), vortices and a boundary layer are formed behind the body. But as long as the flow patterns in front is concerned, the potential theory gives the correct flow lines. Fig 1.2 shows the formation of the vortices in the boundary layer. The comparison of the first and the last photographs shows the flow in the front is unaffected by the formation of vortices, the latter being restricted to the boundary layer.

Hence when dealing with fluids of small viscosity, it is justified to use the potential flow solution for all points outside the boundary layer, while inside the boundary layer the treatment is very complicated. The drag on such a body arises only from the flow inside the boundary layer.

C <u>Slow motion or viscous flow</u>

The other limiting case where the viscous force is very large compared to the inertial force, an exact solution could be obtained, provided the quadratic term in the velocity is neglected. The solution could be made to satisfy the boundary conditions.

In the case of a rigid sphere moving in an infinite incompressible fluid, the solution was given by Stokes. Using the concept of Stokes' stream function (see Lamb 1962, p 596), he obtained the drag on a sphere moving with a velocity, V, as

FIG 1.2

Formation of vortices in the boundary layer - After Prandlt & Tietjens (1957)

PLATE 1.[1]

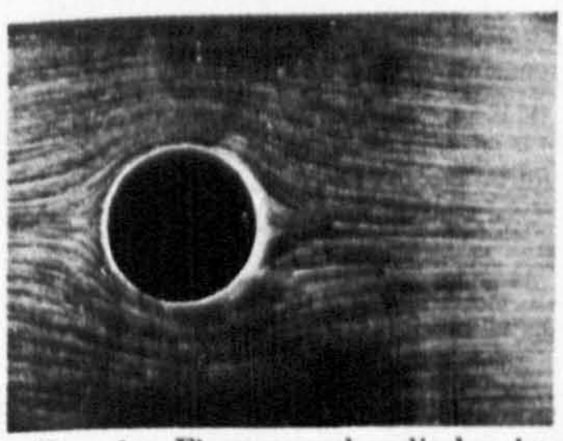

FIG. 1.—Flow round cylinder immediately after starting (potential flow).

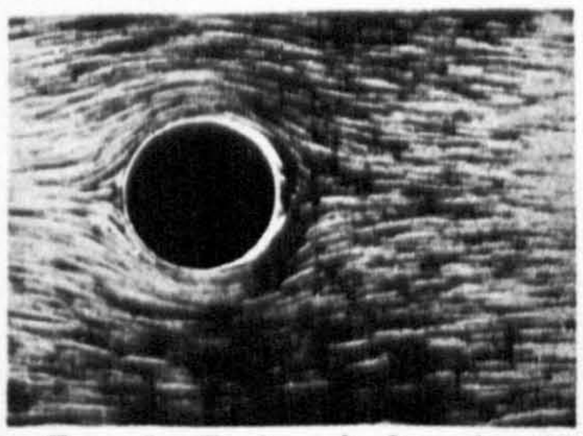

FIG. 2.—Backward flow in the boundary layer behind the cylinder; accumulation of boundary layer material.

PLATE 2.

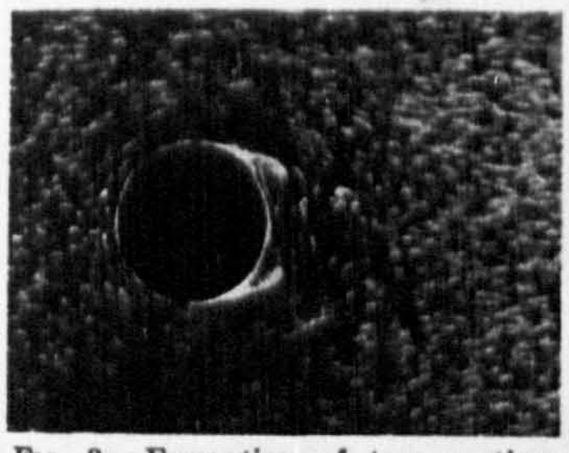

FIG. 3.—Formation of two vortices; flow breaking loose from cylinder.

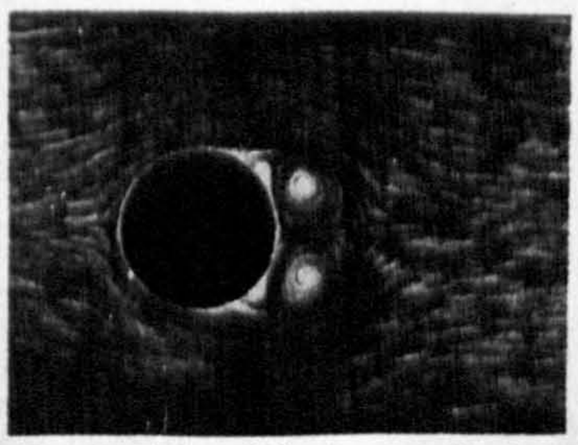

FIG. 4.—The eddies increase in size.

PLATE 3.

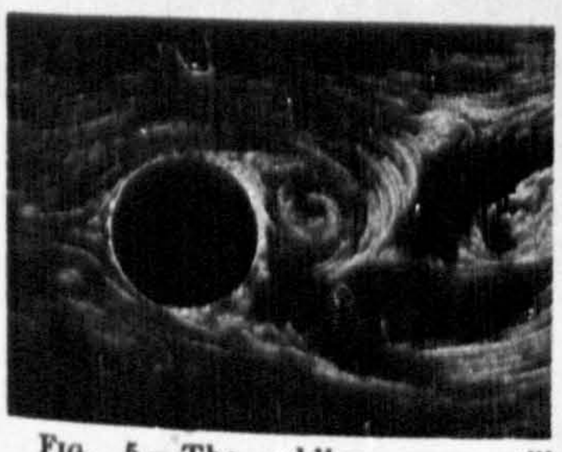

FIG. 5.—The eddies grow still more; finally the picture becomes unsymmetrical and disintegrates.

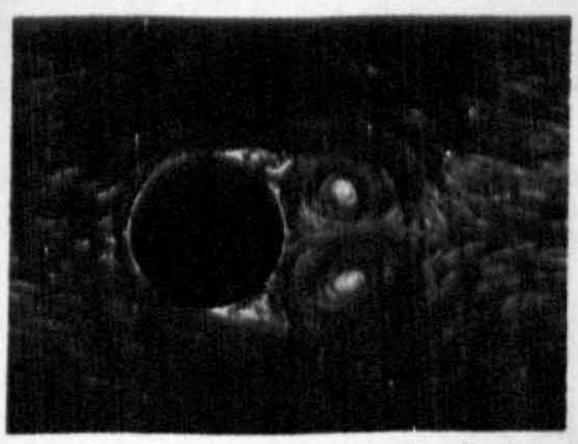

FIG. 6.—Final picture obtained a long time after starting.

The direction of flow is from left to right

$$D = 6 \pi \eta r V \quad \ldots\ldots\ldots\ldots (1.2.4)$$

where, η, is the dynamic viscosity of the fluid and, r, the radius of the sphere.

In terms of the drag coefficient and the Reynolds number, this reduces to

$$C_D Re = 24 \quad \ldots\ldots\ldots\ldots (1.2.5)$$

Hence for very low Reynolds numbers, the drag coefficient is inversly proportional to the Reynolds number.

Using the same assumptions Oberbeck (1876) solved the Navier-Stokes equation for an ellipsoid. The drag for this being

$$D = 3 \pi \eta V d_d \quad \ldots\ldots\ldots\ldots (1.2.6)$$

where d_d is a function of the dimensions of the axes of the ellipsoid and its value also depend on the orientation of the ellipsoid with respect to the flow. It is worthwhile noting that d_d is also the diameter of a sphere which has the same resistance as the particle when moving with the same velocity in the fluid. Hawskley (1954) termed this parameter as the "drag diameter" of the ellipsoid and extended the idea to include any particle.

For spheroids or bodies of revolution, the value of 'd_d' could be computed in terms of the dimensions of the body, from Gans (1911) simplified treatement.

For a thin disc with diameter, d, and thickness, t,

$$d_d = \frac{16}{9\pi} d \qquad \text{when moving edgeways}$$

and

$$d_d = \frac{24}{9\pi} d \qquad \text{when moving normal to the stream.}$$

This gives for a disc moving edgeways

$$C_D \, Re = 21.38 \qquad \ldots\ldots\ldots (1.2.7)$$

where $Re = \frac{2 \, t \, \rho_f V}{\eta}$

and if moving normal to the stream

$$C_D \, Re = 20.34 \qquad \ldots\ldots\ldots (1.2.8)$$

where $Re = \frac{\rho_f V \, d}{\eta}$

For the other limiting case, the infinite circular cylinder, a solution is <u>not</u> feasible from the Gans-Oberbeck method. In this case it is impossible to satisfy the boundary condition that the velocity of the fluid is zero at infinity. Solutions have been attempted by Berry & Swain (1923) and by Wilton (1915). The former authors used a limiting process, but their velocity at infinity does not vanish, but is proportional to $\log_e R$ as $R \to \infty$, while Wilton's solution gives indeterminate values along the front and rear generators of the cylinder. Harrison (1924) attempted to find a solution by satisfying the boundary conditions as far as possible, but has been successful in only making slight improvements on the

solutions of the previous workers.

However, a solution seem to be possible, if the infinite cylinder is bounded by walls parallel to its axis of revolution. This was demonstrated by Bairstow, Cave & Lang (1922) for a special case when the cylinder is mid-way between the two walls five diameters apart. They found that

$$C_D \, Re = 14.2.$$

This result differs considerably from White's (1946) empirical relation, which when extrapolated to this special case gives

$$C_D \, Re = 18.0.$$

Bairstow et al used the maximum velocity of flow (velocity along the axis) to compute the drag coefficient and the Reynolds number, while White used the mean velocity. This could partly explain the discrepancy.

Davies (1947), while discussing the drag for all cases of ellipsoidal particles, derives an expression for the drag on a long but finite cylinder, moving with the axis horizontal and vertical.

For a cylinder falling with the axis horizontal

$$D = \frac{4 \pi \eta V L}{\log_e \frac{2L}{d} + 0.5 + O(d/L)^3}$$

where, L is the length of the cylinder.

This expression was also derived by Burgers (1938)

and the term $O(\frac{d}{L})^3$ was introduced by Boersma (1960).

The condition for pure viscous flow, for which Gans-Oberbeck expression and all its applications are valid, is satisfied only if the ellipsoids move without any preferred orientation. For when the inertial forces are negligible, the body would fall with the orientation in it was released. This is a direct consequence in the derivation of Gans-Oberbeck formula. In fact Gans (1928) make special mention of this, that in a purely viscous flow, a body with three mutually perpendicular planes of symmetry would fall without any preferred orientation.

Using these expressions for the drag, the terminal fall velocities of spheres, dics, and finite cylinders could be computed for pure viscous flow, as the drag is the net weight of the body in the fluid. For spheroids whose ratio of the axes are less than 2 to 1, Green & Lane (1964) show that the error in the computed velocity is small, when the drag diameter, d_d, is replaced by the "equivalent diameter", d_s, which is the diameter of the sphere having the same volume as the particle. But for higher ratios, this substitution gives a smaller value for the fall velocity.

Fuchs (1964, p40) introduces a "shape factor", χ, and computes the fall velocities in the general case of non-spherical particles, from the expression

$$V = \frac{d_s^2}{\chi} \frac{\rho_s - \rho_f}{18\eta} \qquad \ldots\ldots\ldots(1.2.10)$$

where ρ_s is the density of the material of the particle.

Table 1.1, gives the values for this shape factor, χ, as calculated by Fuchs for prolate and oblate spheroids.

The value of, χ, is 1 for a sphere and is greater than unity for ~~all other~~ most other cases. This fact that for a given volume, the sphere has the greatest fall velocity was shown experimentally by Kunkel (1948).

The definitions of the drag coefficients and Reynolds numbers for these irregular particles provide considerable difficulty, due to the ambiquity that arises as to the definition of the "size" of these particles. Pettijohn & Christiansen (1948) and Heiss & Coull (1952), find that for isometric particles and short cylinders, whose shapes are such that the projected area could be represented by $\frac{\pi d_s^2}{4}$, C_D and Re, when defined in terms of the equivalent diameter, d_s, gives the relation

$$C_D \; Re = \frac{24}{\psi},$$

where, ψ, is defined as the ratio of the area of the sphere having the same volume, to that of the particle. This was introduced by Wadell (1934) as "sphericity" and is a measure of the deviation of the particle from the spherical shape.

Hawksley (1951) finds that if C_D and Re are defined as

$$C_D = \frac{4}{3} \; \frac{\rho_s - \rho_f}{\rho_f} \; \frac{g}{\nu^2} \; \psi \, d_s \qquad \ldots\ldots\ldots(1.2.11)$$

$$Re = \frac{1}{\sqrt{\psi}} \; \frac{v \, d_s}{\nu}$$

TABLE 1.1.

Values for the Dynamic shape factor, χ , for ellipsoidal particles. After Fuchs (1964)

Ratio of the axes	Prolate ellipsoids during motion			Oblate ellipsoids during motion		
	Along polar axis	Across polar axis	Average	Along polar axis	Across polar axis	Average
1.1	0.994	1.005	1.001	-	-	-
1.3	0.970	1.027	1.008	-	-	-
1.5	0.940	1.044	1.010	1.072	0.958	0.996
2	0.95	1.09	1.05	1.14	0.99	1.04
3	0.97	1.20	1.12	1.26	1.04	1.11
4	1.01	1.30	1.20	1.38	1.08	1.18
6	1.08	1.47	1.34	1.56	1.17	1.30
8	1.15	1.62	1.47	1.71	1.25	1.40
10	1.22	1.76	1.58	1.83	1.32	1.49
20	1.54	2.34	2.08	2.31	1.59	1.83

the relation between C_D and Re takes the form of that for a sphere.

However, these definitions for the velocity, drag coefficient and Reynolds number could only be applied if the shapes are geometrically similar or not very different from a spherical shape. For extreme shapes these calculations are not valid (Davies, 1947).

So far only the theoretical work on these relations has been discussed.. Hardly any mention was made on their experimental verification.

Stokes' formula for spheres (1.2.4.) has been verified by many workers. Early confimation came from Allen (1900) who, using paraffin wax spheres in aniline, found that for very low velocities, the drag was proportional to the velocity, and that no slipping occurs at the boundary. However, his results show a considerable amount of scatter. Arnold (1911), using metal spheres in oil, compares the viscosity using Stokes' law and Poiseuille's law. He finds deviation from Stokes' law occurs for Re as low as 0.01. Schiller (1932), discussing the various verifications of the Stokes' formula, shows that for $Re < 0.5$, the deviation from Stokes' formula is less than the experimental error. However, using the more accurate results of Möller (1938), the upper limit to Stokes' law could be placed at Re = 0.1. The deviation at this Reynolds number is - 1.5% (Fuchs, 1964 p31). This corresponds to water-drops of radius 20 μ falling in air at 0°C and 900 mb pressure (See Mason 1957, p421).

All the direct experimental verifications of Stokes' formula have been carried out in liquids and not in gases. In the latter medium, it becomes difficult to obtain low Reynolds numbers without using small spheres. This gives rise to slip and uncertainity in the measurements of their diameters, added to this is the practical difficulty to obtain true spheres. But, by the determination of the electronic charge, e, Millikan (1917) who used Stokes' formula to compute the radius of the oil drops, indirectly verified Stokes' law. However, an approximate verification had been carried out by Zeleny & McKeehan (1910) in the study of fall velocities of Plant spores of spherical shape.

For non-spherical particles, Fuchs justified his calculations for the dynamic shape factor from the results of McNown & Malaika (1950) and also explores the possibility of using his values for elongated bodies, by treating them like prolate or oblate spheroids having the same axial ratio. Support for this possibility is seen in the experiments of Heiss & Coull (1952).

For thin discs, the experimental evidence is rare. But Schmiedel's (1928) results justify the accuracy of the formula (1.2.8) for discs falling normal to the stream. Squires & Squires (1937) attempted to verify the relevent formulae for discs falling edgewise and normal to the stream. But unfortunately their results were very much affected by

the proximity of the walls. Also these authors fail to mention the Reynolds number for which they justify the use of Gans-Oberbeck formula. For finite long cylinders there is hardly any satisfactory experimental data.

Using the Stokes' stream function , it is possible to map the contours of stream lines for a moving body. These lines represent the direction of the flow at any point. The magnitude of the velocity is given by the differentials of the stream function. E.g. in Cartesian co-ordinates for two dimensional flow

$$V_x = -\frac{\partial \Psi}{\partial y} \qquad \text{and} \qquad V_y = \frac{\partial \Psi}{\partial x}$$

Stream lines for a sphere moving in a viscous fluid, calculated by Lamb (1962, p599) is shown in fig 1.3. The direction of motion is along $x\ x'$. The flow lines are completely symmetrical and show no wake behind the sphere.

D <u>Limitations to viscous solution</u>

Other than for very low Reynolds numbers, the Stokes' law for spheres requires that

(1) the sphere is rigid

(2) there is no slip at the surface,

(3) the diameter of the sphere is large compared to the mean free path of the fluid molecules,

(4) the fluid is non-compressible and infinite in extent, and

Fig. 1.3 FLOW ROUND A SPHERE. after Stokes.

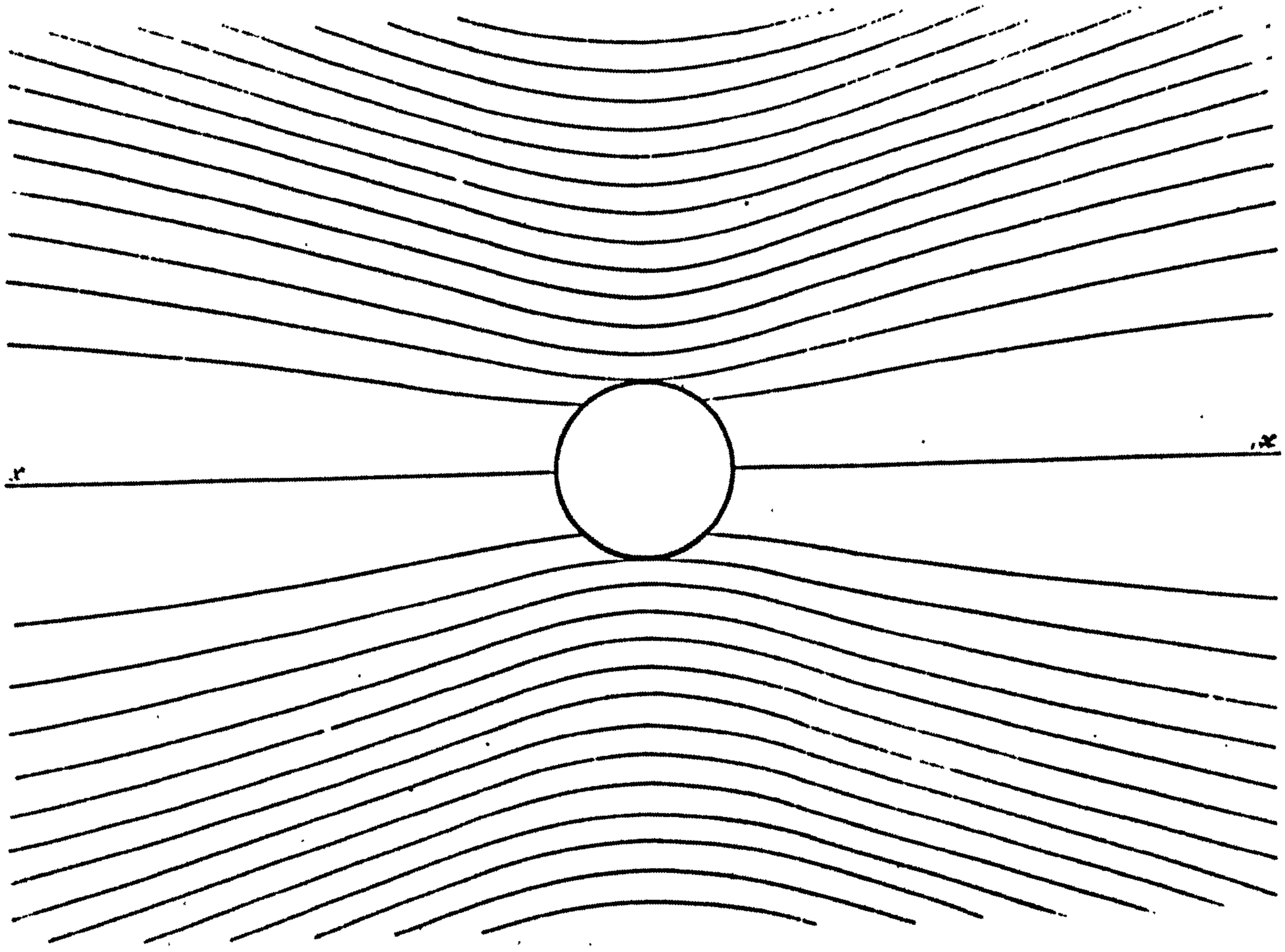

(5) the velocity is uniform.

If the sphere is not rigid, for example liquid drops, and if the viscosity of the fluid making the drop is comparable to that of the medium, circulations develop inside the drop causing a decrease in the drag. Lamb (p600) gives the modified expression for the drag as

$$F = 6\pi\eta r V \frac{1 + 2\eta/\eta_p}{1 + \eta/\eta_p} \quad \ldots\ldots(1.2.12)$$

where η and η_p are the dynamic viscosities of the medium and the fluid drop.

If the viscosity of the drop is very much larger than that of the medium, as for water drops in air, this effect can be neglected.

The condition of slip is also discussed by Lamb (p602). This correction, which also gives a decrease in resistance, is caused, by the fluid adjacent to the moving sphere not having the same velocity as the sphere. This effect becomes important only when dealing with spheres moving in gases (Fuchs 1964, p25).

If the diameter of the sphere becomes comparable with the mean free path of the fluid molecules, then the fluid cannot be considered as homogeneous. The modified expression for the drag was shown theoretically by Cunningham (1910) and experimentally by Millikan (1923) to be

$$D = \frac{6\pi\eta r V}{1 + 0.864\frac{\ell}{r} + 0.290\, e^{-1.25 r/\ell}} \qquad \ldots\ldots(1.2.13)$$

where the mean free path $\ell = \dfrac{\eta}{0.3502\ \rho\ \bar{c}}$

$\bar{c}$ is the average molecular velocity.

This, again, is important only for very small spheres $< 3\mu$ diameter falling in air. But if the sphere diameter exceeds $10\ \mu$, this expression reduces to Stokes' formula (Dryden, Bateman and Murnaghan, 1956). Hence in dealing with water drops of diameter greater than 10μ falling in air, Stokes' law may be assumed, provided $Re < 0.1$.

The in-compressibility of the fluid does not become at all significant for these low velocities, for which Stokes' law is valid.

All the limitations so far discussed are negligible for solid spheres falling in liquids. Even though the corresponding cases for non-spherical bodies have not been worked out, it may be assumed that all these limitations may be neglected for all solid particles falling at low Reynolds numbers in a liquid.

However, the assumption that the fluid is infinite in extent is something which can never be achieved in practice. Lamb's theoretical curves for the stream function shows (see fig 1.3) that the outer boundary greatly modifies the flow patterns. This is to be expected as, in a pure viscous fluid the effect of any shear in the fluid is transmitted

all along the fluid. The photographs of the flow round a sphere moving in glycerine solution obtained by Ellis-Williams (1915) show the extent to which the presence of the walls changes the flow lines.

Modification of the stream lines correspond to a change in the drag on the moving sphere. This effect has been investigated in detail both theoretically and experimentally by many workers. Basically the presence of the walls causes a increase in the drag on the body. For small values of r/x, where, r and x are representative dimensions of the particle and the wall, the increase in the drag is given by the factor

$$1 + b \frac{r}{x} ,$$

where,b is a constant which depend on the type of the particle and the bounding wall.

For a sphere moving along the axis of a cylindrical container, Landenberg (1907) showed that b=2.4. Later Faxén (1923), while extending the correction factor to include higher powers of (r/x), also pointed out that due to a mathematical error, the constant, b, should 2.1. His improved expression is

$$1 + 2.104 \frac{r}{x} + 2.09 \left(\frac{r}{x} \right)^3 + 0.95 \left(\frac{r}{x} \right)^5 \quad \ldots\ldots(1.2.14).$$

Fuchs (1964, p 24) quotes Bacon's (1936) experimental verification of this result upto $\frac{r}{x} \simeq 0.3$ and $Re \leq 0.02$.

Brenner (1962) extended this result to include all particles. For a particle moving parallel to one of its three mutually perpendicular planes of symmetry, close to a boundary having planes orthogonal to the principal axes of the particle, Brenner showed that

$$D = \frac{D_\infty}{1 - b\frac{D_\infty}{6\pi\eta V x} + O\left(\frac{r}{x}\right)^3} \qquad \ldots(1.2.15)$$

where, D is the drag on the particle moving with a velocity, V, in a bounded fluid and D_∞, the drag for the same particle moving with the same velocity in an unbounded fluid.

This reduces to Faxén's expression for a sphere, when D_∞ is substituted by the Stokes drag $6\pi\eta Vr$.

Brenner's expression is of general application. He supports his theory by the experiments of Pettijohn & Christiansen (1948), Heiss & Coull (1952) and of Squires & Squires (1937) for single bodies falling in an enclosed medium, and accounts for the discrepancy between the theoretical curve of Kynch (1959) and the experimental values of Eveson, Hall & Ward (1959) for the sedimentation of two equal spheres in a liquid.

E <u>Oseen's approximation and "relaxation" methods.</u>

The solutions of the Navier-Stokes equation so far discussed, were for the two extreme cases. The potential flow solution, which neglects the viscous term, was erroneous in the

boundary layer of the body, due to the importance of even a slight amount of viscosity. ~~But~~ However, for all points outside this layer, the solution is very satisfactory. The type of flow from this solution is irrotational.

On the other hand, the viscous flow solution completely neglects the inertial terms, and obtains satisfactory values for the drag and streamlines at low Reynolds numbers. The neglect of the inertial forces in comparison with the viscous forces at all points in the flow field, is an absolute necessity in this solution. But as the distance from the body increases, the viscous forces decrease at much faster rate than the inertial forces. So that at large distances from the body, the inertial forces will become sufficiently comparable with the viscous forces, not to justify their neglect. Hence theoretically, unless $Re \to 0$, the viscous flow theory cannot be applied at large distances from the body. However, from a practical point of view, negligible error arises for $Re \leq 0.01$, as stated earlier. Oseen (1910), using this argument, made a fundamental improvement to the viscous flow theory.

In the solution of the Navier-Stokes equations, it is necessary to consider the body at rest in a steadily moving fluid, or the body moving steadily in a stationary fluid. These two cases are identical. For, by making the origin move with the body, the latter case could be transformed to the former, Thus in both cases, the velocity of the fluid

relative to the origin (viz body) has a fixed constant value $\bar{U}$ (say) at large distances from the body. Now the non-linearity of Navier-Stokes equations arise from the quadratic term $\bar{V}.\nabla\bar{V}$. Oseen linearised this term by writing $\bar{U}.\nabla\bar{V}$ instead of $\bar{V}.\nabla\bar{V}$. This simplification is justified so far as the importance of the inertial terms are limited , only at large distances from the body.

For a sphere, using this approximation, Oseen obtained the relation between the drag coefficient C_D , and the Reynolds number Re, to the first order of Re as

$$C_D\ Re = 24\ (\ 1 + \frac{3}{16}\ Re\ ) \qquad .....(1.2.16\ a).$$

later to be improved by Goldstein(1929) to include higher powers of Re, to the form

$$C_D\ Re = 24\ \left(\ 1 + \frac{3}{16}\ Re - \frac{19}{1280}\ Re^2 + \frac{17}{20480}\ Re^3 + \ldots\right)$$

$$.....(1.2.16\ b\ ).$$

Goldstein gives his result for much higher powers of Re, so that the drag could be calculated upto Re=2.0. But such tedious computations are unnecessary as deviations from experimental values occur even at Re=0.5. Fig 1.4 shows the C_D - Re curve for a sphere. The theoretical curves of Stokes and Goldstein-Oseen are compared with the experimental values listed by Fuchs (1964. p32).

Using the analytical solution of Goldstein, Pearcey & McHugh (1955) computed the flow round a sphere

Fig 1.4 $C_D - R_e$ Curve for spheres

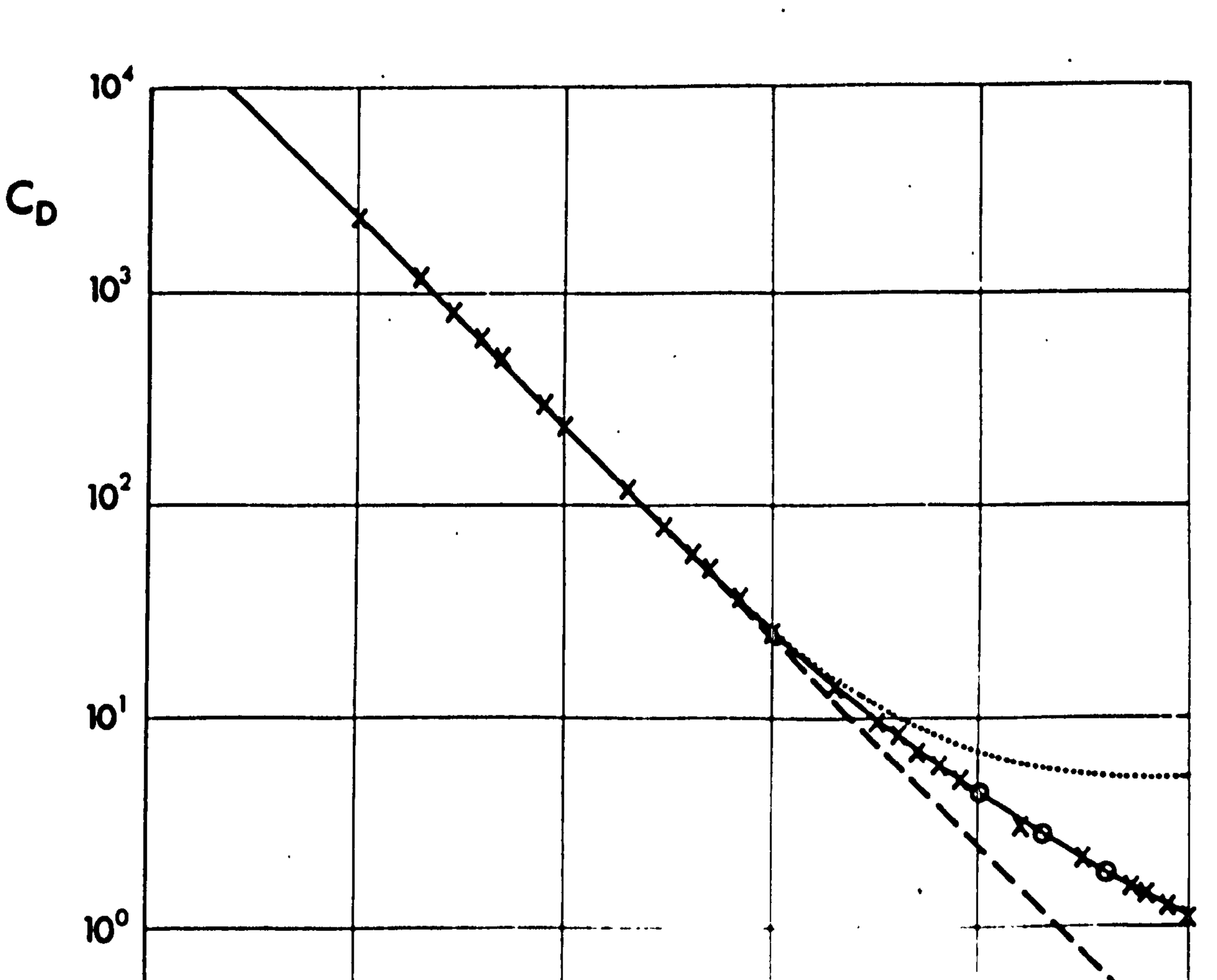

for Re = 1. 4. and 10.

These authors divided their flow field into two regions. One where the flow is essentially irrotational and the other of vorticity or rotational flow, called the " wake". The division is provided by a third region, where the magnitude of the velocity of the fluid is very small, and changes direction very rapidly. The "thickness" of this transition region decreases with increasing Reynolds number, such that at Re = 4 and 10, a clearly well defined wake is evident, but even at Re = 1, the establishment of the wake is apparent.

The flow lines in the wake also indicate that the velocity of the fluid is directed towards the sphere, and at large distances decreases inversly as the distance from the sphere. The velocity in front of the sphere, is directed away from the sphere and decreases as the inverse square of the distance. The magnitude of the flow velocity at a particular distance in the wake increases, while in front of the sphere, it decreases as the Reynolds number increases.

Even though a clear distinct wake was observed at Re = 10, their calculations do not show an existance of a stationary eddy behind the sphere.

Apart from the flow lines, these authors do not indicate any values for the drag coefficients. But presumably since they used Goldstein's analytical solution, any values for the drag coefficients would not be any better than Goldstein's

values.

Proudman & Pearson (1957) went a step further. They used two linear equations for the distances, close to and far away from the sphere. The successive terms in the expansions for the two stream functions, thus obtained, were determined using a "matching" procedure. They do not show their flow lines or calculate the values of the flow velocities, but indicate the formation of a closed eddy behind the sphere at Re = 8. Nevertheless an expression for the drag coefficient was obtained, which includes a logarithimic term in the Reynolds number as

$$C_D\,Re = 6\pi \left[1 + \frac{3}{8} Re + \frac{9}{40} Re^2 \log_e Re + O(Re^2)\right] \quad \ldots(1.2.17)$$

Oseen's approximation has been used in case of other shapes as well, Oseen (1927) himself extended his innovation for the flow past a thin disc normal to the stream. Hocking (1958) using a axisymmetric doublet technique extended this work to include higher powers of Reynolds number. His expression being

$$C_D\,Re = 20.34 \left[1 + 0.1591\,Re - 0.0009\,Re^2 + \ldots\ldots\right] \quad \ldots.(1.2.18)$$

The term in Re was deduced by Oseen.

This expression is compared with the experimental results of Schmiedel (1928) and Willmarth, Hawk & Harvey (1964) in fig 1.5.

Hocking using his technique for higher Reynolds

Fig 1.5 $C_D - R_e$ Curve for discs normal to flow

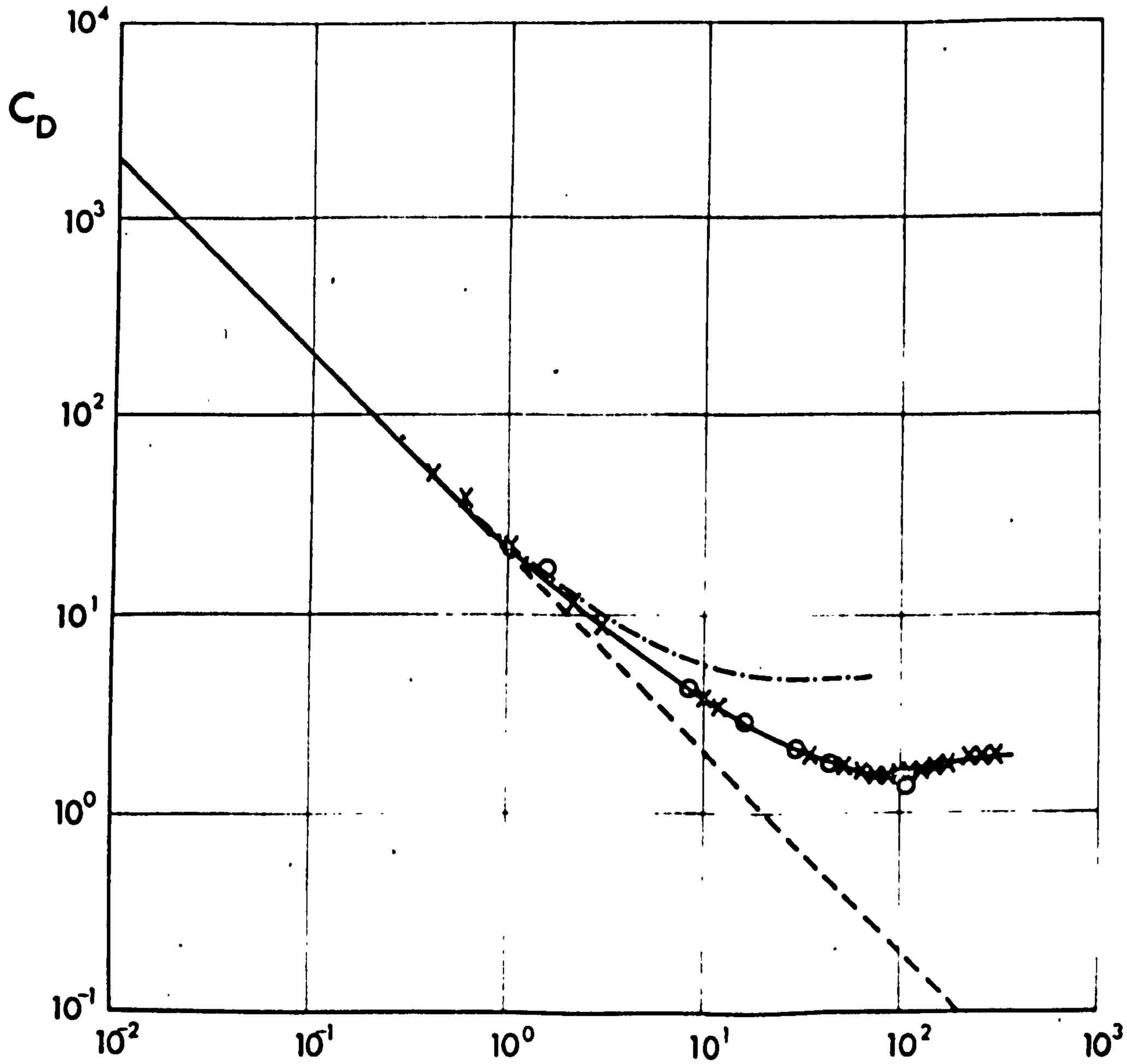

numbers (100 to 200), found that the drag coefficient remains constant, but is more than two times too high,(3,69 compared to 1.8).He also indicate that a stationary eddy exists behind a disc normal to the stream for all Reynolds numbers.

Aoi (1955) gives a detailed theoretical discussion in the cases of prolate and oblate spheroids. The expression for the oblate spheroid reduces to Oseen's result in the limiting case of the disc.

The accuracy of Oseen's approximation is very limited Linearisation of the inertial term enhances its effect on the drag, thereby giving much higher values for the drag coefficient. Hence the validity of Oseen's solution does not extend , at all very far from the viscous solution, and does not justify the tedious computations involved.

But, the importance of Oseen's idea was seen in the solution for the flow past an infinite cylinder. It was stated earlier that no solution is possible for this case using the viscous flow theory. Lamb (1962, p614) using a method similar to Os$en, obtained the follcwing equation for the drag coefficient of a long thin cicular cylinder ($\frac{d}{L} > 100$).

$$C_D = \frac{8\pi}{\frac{1}{2} - \gamma - \log_e \frac{Re}{8}} \quad \ldots\ldots\ldots(1.2.19).$$

where γ = Euler constant 0.577

and $Re = \frac{V d}{\nu}$, d being the diameter of the cylinder.

Finn (1953) using long wires suspended in a wind tunnel directly confirmed this equation for $Re < 0.2$, while extensions of the C_D-Re curves of Wieselsberger (1921) and Relf (1914) join smoothly with Lamb's theoretical curve.

Bairstow, Cave & Lang (1923), Sidrak (1950) and Tomotika & Aoi (1950, 51), extended Lamb's analysis to include higher powers of Reynolds number, in an expression of the type

$$C_D = 8\pi \sum_{n=0}^{\infty} A_n$$

where, $\sum_{n=0}^{\infty} A_n$ could either be solved numerically for special values of Re or expanded as a power series in Re.

Fig 1.6 compares these theoretical curves with the experimental values. The series solutions though giving closer values than Lamb's, still do not justify (as in the case of other bodies) the rigorous calculations. However, the validity of these solutions could be placed at $Re \leq 1$.

Inability to improve the solutions using linearised equations, led some workers to try numerical solutions using the exact non-linear equation. In 1933, Thom used a method of repeated interpolation, in a field of initially assumed values. He divided the flow field into squares, and placed initially assumed values of the stream function, ψ, and vorticity, ζ, at each corner. These values were then used to find the values of ψ and ζ at the centre. The new computed value at the centre was used to find the values at the original corners. This process was repeated

Fig 1.6 $C_D - R_e$ Curve for infinite circular cylinders

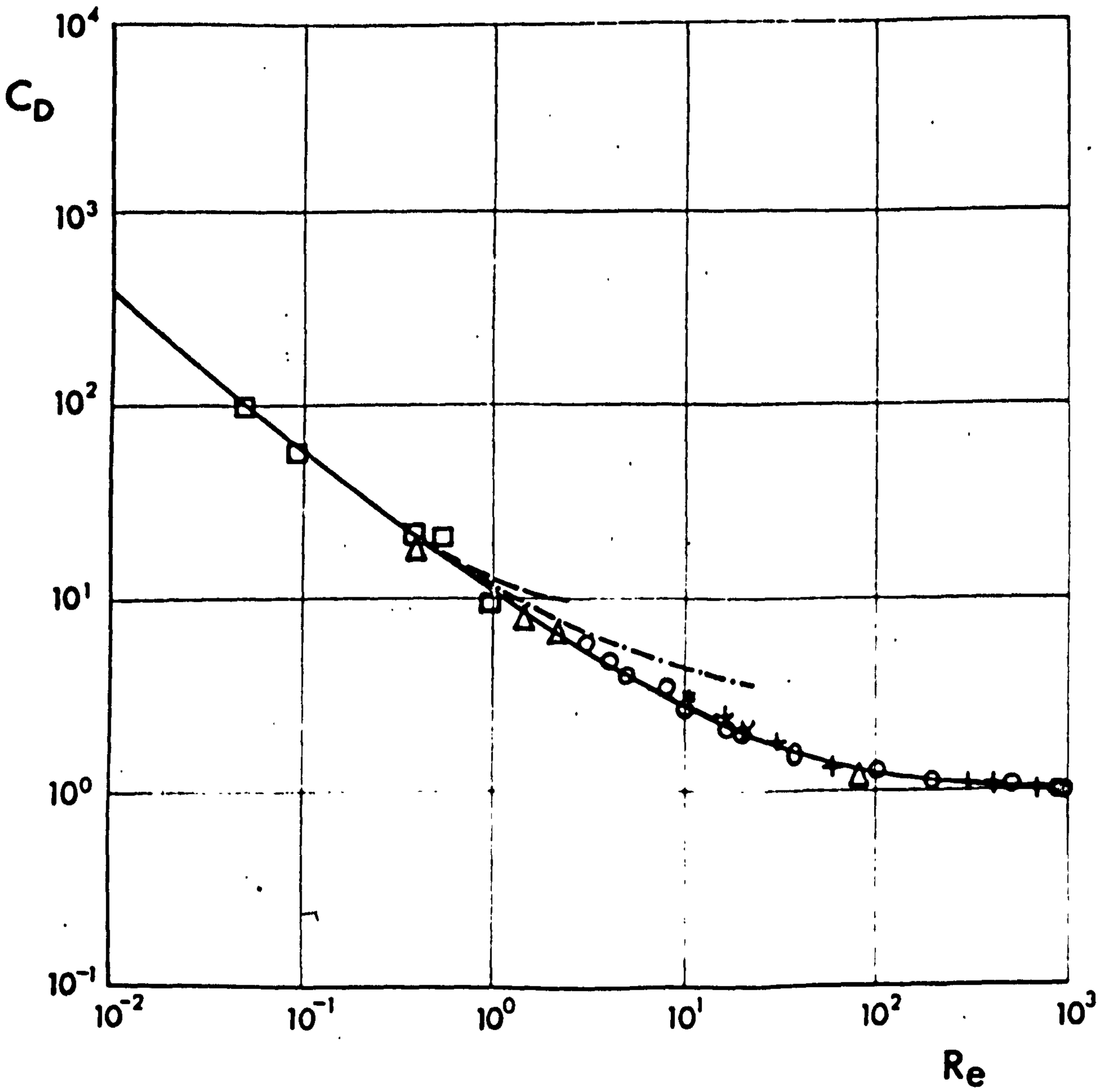

over and over again, until the values of, ψ , and, ζ , all over the field were determined.

Using this rather tedious process Thom computed the flow field and the drag coefficient for the flow past a infinite circular cylinder at Re = 10 and 20. These compare very well with the experimental observations (see fig 1.6).

In principle , this is a finite difference method, the residues being liquidated by repeated interpolation. Kawaguti (1950) used this method for the flow past a sphere at Re =20 and for a circular cylinder at Re = 40,(in 1953).

This method which gives very satisfactory results was later developed into a "relaxation" method by Allen & Southwell (1955) for cylinders at Re= 0, 1, 10, 10^2, and 10^3 and by Jenson (1958) for spheres at low Reynolds numbers (<40). These authors outline the principaleof this method very clearly. In the words of Jenson " the principle of relaxation is to cover the field with a lattice, and approximate to the solutions of the differential equations by satisfying a similar finite difference equations which relates the values at neighbouring points. The solution to the problem is thus found at a finite number of points and the complete solution is obtained by interpolation between lattice points".

Though the basic priciple used by these authors is the same, the treatement however differs mainly through the chioce of co-ordinate systems. Allen & Southwell, solve the

two-dimensional equation for the cylinder, using two transformations for the stream function, ψ , and vorticity, ς , The new values, ψ'' and ς'' , then becomes independent of the Reynolds number. The Reynolds number being absorbed into the Laplacian operator. The lattice points are determined by changing the cartesian co-ordinates, x and y, to α and β , the velocity potential and the stream function for irrotational flow.

Jenson, on the other hand, transforms the equations into spherical polar co-ordinates and his lattice spacings are accomodated in radial co-ordinates by substituting, $r = e^z$, and drawing lattice lines at regular intervals of z. Jenson uses a finer lattice near the surface of the sphere as ψ and ς vary most rapidly in this region.

The flow lines and the values for the drag coefficients obtained by this method are by far the best available. Kawaguti and Allen & Southwell show that laminar solutions are possible for cylinders for Reynolds numbers (> 40) above which vortex rings are shed behind the cylinder. But indicates that such steady regimes could not be realized in experiments because the smallest disturbance can upset them. Hence this method seem to fail once the flow behind the cylinder becomes unsteady.

Fig 1.7 shows the stream lines and vorticity contours for spheres at Re = 5, 10, 20, and 40, after Jenson. He also

Fig. 1.7 FLOW ROUND SPHERE. after Jenson.

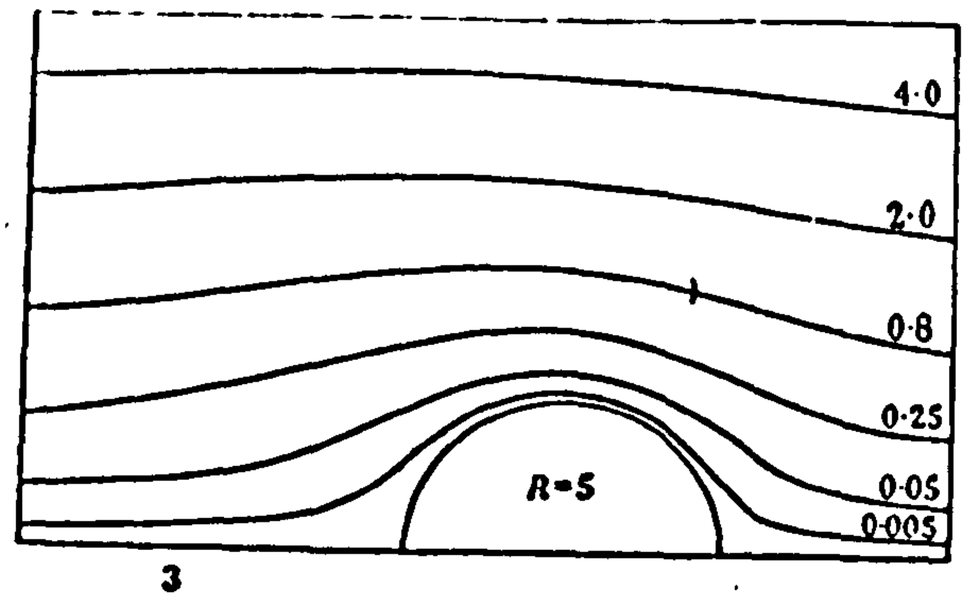

3

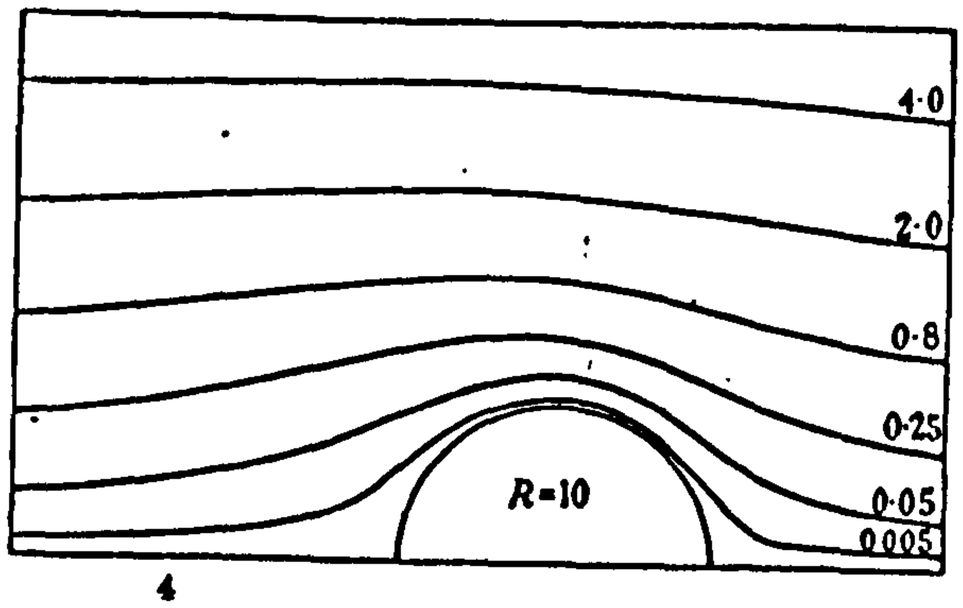

4

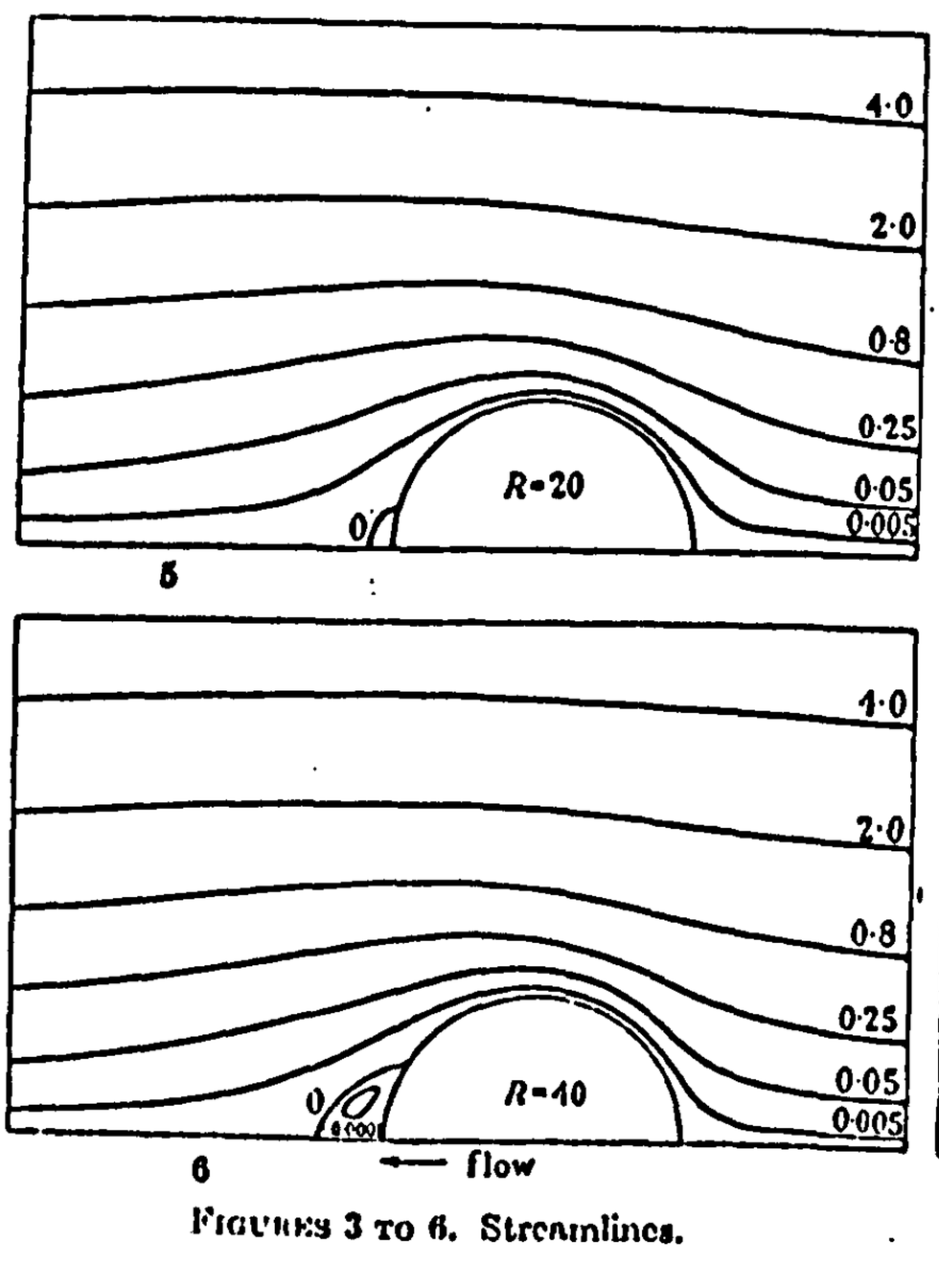

5

6

Figures 3 to 6. Streamlines.

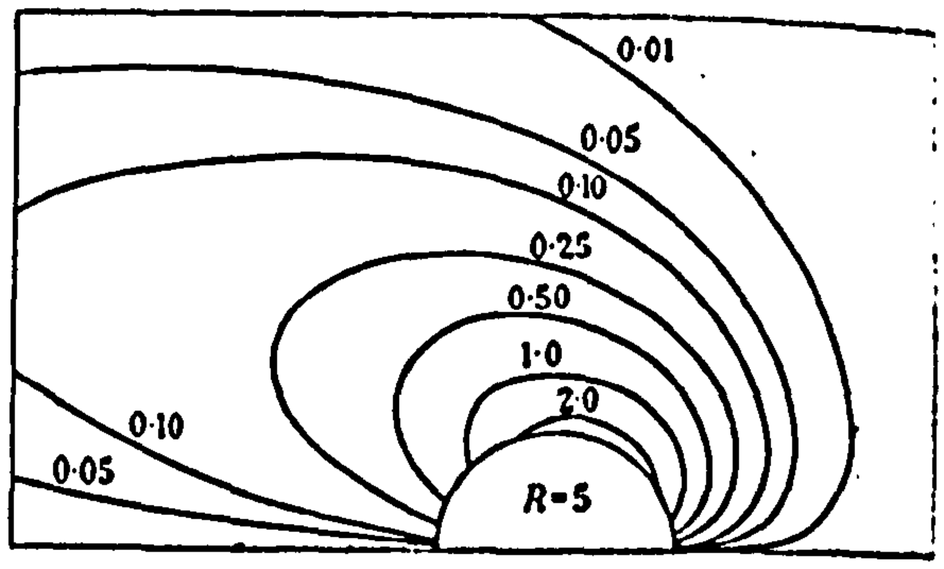

7

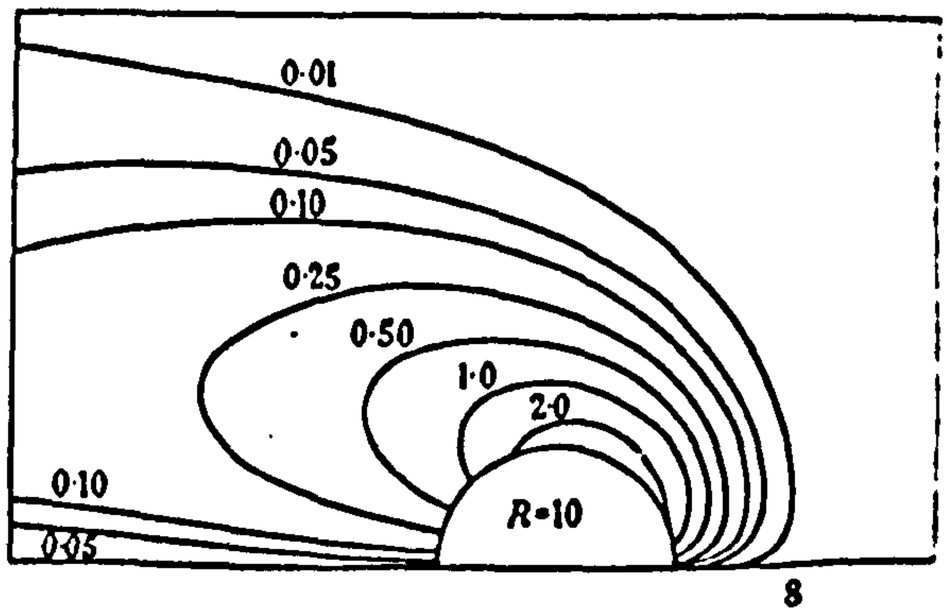

8

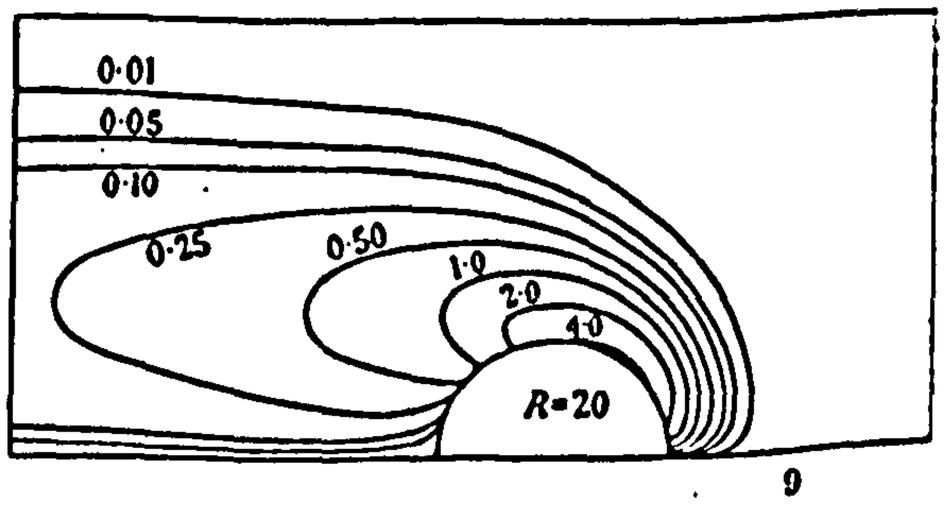

9

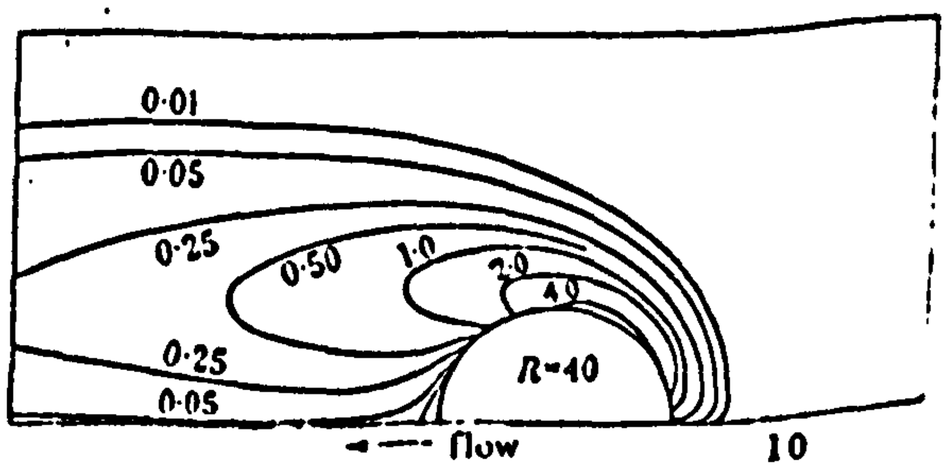

10

Figures 7 to 10. Vorticity.

predicts that a closed eddy behind a sphere is first formed at Re = 17. The values of drag coefficients for the above Reynolds numbers compare very well with the experimental values (see fig 1.4).

Summarising all the theoretical computations for the flow past spheres, all solutions using Oseen's approximation are not valid beyond Re = 2, while that of Proudman & Pearson's improved solution may be extended upto Re = 5. Using relaxation methods, very accurate values can be obtained for particular values of the Reynolds number as long as no unsteady motion exists behind the sphere.

Similar regimes exist for all other shaped bodies as well.

No series solution warrants any accuracy for Re > 5. But, however, empirical relations have been proposed by many authors. Of these, that of Kalycko (1934) merits best credit. His expression is valid within 2% for the range $2 < Re < 400$ and takes the form

$$C_D = \frac{Re}{24} + \frac{4}{\sqrt[3]{Re}} \qquad \text{.....(1.2.20).}$$

This provides a very convienient formula for computing the drag coefficients, but nevertheless, one still has to depend on the theoretical calculations for the flow patterns.

Another important fact, that emerges from the theoretical computations of the flow lines, is that they show that vorticity gets concentrated more and more behind the body as the Reynolds number increases, while irrotional flow exists elsewhere. Hence the effect of the boundirg walls or wall effect gets very much reduced as the Reynolds number increases. Experimentally, McKnown & Malaika (1950) showed that the walls have neglible effect above Re = 1. On physical grounds too, this fact is obvious. For increase in Reynolds number correaponds to a decrease in viscosity. For lower viscosity, any shear in the fluid is transmitted only a short distance from the cause of the shear. So that for a body moving in a low viscous fluid, the velocity of the fluid becomes negligible not far from the body. Hence the condition that the fluid velocity at the bounding wall is zero becomes redundant.

1.3 ORIENTATION OF FREELY FALLING BODIES

The drag on a body depends on the orientation in which it falls. For very low Reynolds numbers, for which Gans-Oberbeck theory is applicable, a body could fall in any orientation. But for an ellipsoid of revolution in translational motion in an ideal fluid, Kirchoff (1869) pointed out that, there are three mutually perpendicular directions of permanent translation. A ellipsoid set in motion in any of these directions,

without rotation, would continue to move in this manner. Of these three directions,he also showed that the direction along the shortest axis is most stable. The streamlines round a flat plate for irrotational flow, computed by Lamb (1962, p86) show the cause for this orientation. Lamb (p171) also gives a detailed mathematical proof for the above mentioned behaviour of a freely falling ellipsoid, at high Reynolds numbers.

In the light of this analysis, long cylinders would fall with their long axis normal to the stream, and thin discs with their short axis along the stream. Bodies which are neither flat nor long and whose shapes do not vary very much from spherical, do not show a strong tendency to orient themselves. But eventually they, too, show this type of preferred orientation, but at much higher Reynolds number. While discs fall with a preffered orientation above Re = 1 (Willmarth et al 1964), isometric bodies like tetrahedrons did not show a preferred orientation until the Reynolds number exceeds over 100 (Pettijohn & Christiansen 1948). For more spherical bodies like a octo-hedron, or as the sphericity approaches unity, this Reynolds number is much higher.

Hence, beyond the viscous regime, bodies fall in such a way as to present the greatest resistance to motion. Extreme shapes show this tendency very rapidly. Near spherical bodies, whose projected areas are anyway not much different, have much less tendency to orient themselves.

As the Reynolds number increases, with the shedding of vortex rings, the fall behaviour of bodies become very unsteady. Discs show a fluttering motion when Re > 80, as shown by Schmiedel (1928). Miller & M'Inally (1936) found that, for high Reynolds numbers (>500) rectangular prisms and long cylinders generally spun or rolled about their long axis. Rough spheres and cubes also showed a spin. These oscillations cause the body to deviate from a vertical path.

Recently Shafir, in a note to the Scientific American, said that smooth cannon balls dropped from a helicopter did not fall vertically but were subjected to a spiralling motion. In discussing the hydrodynamics of wind sensors, Scoggins (1964) shows photographically that, in very calm atmosphere, smooth balloons show a spiralling motion. However, it should be noted that the Reynolds numbers in these cases are very high ($>10^5$).

Further investigations on this type of behaviour of different types of bodies were carried out in the present experiments and are described in the relevent chapters.

1.4 TWO OR MORE BODIES FALLING IN A VISCOUS FLUID

The behaviour of two bodies falling in close proximity has been investigated only in the case of spheres.

For very low Reynolds numbers, Smoluchowski (1911, 12) made the first theoretical investigation of the sedimentation of

two equal spheres. The method was to superimpose the motions produced by each sphere in isolation. The superimposition in this way, is valid only when the separation 's' between the centers of the spheres is large compared to the radius 'r'. Smoluchowski's results could then be valid only for small values of $(\frac{r}{s})$. By introducing terms to satisfy the boundary conditions on one sphere and then on the other, Faxén (1925) found that the drag for two equal spheres moving along their line of centres as a series in$(\frac{r}{s})$ upto $(\frac{r}{s})^5$. Stimson & Jeffery (1926) also worked out an expression for the drag force for spheres falling one behind the other, when there is axial symmetry.

The drag force on each sphere, in all these cases,is the same and could be expressed as

$$D = 6 \pi \eta r V \lambda \qquad .....(1.4.1)$$

the value for λ depends on the orientation and separation.

The most rigorous treatement was given by Stimson & Jeffery. These authors, however, tabulate values of λ for various ratios of $(\frac{s}{r})$ from 1.128 to ∞ , These values could be regarded as the best values for the motion when one sphere is directly behind the other. But since the solution involves axial symmetry, it cannot be used for more than two spheres or when moving in any other orientation.

Recently Kynch (1959) extended the analysis to higher powers of $(\frac{r}{s})$ to facilitate closer comparison with

experiments for smaller separations.

The main predictions of these workers could be summarised as follows.

(1) Pair of equal spheres always fall faster under gravity, than do single sphere falling alone.

(2) This enhancement in the rate of fall is more marked when the spheres are close together.

(3) The pair always maintains the same constant separation and orientation.

(4) Vertical fall is observed only if the line joining their centres is either vertical or horizontal. Otherwise their velocity has a component in the downward sense along the line joining their centres.

Eveson, Hall & Ward (1959), using small perspex spheres of diamter 0.327 to 0.477 c.m. in castor oil verified these predictions. With a suction device, they were able to release the spheres with any separation and orientation. The motion of the spheres was followed using a cathetometer. The Reynolds numbers in these experiments were usually less than 0.01.

These authors also state that no rotation was observed even when the spheres were almost touching. But after a letter by Matthews & Smith (1960), Eveson (1960) reported having observed a slow rotation with a pair of spheres falling side by side.

Absence of a relative velocity between the two equal spheres in the viscous regime makes this problem irrelevent to Cloud Physics. Hence the motion of two unequal spheres has been throughly investigated. The behaviour of a small cloud droplet when being approached by a larger drop, is one of the central problems of Cloud Physics.

The trajectory of a small droplet in the vicinity of a larger drop was calculated by Langmuir (1948) for both viscous and potential flow round the larger drop. An expression for the collision efficiency was deduced using these trajectories. The collision efficiency was defined as the ratio of the actual collision cross-section to the true cross-section of the sphere. For the intermediate region between viscous and potential flow, Langmuir gives an interpolation formula. A serious set back in these derivations is that Langmuir assumed that the smaller droplet had negligible size and caused no disturbance on to the flow round the collector.

Since then, various workers have improved on Langmuir's trajectories. The best contribution was made by Hocking (1958). In his method, Hocking allowed fully for the mutual interference of the two drops. He also computed the drag for each sphere as a series in (r/s) retaining terms upto $(r/s)^7$. Kynch (1959) also treated the motion of two unequal spheres. Important predictions that resulted from these analyses were that

(1) in this case too, there is an enhancement in the velocity of each sphere, and

(2) if two spheres of unequal size, but having the same individual terminal velocity, fall together, the smaller will always move faster than the larger.

The latter prediction was verified by Slack in Porton for Re = 0.3 and 1.8. This work is published in Jayaweera, Mason & Slack (1964).

For higher Reynolds numbers, with the flow becoming increasingly asymmetrical, the behaviour of two spheres changes considerably.

Oseen (1927), using his own approximations showed that, if two equal spheres move along their line of centres, the trailing sphere moves faster than the leader. When they move perpendicular to the line of centres, there is a repulsive force between them, inducing separation.

The existance of a wake behind a sphere due to the inertial forces,causes a trailing sphere to catch up with the leader. This sucking in, which eventually causes capture or collision is called "wake capture", and is observed experimentally for various combinations of materials of spheres and fluids. Happel & Preffer (1960) using plastic spheres in a glycol solution sets the lower limit for wake capture at Re =0.25. Woods & Mason (1965) find that for water drops in air, the radius should exceed 35 μ, corresponding to Re =1.

The difference between these two results is understandable. The former authors were able to detect any slight closing up of the two spheres, by measuring the separations at two points 30 c m. apart, while in the experiments of Woods & Mason the approach velocity has to be at least one-tenth the individual terminal velocity at about ten drop radii apart, so that the wake capture effect could be differentiated from any other spurious effects. Corresponding approach velocity for 40 μ radius drop is about 3 cm per sec.

From these two experiments, it may be concluded that wake capture is noticeable even at Reynolds number of 0.25, but will not be appreciable enough to cause capture of two equal water drops in air unless the Reynolds number is greater than one.

Even for higher Reynolds numbers, between 25 and 100, Rowe & Henwood (1961) showed that there is a decrease in drag on a sphere in the presence of another, the decrease being much higher when the interfering sphere is in front than behind with respect to the stream. Their experiments also showed that the ratio of this increased drag to that of single sphere is independent of the Reynolds number, within the limits of experimental accuracy. However, the errors in their observations are as high as 30%. The drag reduction was observed upto 100 diameters, but the effect is prominent only about 30 diameters away. For two spheres with their line of centres perpendicular

to the stream, a very small repulsive force was detected by these authors even for these high Reynolds numbers.

In the literature, no work is mentioned for the behaviour of few particles in a cluster. However, work has been done for large numbers of sedimenting particles (see Fuchs 1964 and Green & Lane 1964).

Recently after the publication of the present work on spheres (Jayaweera, Mason & Slack 1964), Hocking (1964) and Bretherton (1964) considered the behaviour of small clusters of spheres moving in a viscous fluid, in an attempt to explain the present observations theoretically. Hocking used the slow motion theory and was able to explain most of the observations pertaining to low Reynolds numbers. Some of the discrepancies arising from Hocking's analysis, which he attributes to the inertial effects, was partly explained by Bretherton using Oseen's flow field. More detailed discussion of these two analyses is given in section 2.4, chapter 2.

1.5. MODEL EXPERIMENTS

The principle of dynamic similarity is enunciated by Bradshaw (1964) as "a necessary and sufficient condition for similarity is that all possible, non-dimensional combinations of the geometrical and dynamic scales of the system, together with the properties of the fluid, shall be the same in the two cases considered". Once these requirements are fulfilled, then

the flow past the two systems is identical, and does not depend on the properties of the fluid or that of the solid, taken separately.

For a greater number of flow phenomena, these requirements are basically represented by

(10 geometric similarity, and

(2) equality of Reynolds number

the former controlling the geometric scales and the latter, the dynamic scales of the systems.

Fuchs (1964) points out that these are the only conditions necessary for matching the flow properties only if the motion of the body is uniform and rectilinear. In other words, these are applicable only if the body falls with its terminal velocity. But if the body moves under a external force in a curved path or with non-uniform velocity, then an additional condition has to be satisfied.

Hocking (1958) in discussing the motion of two spheres in a fluid, showed that, unless the ratio of the density of the fluid to that of the material of the body (ρ_f/ρ_s) is small, unsteadiness of the motion cannot be neglected. The motion of one sphere in the vicinity of another is, no longer uniform. It has to be represented by the unsteady equations of motion. In the Stokes' regime, the first term in this equation, which indicated the degree of unsteadiness, is a function of the density ratio. Hence, even if the Reynolds numbers for the

two geometrically similar systems are the same, the motion would not be the same unless the density ratio, (ρ_f/ρ_s), is also matched.

Fuchs introduced ~~the same idea through~~ the concept of the "Stokes' number", S. This is defined as the ratio of the distance, l, traversed by the particle against the viscous drag, if projected with a velocity, U, to that of a dimension, r, of the particle.

Thus

$$S = \frac{l}{r} = \frac{\tau U}{r} ,$$

l is also called the stopping distance

and, τ, the "relaxation" time

~~The stopping distance, l, or the relaxation time, τ, is a function of the density ratio.~~ The additional condition required with this concept being the equality of the Stokes' number.

Fuchs also indicates that, if the Reynolds number is large, so that the resistance is not proportional to the velocity, then the use of similarity theory becomes complicated and affords no advantage except for steady rectilinear motion.

When there are two or more bodies in a cluster, no steady rectilinear motion is possible. Each body moves under the external force arising from the motion of others. So that unless the density ratio or the Stokes' number is also matched as well, it is impossible as well as meaningless to apply the

results of model experiments to that of the real case.

Failure of model experiments in this respect, is shown in the collision efficiency experiments of Sartor(1954) and Schotland (1957). The former used water drops in a viscous liquid for Reynolds numbers between 0.02 and 1, to match water drops . $< 40\,\mu$ radius falling in air. The values of the collision efficiencies were two or three times larger than the computed values of Langmuir or Hocking. Schotland used the simplifying assumption that, as the Reynolds number is small, the fluid density is no longer a significant parameter, thereby making the last condition unnecessary. Theoretically this assumption is correct. For very low Reynolds numbers, the inertia of the fluid can be neglected. But however, this authors intention was the study of wake capture between two equal spheres, which itself requires that the Reynolds number should be, at least, greater than that of Stokes regime. Hence no weight could be attached to his assumption that, the fluid density is not significant. Anyhow the collision efficiencies obtained were far too high.

In the present experiments, the density ratio ρ_f/ρ_s, is never less than 10^{-1}, while that for the case of water or ice in air, this is of the order 10^{-3}. Due to this difference in the density ratios and in the light of the failure of model experiments, the direct applicability of the present results in the case of behaviour of clusters, to

atmospheric particles, is very limited. But these observations would give a qualitative picture of the behaviour to be expected, and further could help in the solution of the flow trajectories for more than two bodies in a cluster. At the same time the orientation and other behaviour of steady motion of a single body, could be applied directly as long as the equality of Reynolds number and the geometric similarity are satisfied.

CHAPTER 2

SEDIMENTATION OF SPHERES

2.1 EXPERIMENTAL ARRANGEMENT

The experiments were conducted in three rectangular tanks, one of which is shown in fig 2.1, each containing a different liquid. A larger tank 2'x 2'x 5' was used with water, while smaller tanks 30 cm. x 30 cm. x 70 cm. was used with sugar solution and liquid paraffin. The last two tanks had a glass bottom as well. The spheres are collected in a transparent cage placed at the bottom of each tank, which is lifted up at the end of the experiment to recover the spheres.

With liquid paraffin, the experiments were performed in a well insulated room, where the temperature could be varied by either heating or refrigeration. The temperature of this room could be maintained steady to within $\frac{1}{2}^{o}$C. The air inside the room was well circulated to ensure constant temperature throughout the room.

The temperature of the liquids was recorded continously, during the experiment, using two mercury thermometers, one placed at the top close to the centre and other at the bottom, close

FIG 2.1

Tank and the suction system

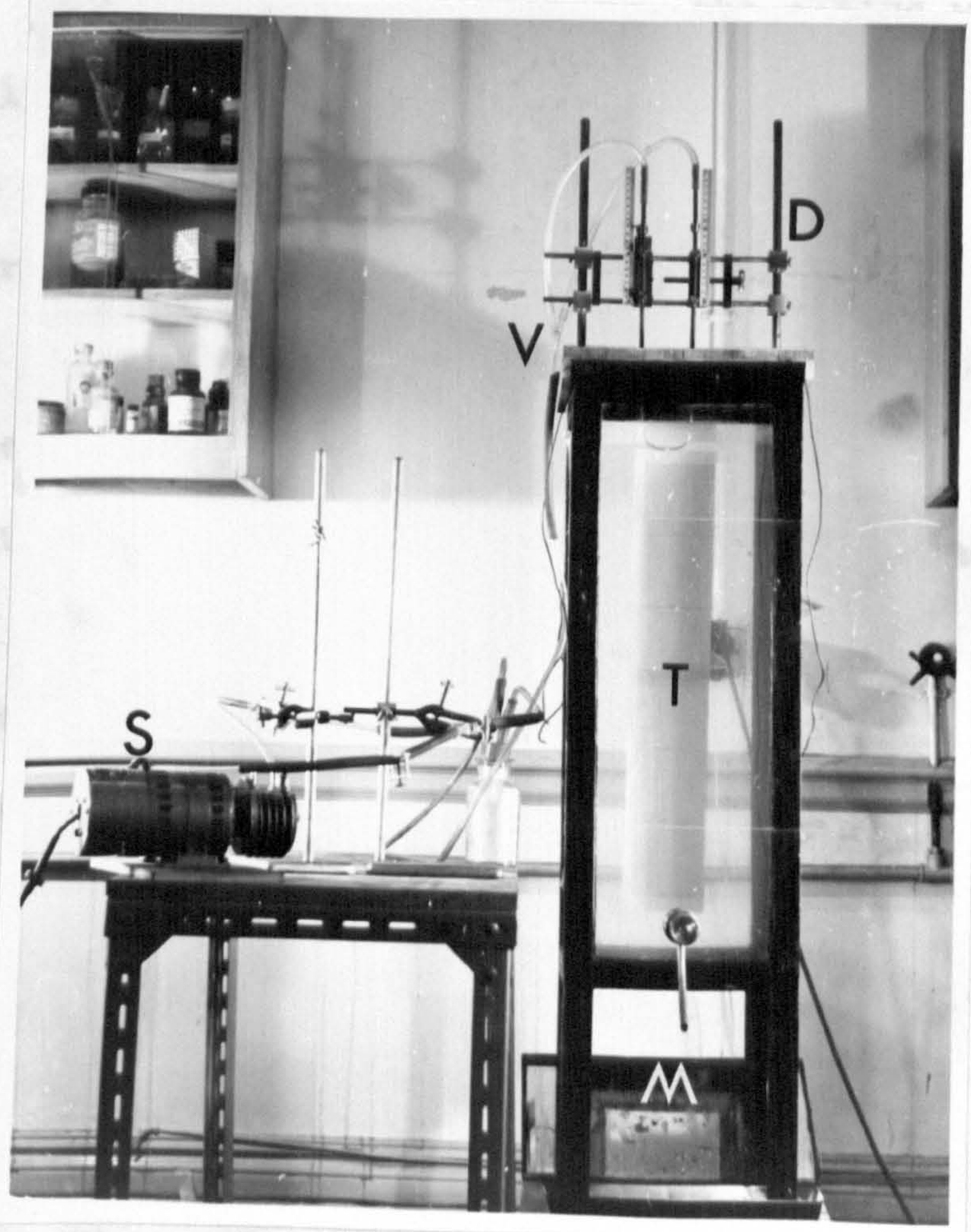

T = Tank (30 cm. x 30 cm. x 70 cm.) D = Dispenser

S = suction pump M = 45° plane mirror V = V-tube

to a side wall. The illuminations were such that no rise in temperature occurs during the experiment.

For photographic purposes, the camera was mounted in a vertically movable carriage (fig 2.2). Two microscopic lamps were fixed on to this carriage so as to illuminate only the region where the camera is in focus. Since the spots of light follow the falling spheres, no part of the fluid was exposed to heat by the lamps for a long time to cause a temperature rise in the liquid.

The spheres were released just below the surface of the liquid. This ensured that the temperature of the spheres was the same as that of the liquid, and that there ~~was~~ were hardly any air bubbles on the spheres. In any case, spheres with air bubbles were not used.

Two types of dispensers were used for the release of spheres. The one shown in fig 2.3, released two spheres with known orientation and separation. The other shown in fig 2.4 a, released coplanar clusters of known geometry and spacing. (These two dispensers will be hereafter referred to as dispenser 1 and dispenser 2 respectively). In both cases the spheres were held under suction and suspended just below the surface of the liquid, and the spheres fell smoothly once the partial vacuum was released.

The dispenser 1 (fig 2.3) was of a very similar type

FIG 2.2

Movable Carriage

M = Microscopic lamps

S = Shackman camera

C = Counter weight

T = Timing unit

FIG 2.3

Dispenser 1

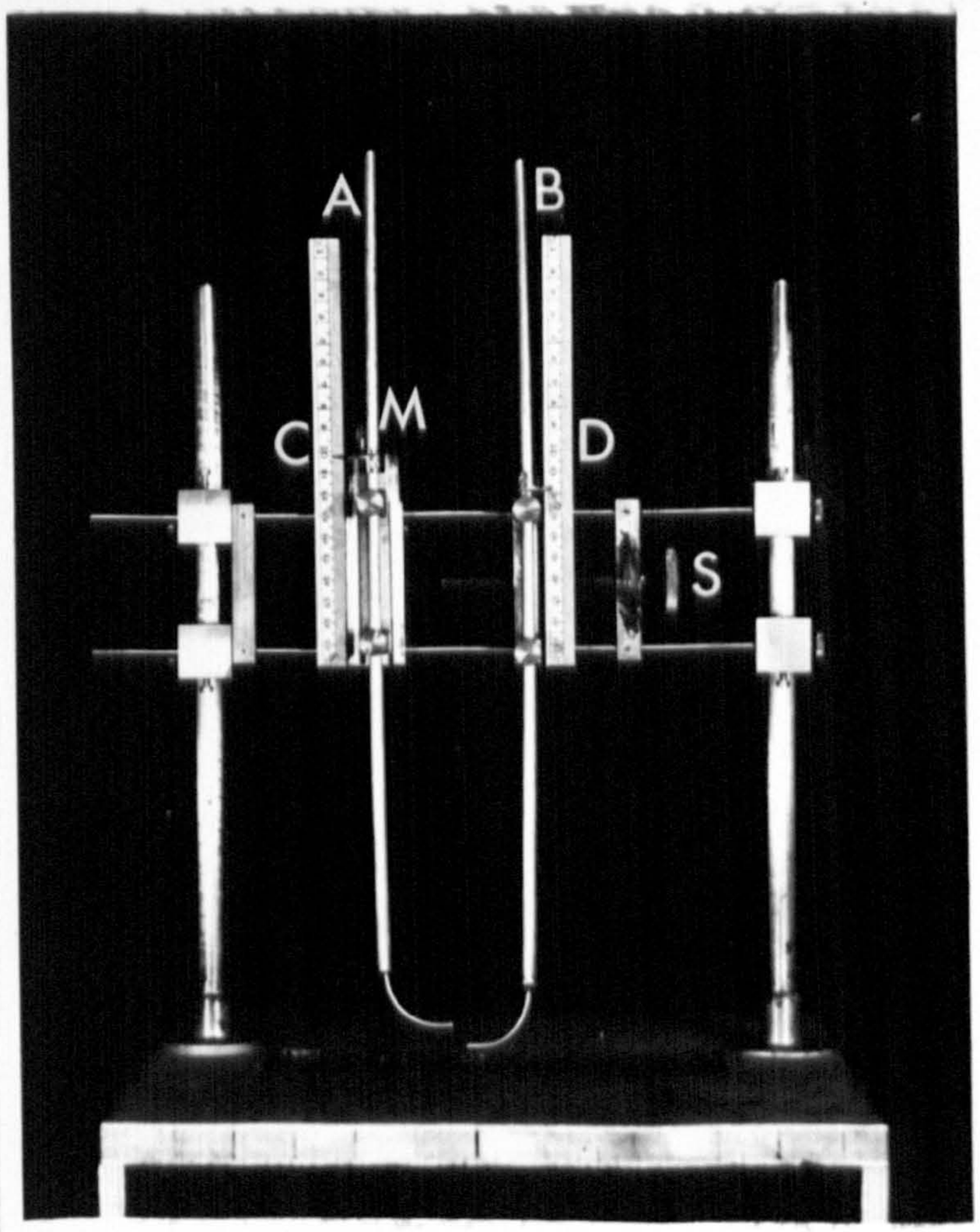

(a) (b)

A, B = Brass tubes C, D = Millimetre scales

S = Screw, (1 mm. per revolution) M = Micro- screw

FIG 2.4

Dispenser 2

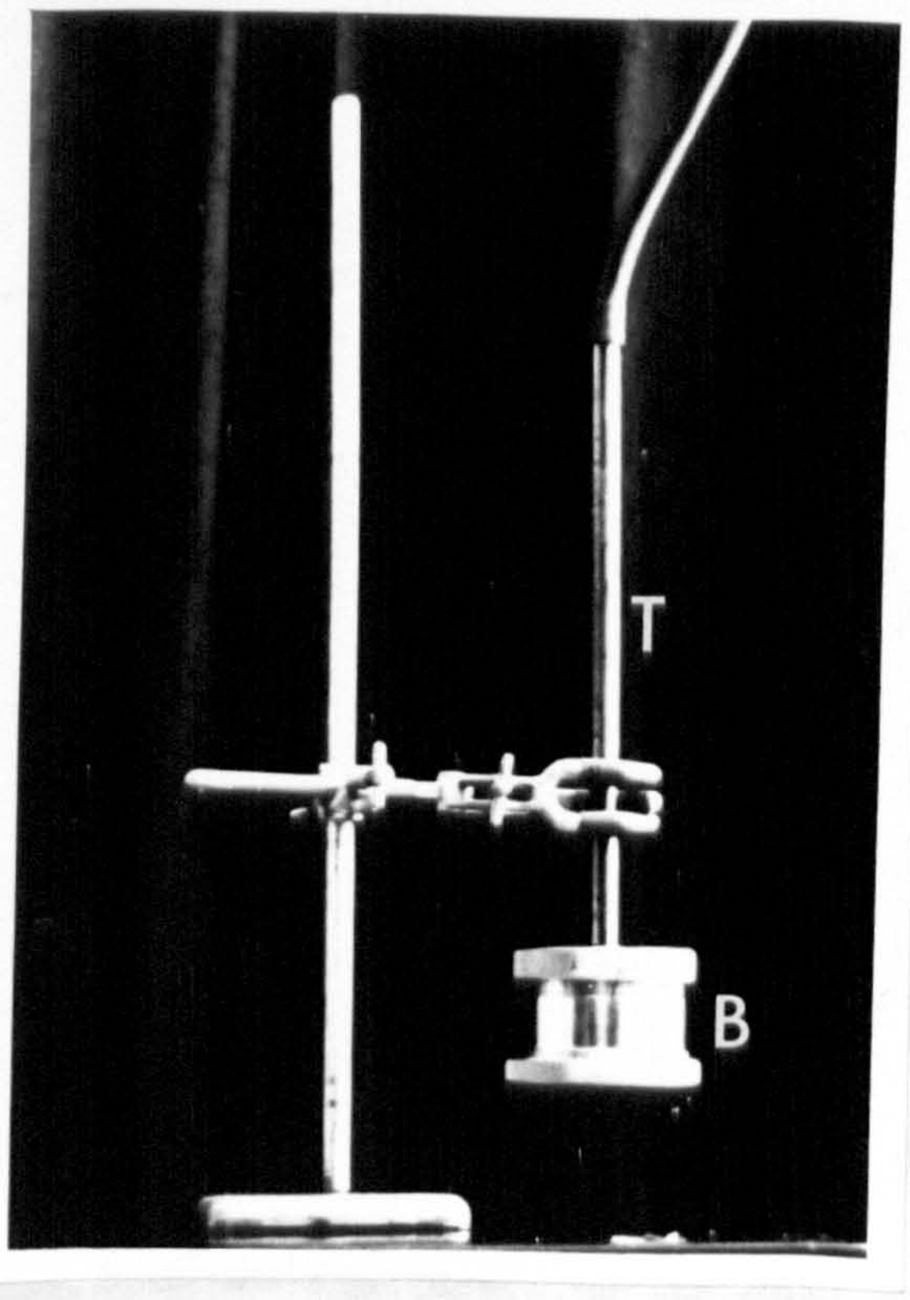

(a)

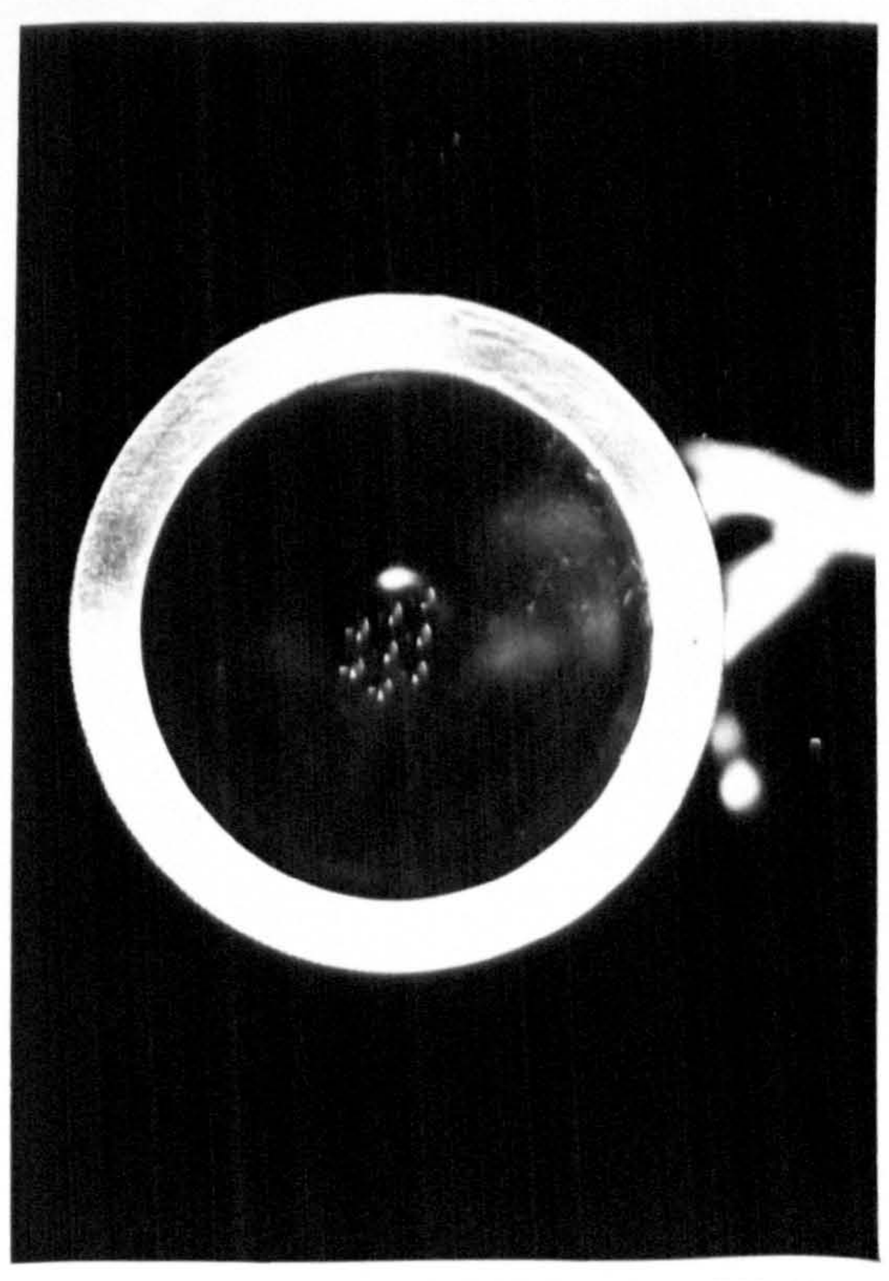

(b)

B = Barrel

T = Brass tube

Perspex plate

to that
~~as~~ used by Eveson et al (1959). This essentially consists of two brass tubes A and B of internal diameter 3/16". The spheres were suspended from the two curved tubes of internal diameter 1/16" sealed to the bottom ends of A an B. The two tubes A and B can be moved vertically and independent of each other along the two millimetre scales C and D. The screw M enables any minor vertical adjustments, upto a centimetre, of the tube A. The horizontal separations of the two tubes was varied by the screw S, which has a pitch of 1mm per revolution. With this device, the horizontal separation of the two spheres could be estimated upto 0.1 mm. The dispenser was mounted on a wooden base, so that it could be firmly placed on the tank in such a way that the plane containing the two tubes was parallel to any of the opposite pairs of the walls of the tank. A wide slit at the centre of the wooden base allowed the tubes to pass through. The two tubes were connected by P.V.C. tubing via a V-tube to the same suction pump.

The dispenser 2, (fig 2.4a), consists of a cylindrical barrel, B, of 9 cm. diameter and 6 cm. high made of Aluminium. The top was firmly closed but connected axially to a brass tube, T, 2.5 cm. internal diameter and 30 cm. long. To the base a perspex plate of thickness 0.96 cm. (3/8") with holes drilled in it (see fig 2.4b) was screwed firmly. This plate could be removed, so that any other similar plate with a different configuration could be replaced. The holes in the plate were of a funnel shape and of size to hold the spheres securely under suction.

The details of the spheres and the liquids used are listed in Table 2.1. With different combinations of these liquids and spheres, it was possible to investigate the behaviour of spheres for Reynolds numbers, defined as $Re = \frac{Vo\ d}{\nu}$, where Vo is the terminal velocity, d the diamter of the sphere and ν the kinematic viscosity of the liquid.

The viscosities of the liquids were measured using a calibrated Ostwald's viscometer, and the density by a 20cc specific gravity bottle. The diameter of the spheres were measured by a micrometer screw gauge and only smooth spheres with diameter correct to within $\pm$ 0.5% were selected.

The spheres were timed over a distance of 80cm. in the water tank and 40 cm. in the other two tanks to calculate their terminal velocities. A stop watch which could be read to 0.1 sec. was used for this purpose. A minimum distance of fall of 30 cm. in the water tank and 15 cm. in the other two tanks was allowed to ensure the attainment of the terminal velocity . (see Appendix 1).

2.2 DRAG COEFFICIENTS AND FLOW PATTERNS FOR SINGLE SPHERES

The drag coefficient for a smooth sphere as a function of the Reynolds number has been very accurately determined by many workers for freely falling or ventilated stationary spheres. A detailed description of these determinations upto a Reynolds number of 10^4 is given by Davies (1945). Further as the already

TABLE 2.1

Spheres

Material	Density $g.\ cm^{-3}$	Diameter range at intervals of 1/16"
Perspex	1.19	1/8" to 3/8"
Nylon	1.14	"
Polystyrene	1.09	"
Polyethylene	0.98	1/8" to 1/2"

Liquids

Material	Density $g.\ cm^{-3}$	Viscosity centistokes	Reynolds number range
Water	1.00 at 20°C	1.00	150
Sugar sol. Conc. 25%	1.10 at 20°C	3	30 to 200
Liquid Paraffin	0.884 at 15°C	340	0.01 to 15
	0.875 at 37.8°C	80	

existing results agree well with each other, any attempt to make further improvements seem unnecessary. However, measurements of the drag coefficients were made to check the accuracy of the present experiment. Fig 2.5, shows that the present values compare very well with the experimental values listed by Fuchs (1964, p32). The drag coefficients were calculated from the measured terminal velocities of fall, and have a error of ± 5%. No correction was made for the wall effects. The ratio of the diameter of the sphere to the distance between the walls was always less than 0.03, and the good fit with the previous results indicates that wall effects could be neglected at least to within the experimental accuracy. Anyway above Re= 1, the wall correction is negligible.

The flow behind a falling sphere was investigated by using a soluble dye. "Biebrich Scarlet R" oil soluble dye was used with liquid paraffin, and a water soluble aniline dye was used with water and sugar solution. A thin layer of dissolved dye was coated on the sphere, which leaves a trail corresponding to the flow behind the sphere when falling through the liquid.

Laminar flow exists for Reynolds numbers less than about 0.5, but as the Reynolds number increases, the flow becomes increasingly asymmetrical. The first visual standing eddies behind the sphere were formed at Re= 24.5. This value is higher than Jenson's(1959) theoretical value of 17. The inability to observe visually the presence of very small eddies may be the

Fig 2.5 $C_D - R_e$ Curve for a sphere

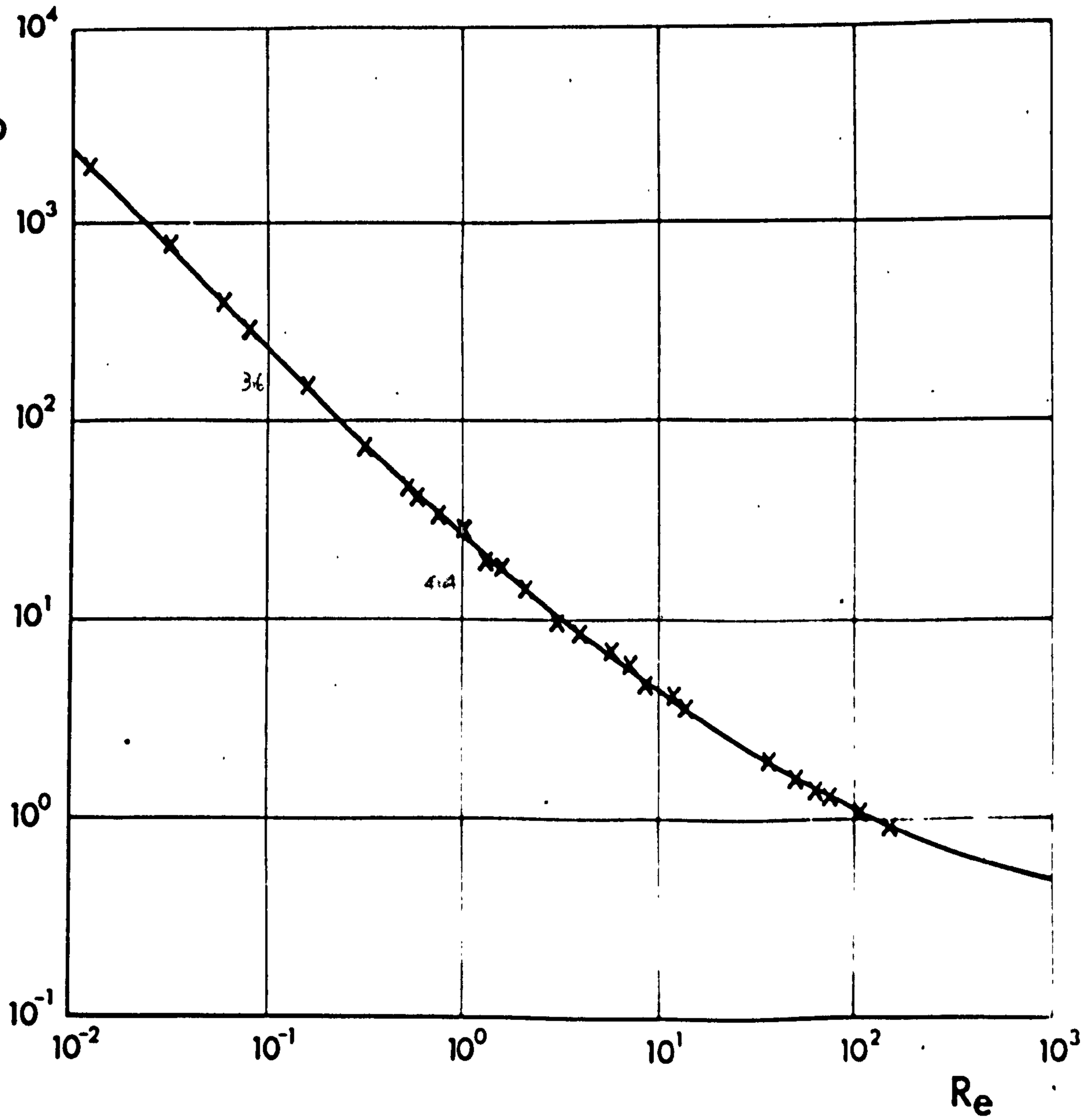

——— From Fuchs (1964)

x Present experimental values

cause of the higher value obtained.

The ~~two standing eddies~~ toroidal vortex ring behind the sphere, shown in fig 2.6a, becomes elongated as the Reynolds number increases upto 180, beyond which the ~~eddies~~ rings get separated from the sphere shedding vortex rings. These are shed alternately from the opposite sides of the sphere, and as each ring is shed the sphere is deflected from the vertical path. This zig-zag motion of the sphere is evident from fig 2.6b.

At higher Reynolds numbers, the rate of shedding of eddies increases, and above Re= 400, the flow becomes turbulent, with the result the zig-zag motion gets gradually transformed into a spiralling motion. Since the zig-zag motion is caused by the shedding of eddies, the spiralling motion may also be due to the shedding of eddies at a greatly increased frequency.

It was stated in section 1.3, that smooth cannon balls falling in air and ballons rising in very calm air at super-critical Reynolds numbers ($>10^5$), showed a spiralling motion, No satisfactory explanation for this motion has yet been put forward. It may be that, the cause for these is also tha break-up of the flow behind the spheres. Correlation between these and the present observations cannot be made until the motion for $10^3 < Re < 10^5$ is studied. ~~However, it is evident that smooth spheres do not fall vertically for Reynolds numbers beyond which vortex rings are shed.~~

FIG 2.6

Flow behind a sphere

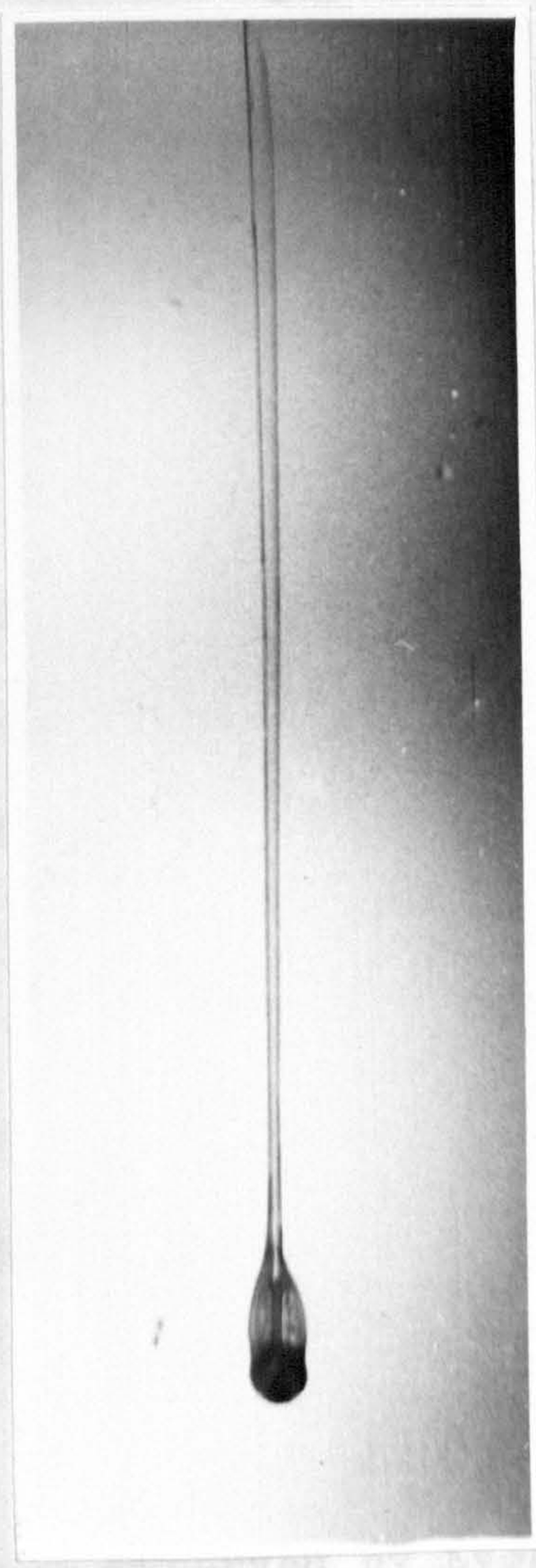

(a)

Standing eddies

$24.5 < Re < 180$

(Perspex $\frac{1}{4}$", Re = 120)

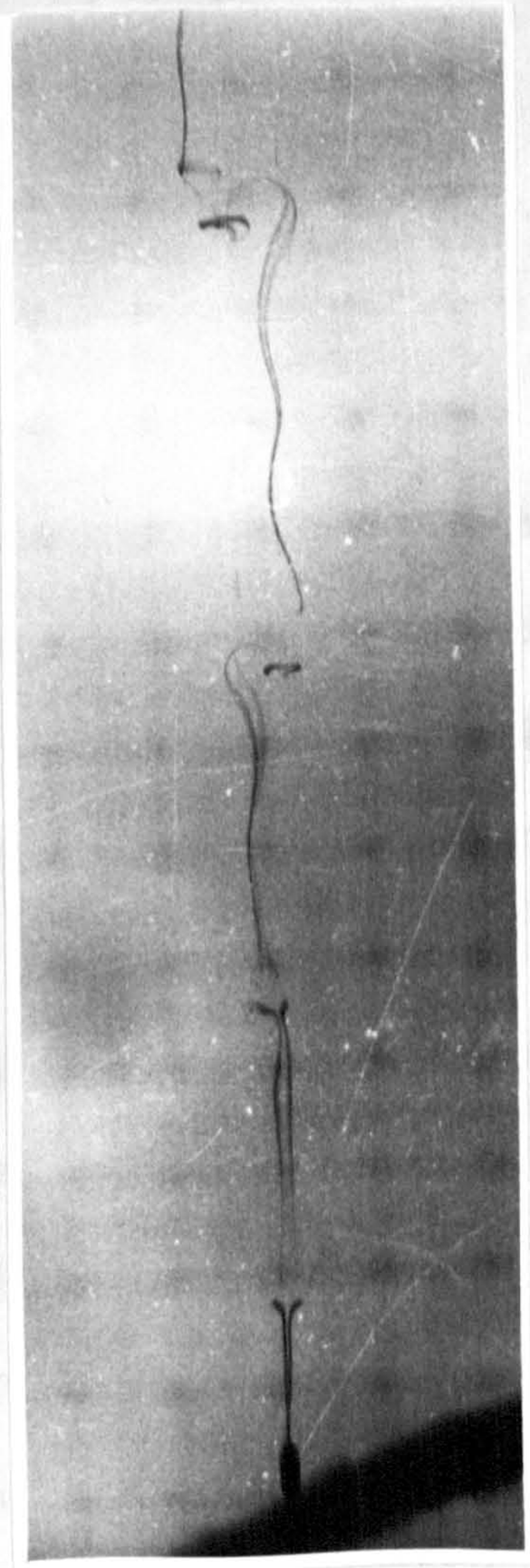

(b)

Shedding of eddies showing the zig-zag motion

$Re > 180$

(Perspex 1/8", Re = 295)

2.3 THE BEHAVIOUR OF PAIRS OF SPHERES

A Two equal-sized spheres falling side by side

For very low Reynolds numbers, < 0.01, sedimentation of pairs of equal spheres have been investigated by Eveson, Hall & Ward (1959). But for higher Reynolds numbers, there is hardly any experimental data. The Reynolds number refer to a single sphere falling in the absence of the other.

When the Reynolds number exceeds about 10, two spheres initially touching each other show a sudden horizontal separation and fall vertically with their individual terminal velocities. Hence no detailed investigations were made for Re > 10.

For all lower Reynolds numbers, the rate of fall of both spheres is greater, in all cases, than that of either sphere falling individually. This enhancement in velocity of fall is greater when the spheres are close together.

When Re < 0.03, the behaviour is exactly the same as that observed by Eveson et al (1959). The spheres showed no tendency to separate or rotate. But for Re > 0.05, each sphere rotates about a horizontal axis through its centre and normal to the line of centres. The left hand side sphere rotates in a clockwise sense, while the right hand side sphere in an anti-clockwise sense. This type of rotation, which will be referred to as "inward" rotation was made visible by half

painting the spheres, and is shown in fig 2.7. The rotation is accompanied by separation of the two spheres, but the spheres remain separated with their line of centres horizontal throughout the fall.

The rate of separation and rotation increases with increasing Reynolds number, but decreases as the spheres separate. Thus the rotation and separation cease.. to exist after the spheres have reached a particular maximum separation.

The separation of the two pairs was recorded at constant intervals of time ($\frac{1}{2}$ or $\frac{1}{4}$ sec.) using a Shackman camera incorporated with a timing device. The two spheres were released using the dispenser 1 so that the axis of separation was parallel to the wall of the tank facing the Shackman camera, S. The camera was mounted on the moveable carriage and focussed on to the spheres. The axis of the camera lens was kept perpendicular to the line of separation of the spheres. The lens being an ordinary 3.5, 5 cm. lens. Another camera V (Vito C) was placed with its axis horizontal and along the line of centres of the two spheres. The arrangement is schematically represented in fig 2.8. The camera V just takes one photograph when the two spheres are in line with its axis. This ensured that the camera S records the actual separation between the two spheres. If the camera V showed a displacement of the two spheres, the run was discarded.

The two spheres always separate along their line

FIG 2.7

Separation and rotation of horizontally separated two equal spheres. After Jayaweera, Mason & Slack (1964).

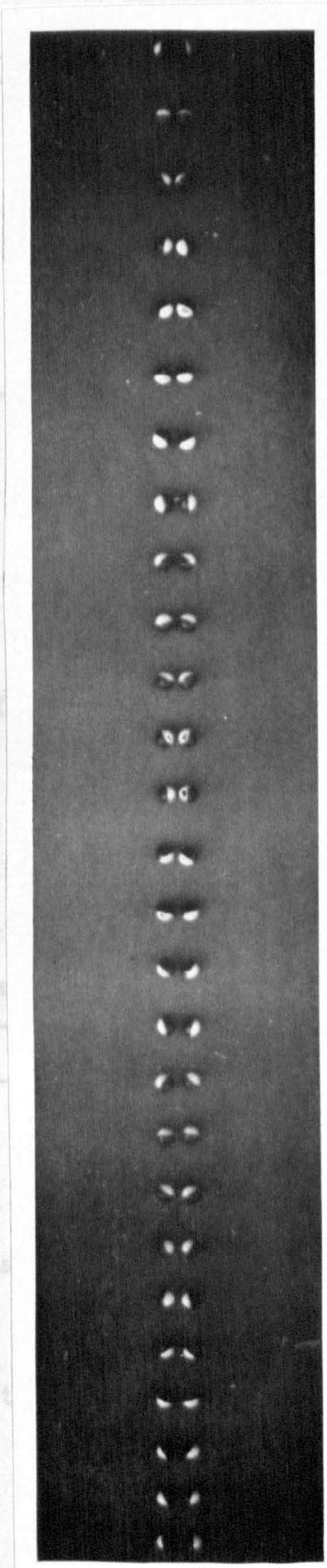

Perspex d =3/8"

Re ≃ 0.1

Photographed at intervals of 2 sec.

FIG 2.8

Photographic arrangement to measure the horizontal separation of two spheres. (Plan view).

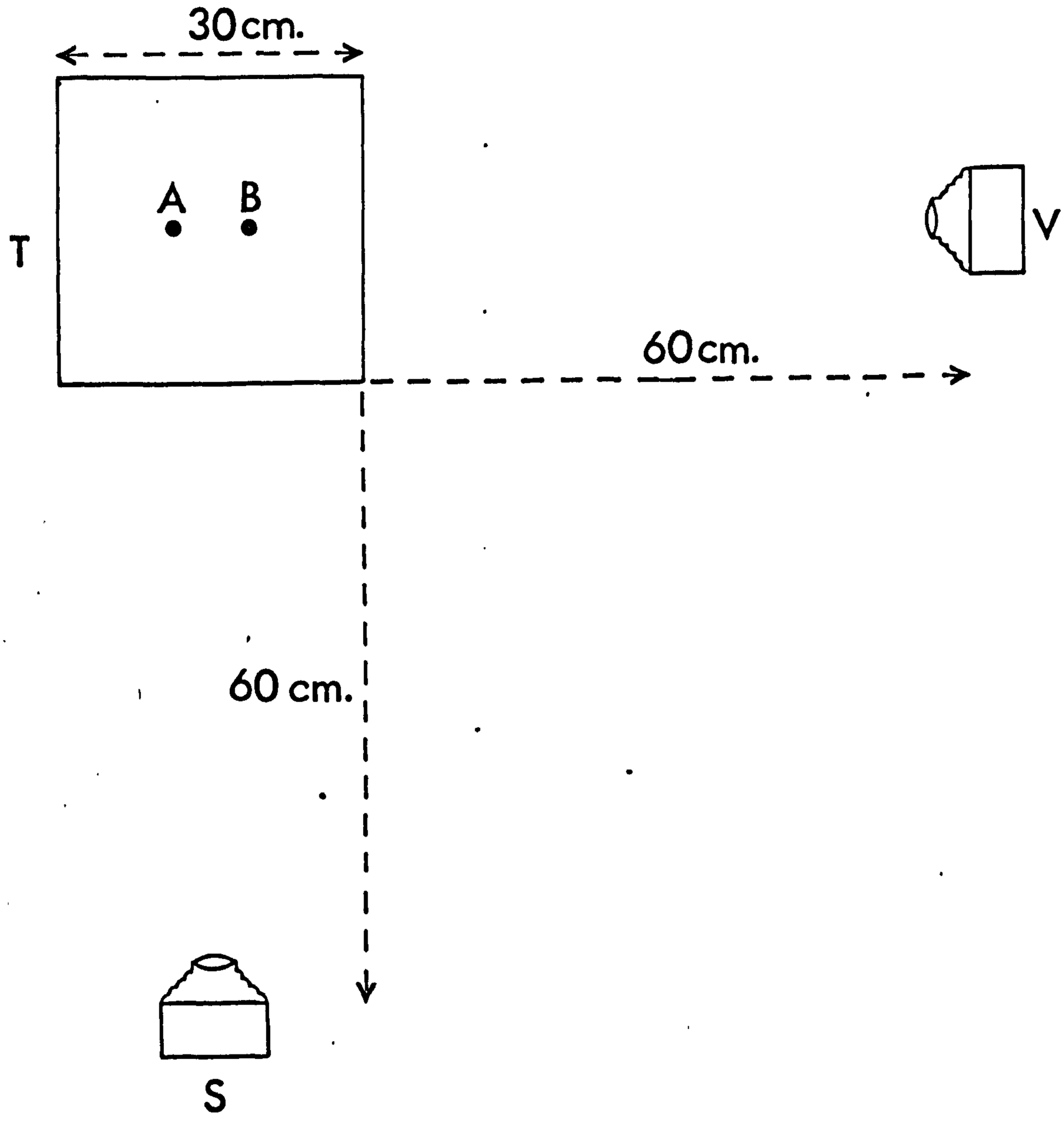

T = Tank

S = Shackman camera (movable vertically)

V = Vito C camera (fixed)

A and B = the two spheres.

of centres. This was found by interchanging the positions of the cameras V and S, and taking photographs at regular intervals of time with camera S. In all cases the spheres were one behind the other, showing the separation always take place along the line of centres.

The Shackman camera always moved so that the spheres were in the centre of field of view. The separation between the two spheres was read using a micro-film reader. The outline of the spheres was very sharp, so that separations could be very accurately determined. To calibrate these separations, a photograph of a 5 cm. scale suspended horizontally in the liquid on the same plane as that in which the spheres fall, was taken.

These measurements, made either at $\frac{1}{2}$ or $\frac{1}{4}$ sec intervals depending on the velocity of fall, showed that for a given pair falling in the same fluid, whatever the initial separation they reach the same maximum limiting separation, X_m. This is a function of the Reynolds number and the diameter of the sphere, as shown in fig 2.9. (X_m / d) decreased from 7.8 at Re= 0.5 to a nearly constant value of 3 for Re $>$ 8. The rotation of the spheres exists until this maximum separation was reached.

B Two equal-sized spheres falling vertically one behind the other

This investigation was also carried out using the

Fig 2.9 Limiting separation X_m for two equal spheres as a function of Reynolds number

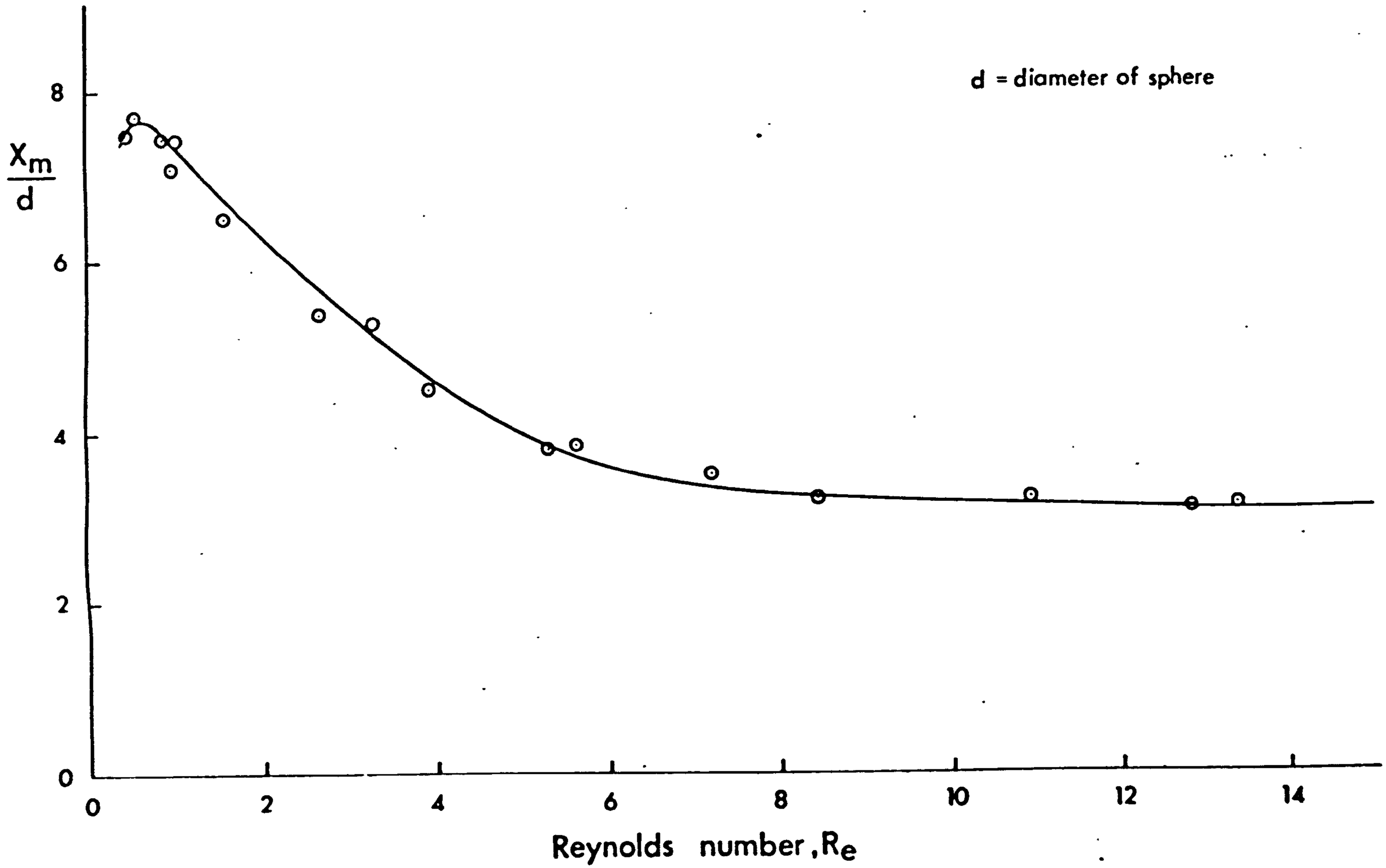

same experimental arrangement as in case A, except that the use of the camera V becomes unnecessary. To make certain that the spheres are vertically one behind the other, a plumb line made with a thin white silk thread (gauge 40) was hung about 10 cm. from the line of centres of the spheres and in focus for the camera. The thread has no effect on the motion of the spheres.

When the two spheres are released vertically one behind the other, they remain this way but the separation decreases, as they fall. For Reynolds numbers as low as 0.3, in accordance with the observations of Happel & Preffer (1960), there is a decrease in the separation but the velocity of approach was so small that the rear sphere never overtook the front sphere, even when the initial separation was only three diameters. For Re = 0.32 (3/16" diameter perspex sphere in liquid paraffin at 18°C) the separation changed only from 2 cm. to 1.5 cm. after a fall of 40 cm. But if Re > 1, the rear sphere gets accelerated in the wake of the front sphere and tends to overtake it. When Re exceeds 4, this acceleration is already noticeable when the spheres are ten diameters apart.

At large distances apart, the velocity of approach varies inversely as the separation but settles down to a nearly constant value at small separations - see fig 2.10a. The relative velocity on apparent contact is little less than half the terminal velocity of an individual sphere at Re ~ 10 and about

Fig 2.10a Relative velocity of approach V as a function of separation S

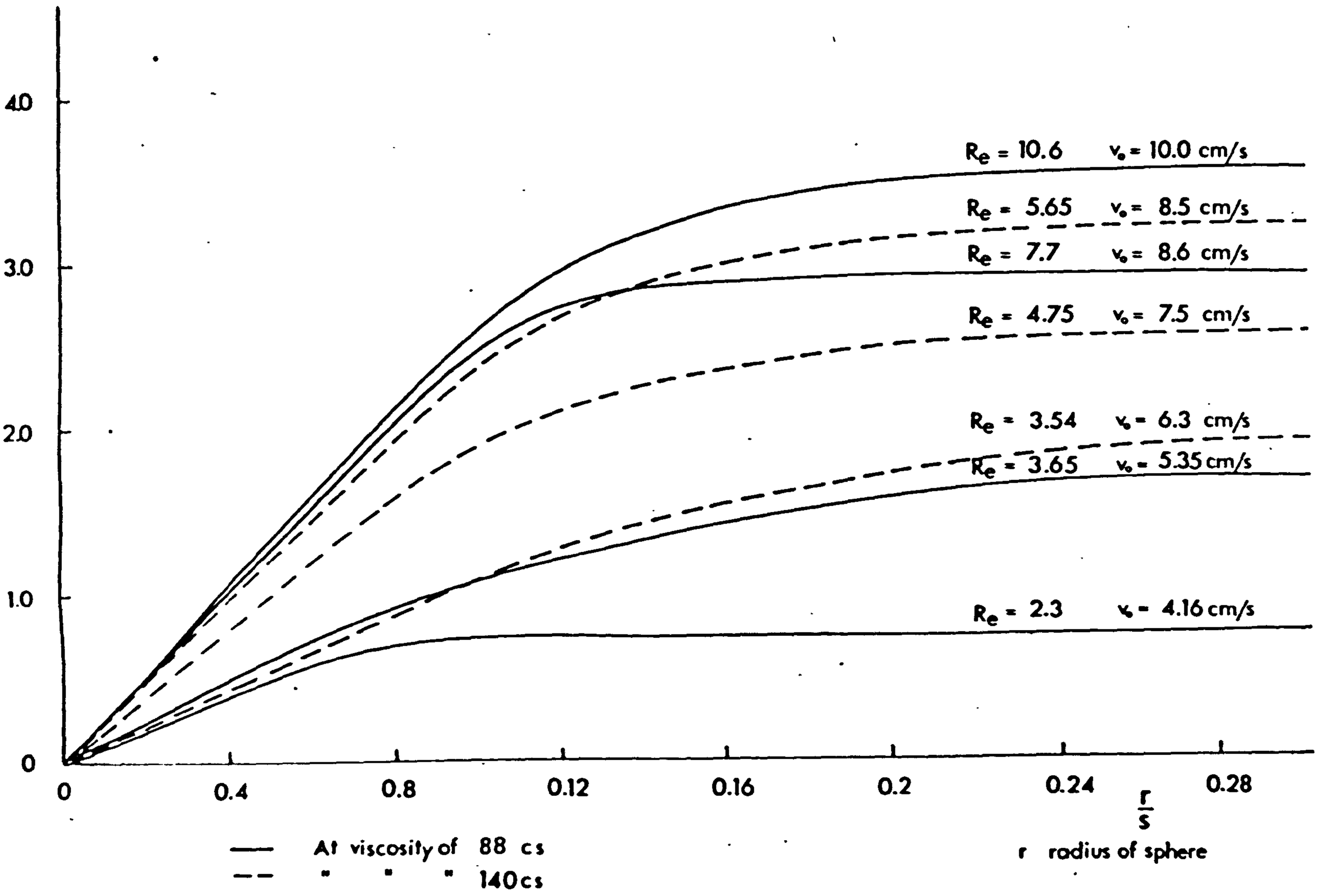

0.15 for Re~2.

No rotation of the spheres were observed until the two spheres were almost touching, after which the rear sphere slides round the leader, and when the line of centres become horizontal, the spheres separate and rotate in opposite directions, and continue to diverge laterally as they fall just as in (A).

For separations greater than ten radii, the velocity of the front sphere was unaffected and moved uniformly with its own terminal velocity. But for shorter separations there was an increase in the velocity of the front sphere as well. Referring to fig 2.10a, the region where the velocity of approach increases with decreasing separation is when the velocity of the front sphere is unaffected, while the other region where the velocity of approach is nearly constant, is when the front sphere also moves with a non-uniform increasing velocity.

Pearcey & McHugh (1955) showed that the flow behind a sphere is directed towards the sphere and for large distances, the velocity, V, of the fluid is given by

$$\frac{V}{V_o} = m\ (r/s)$$

V_o = terminal velocity of the sphere.

For

Re = 1,	m = 3.526
= 4,	= 4.87
= 10,	= 7.17

For a particular Reynolds number, the velocity of the fluid is inversely proportional to the separation, so is the velocity of approach at large distances from the experimental results. This suggests that the rear sphere at large separations (>10 radii) moves in response to the flow field created by the front sphere. To check this the values of 'm' was compared with the corresponding experimental values and is shown in fig 2.10b. Good agreement exists for Re= 1 and 4. However, for Re= 10, Pearcey & McHugh's value is too high.

For small Reynolds numbers, when the density of the fluid is comparable to that of the sphere, the time taken for any sphere to adjust its velocity in response to changes in the fluid velocity can be neglected (Hocking 1958). The present experimental values show, at least for large separations, that such a situation exists for Reynolds numbers as high as 4.

C <u>Two unequal spheres falling vertically one behind the other</u>

In this case too, the rear sphere moves with a greater velocity than its individual terminal velocity. Measurements revealed that the relative motion of two unequal spheres is equivalent to a linear superposition of their difference in terminal velocities upon the motion of two equal spheres. The rear sphere being controlled largely by the flow behind the front sphere.

Fig 2.10b m versus R_e where $m = \frac{v/v_0}{r/s}$ at small r/s

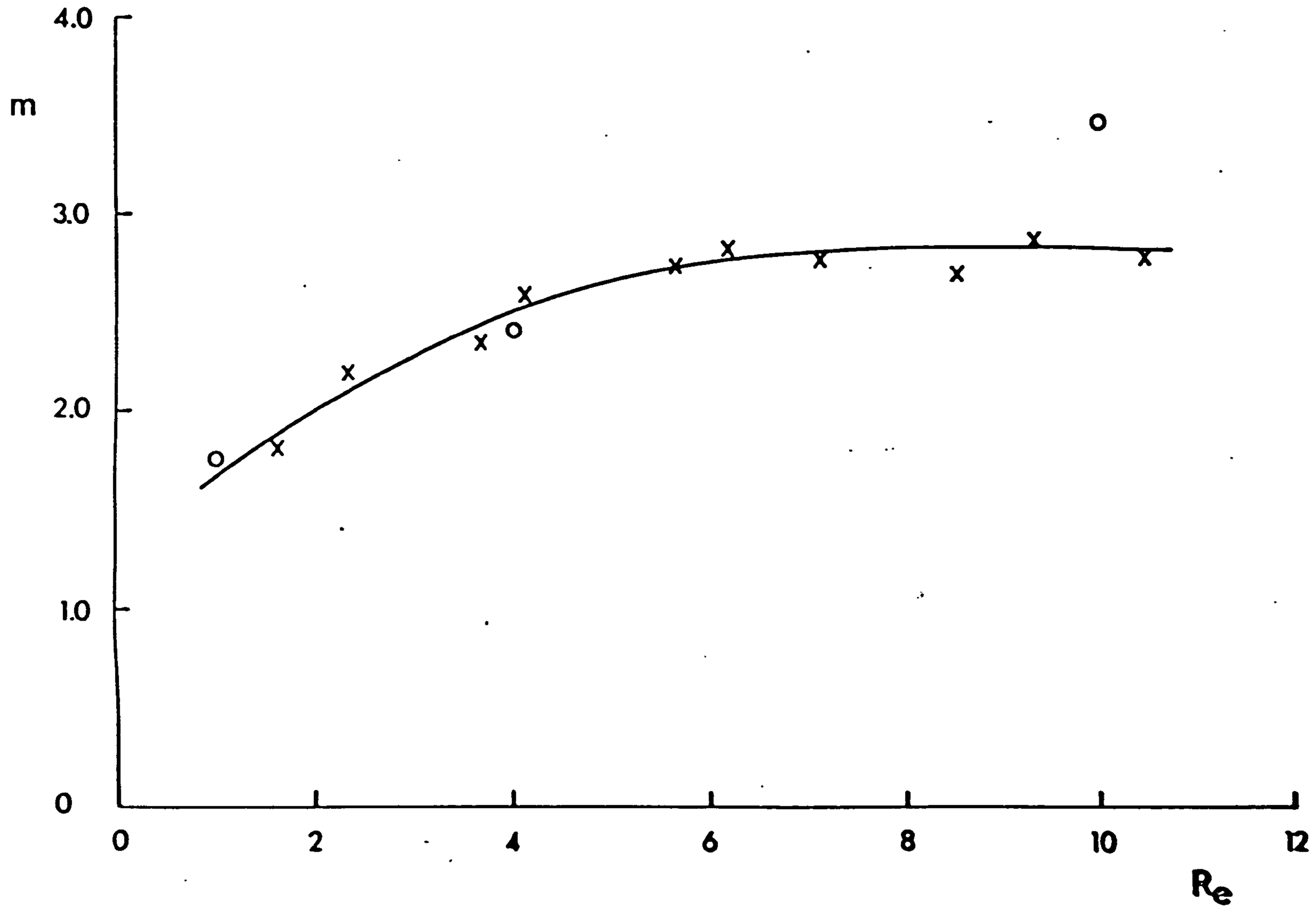

Thus if the rear sphere has a lower terminal velocity than the leader, it will catch the leader, only if the difference in the terminal velocity is less than the approach velocity of two spheres identical to the leader, at the particular distance apart. When such a capture occurs, the two spheres initially rotate and separate, but eventually the sphere with the greater terminal velocity moves ahead.

D Two equal-sized spheres with the line of centres inclined to the horizontal

A pair of equal spheres, each with $Re > 1$, and initially in different horizontal planes, slide along their line of centres, but at the same time the rear sphere approaches the leader, and ultimately occupies the same horizontal plane, and moves as in (A).

The vertical separation between the two spheres decreases much faster than the horizontal separation. In no case was there even a apparent collision. Fig 2.11 gives a typical path taken by the rear sphere relative to the leader. The two axes correspond to the vertical and horizontal separations in units of the radius of the sphere, and the points are separated in $\frac{1}{2}$ sec. intervals. It is clear from this path that the minimum separation between the sphere is much greater than the diameter of the spheres.

Fig 2.11 Typical path of a rear sphere relative to an equal sphere in front
(Perspex 5/16" in liquid paraffin at 18°C R_e = 1.37; v_∞ = 4.35 cm/sec.)

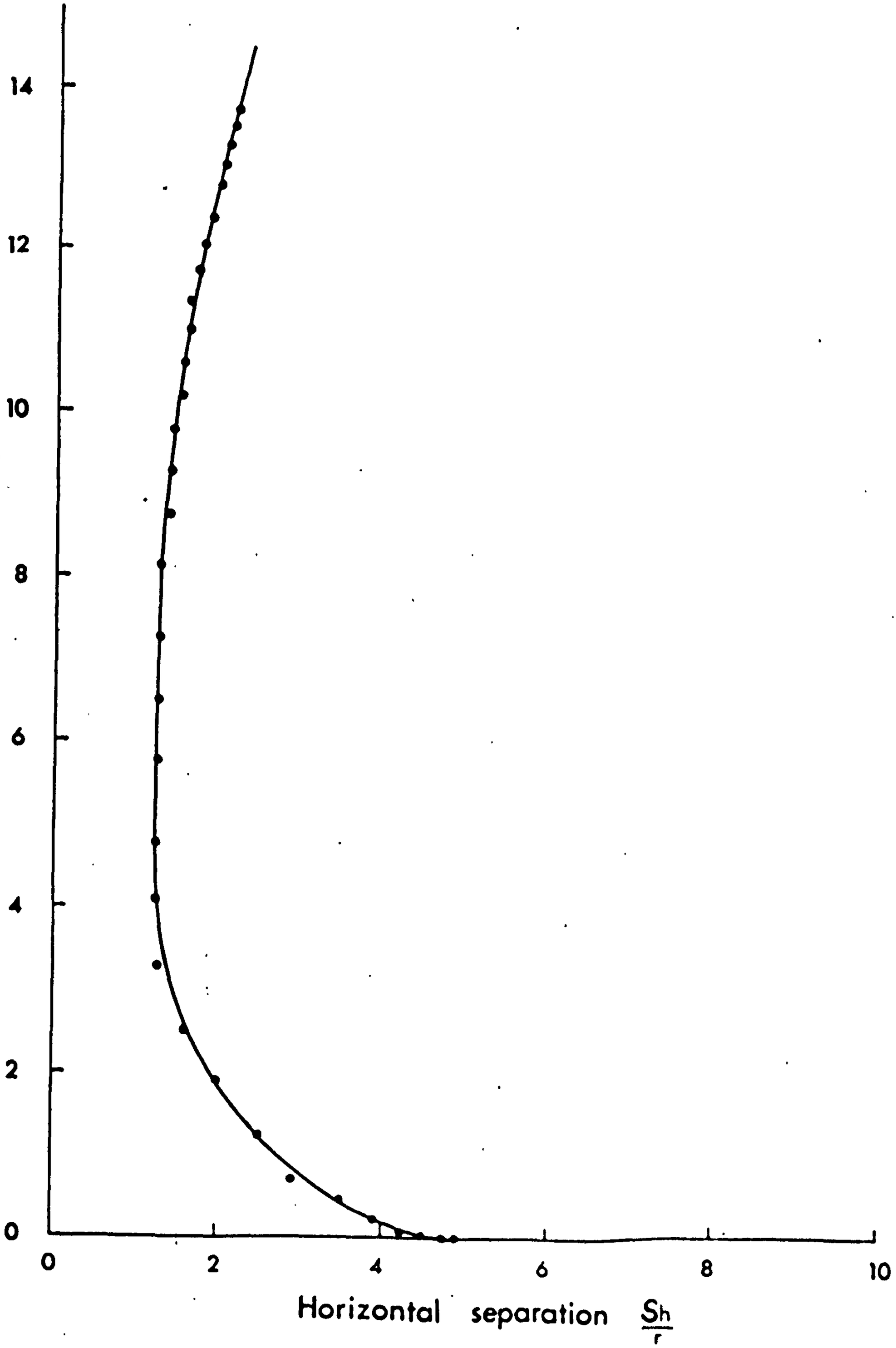

E Discussion

The behaviour of two spheres confirm that if the inertial forces are present, there is an increase in velocity for a sphere falling one behind the other and a repulsive force if separated in a horizontal line. Rotation of the spheres exists only when the spheres separate horizontally.

For two equal spheres not directly one behind the other, the rear sphere initially gets pulled into the wake of the front sphere but later separates without collision. This observation differs from Schotland (1957) who, with a similar experiment, obtained a very high collision efficiency: Schotland explains his high value in terms of the rear sphere getting pulled into the wake of the front sphere. In the present experiments too, the initial pulling indicates that if the separation at the later stages did not occur the spheres would have collided.It seems that Schotland calculated his collision efficiencies only considering the initial stages of the trajectory of the rear sphere.

Collision occurs only if the inertia of the sphere is large enough to squeeze the liquid between the two spheres. But for these low Reynolds numbers and when the densities of the sphere and liquid are comparable, the sphere would move in response to the changes in velocity of the fluid, thereby getting pushed away from the leading sphere.

The present experimental results cannot be directly applied to the case of water drops in air, due to the large difference in the density ratio. However, there is one important point of agreement in that the Reynolds number has to be greater than one, for wake capture to occur in both cases (see Woods & Mason 1965).

2.4 THE BEHAVIOUR OF THREE OR MORE EQUAL-SIZED SPHERES

The behaviour of three or more spheres in a cluster was studied for various initial coplanar configurations. The dispenser 2 was used to release the spheres. With the different combinations of the spheres and the liquids, it was found that the behaviour depends only on the Reynolds number.

A 3 to 6 spheres released in a compact cluster

(a) $Re < 0.06$

The spheres tend to follow their initial configuration, whatever the number in the cluster as long as they are uniformly distributed. But the velocity of fall is more than that for isolated spheres. The enhancement is greater the more compact the cluster. However, the initial configuration even if it is a regular polygon is susceptible to small perturbations.

If the cluster is not uniform, the ~~more~~ denser portion move faster than the other. This cause a tilting of the cluster which then appear to slide along the line of tilt.

(b) $0.06 < Re < 7$

The behaviour of spheres in this Reynolds number range showed that:

(1) Even if the spheres are initially staggered by a few diameters they eventually draw level and ultimately arrange themselves in the same horizontal plane at the vertices of a regular polygon as shown in fig 2.12.

(2) The polygon expands slowly at a decreasing rate during the fall.

(3) The speed of fall is greater than that of a single sphere.

(4)The enhancement of the fall speed is greater more compact the cluster. Hence as the polygon expands the velocity of fall decreases.

(5) The final configuration was achieved more slowly with a large number of more widely separated spheres.

(6) During the early life of the polygon each sphere rotates "inwards" about a horizontal axis that is normal to a lino joining the centre of the sphere to the centre of the polygon.

(7) When the separation exceeds a certain value (about 6 diameters at Re ~1 and 3 diameters at Re ~ 7) rotation ceases, but the separation continues. The regular polygons are not formed if the initial separation exceeded this value. This shows that rotation is necessary for the regular polygons to be formed.

(8) In this case too, as for Re < 0.06, if the spheres composing the cluster are arranged very asymmetrically, the densest portion

FIG 2.12

Clusters of spheres. $0.06 < Re < 7$

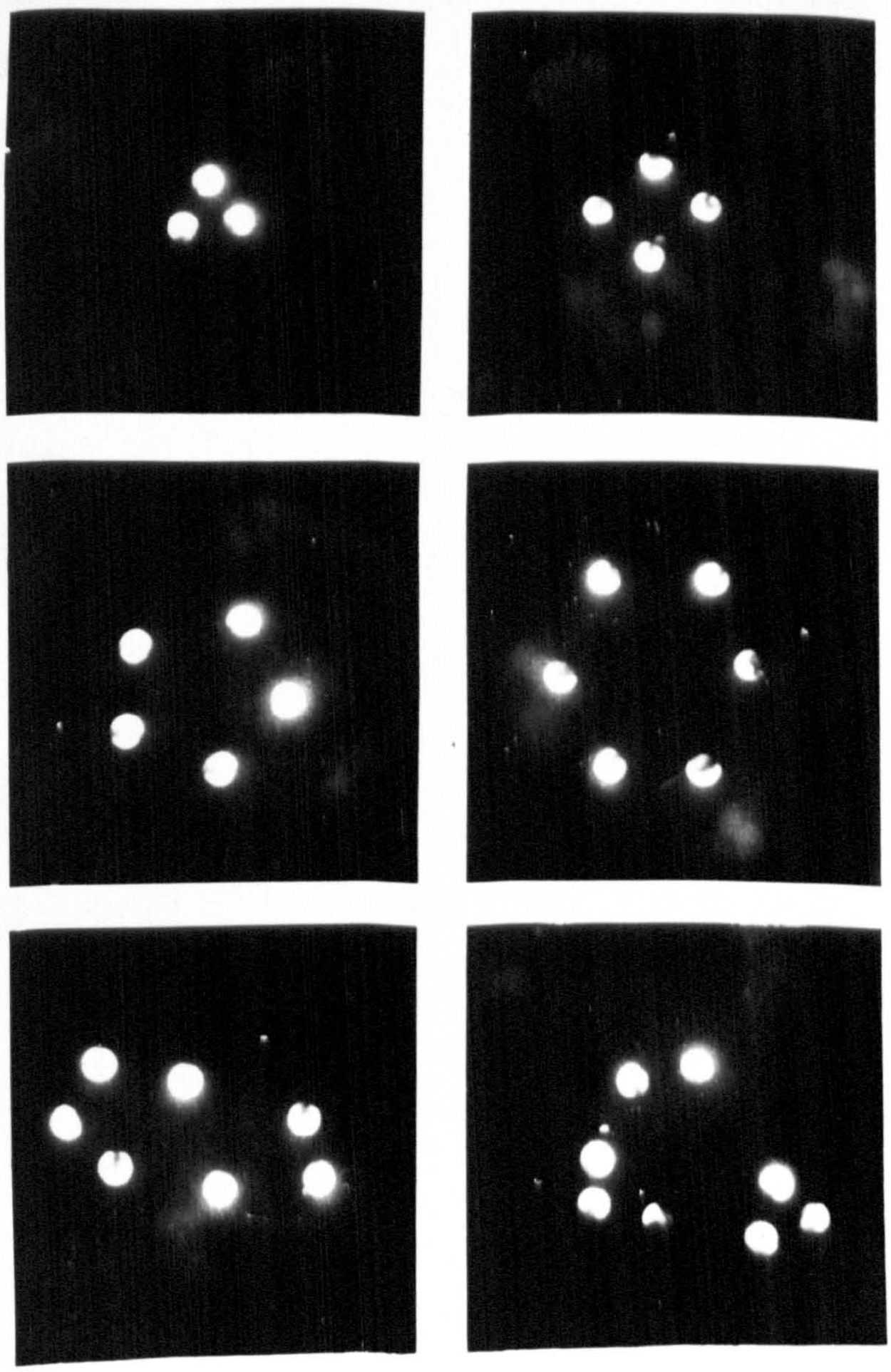

3 to 6 spheres form a regular polygon

7 and 8 spheres break up

(Perspex, d = 3/16", Re = 0.32)

portion travels fastest.

In order to investigate the initial stages of the formation of the regular polygon, three spheres were released in a horizontal isosceles triangle. The apex sphere oscillated in a decreasing vertical spiral relative to the other two, which executed linear oscillations along the horizontal line of centres and moved apart as the apical sphere moved towards them. The initial amplitude of these oscillations depends on the apex angle, which is greater for larger deviations of apex angle from 60°. But the oscillations gradually damp out and the three spheres form a stable equilateral triangle.

Similar behaviour was observed during the formation of 4-, 5-, 6- sided regular polygons. The individual spheres oscillate about their equilibrium positions but eventually achieve a stable regular configuration.

(c) Re > 7

The spheres of the cluster quickly separate with a sudden onset of rotation, which soon ceases, and no regular polygons are formed. The spheres separated to about 3 diameters and fell with the individual terminal velocities.

B 3 to 6 spheres released in a horizontal straight line

The tendency for the spheres to form a regular polygon is much less in this case. The Reynolds number range

$0.06 < Re < 7$ could further be sub-divided where different behaviour occurs.

(a) $0.06 < Re < 0.16$

When three equal spheres, initially in contact or equally spaced within six diameters are released in a horizontal straight line, the centre sphere moves slightly ahead, one of the laggards then moves between the other two, and the third (now trailing) passes between the other two. This interchange of positions continues throught the fall, but the spheres keep close together and do not separate. The sphere temporarily in the lead stops rotating. The three spheres keep to a vertical plane throught the fall.

If the spheres are not equally spaced, then one sphere is always left behind, which sphere, depends critically upon the initial spacings. If the spheres are numbered and separated as

(1) —— a —— (2)——— b ——— (3)

which sphere left behind for the various ratios of b/a are as follows:

b/a	<1.17	1.20-1.30	1.33-1.40	1.5	1.60-2.0	>2.0
sphere left behind	1	2	1	3	2	3

For b/a < 2, one sphere is left behind after one or two interchanges, while for b/a > 2, the sphere 3 is left behind from the start. The two spheres falling together after leaving the third, move in the same way as described in section 2.3.

Two slightly separated pairs initially in a horizontal straight line diverge as they fall, each pair rotating as a doublet. Ultimately the members of each pair separate. If the four spheres are all touching in a horizontal straight line, the behaviour is very inconsistant. They either form into two pairs as in the previous case, or forms a three leaving the fourth behind. With five or six sphores the outer ones move out, re-enter the cluster from behind and cause it to break up.

(b) 0.16 < Re < 3

If three to six contacting spheres are released in a straight line, they separate and eventually form a regular polygon as in the case A(b). Hence for this region, for any initial configuration, as long as the spheres are touching, they form a regular horizontal polygon.

(c) Re > 3

The polygon is not regular, and progressively breaks down until, with Reynolds number greater than seven, the spheres appear to repel each other and separate but show no tendency to form a polygon, the spheres remain in the same horizontal line but with a increased separation between the spheres.

Hence to get a regular polygon between $3 < Re < 7$, the spheres have to be released in a compact cluster, but above Re= 7, no regular polygon is formed whatever the initial configuration.

C 7 or more spheres in a cluster

A compact cluster containing seven or more equal spheres do not form a regular polygon, but breaks into two or more groups (see fig 2.12). Even if the spheres are initially released in a regular polygon, the cluster is unstable. The tendency to break up is higher for larger Reynolds numbers and greater numbers in the cluster. E.g. a regular heptagon gets distorted for $Re < 0.1$, and ~~while~~ breaks up for larger values of Re. If an additional sphere is placed at the centre of a regular hexagon it moves ahead and to one side. This causes the hexagon to tilt towards the sphere, which re-enters the hexagon from the rear side and causes it to break up.

D Discussion

Hocking (1964) made a theoretical investigation to find out how many of these observations can be explained using Stokes' slow motion equations. Hocking made two assumptions in his analysis. The first the necessary Stokes' assumption that $Re \rightarrow 0$, and the second that the separation, s, is large compared to the radius, r. Since Stokes' equations are valid

only for the region near the sphere, Hocking's equations are valid only if

$$Re \ll 1, \quad r/s \ll 1, \text{ and } Re(s/r) \ll 1.$$

These assumptions retain the most important terms in the interactions of the spheres and enables the fluid motion to be found by the superposition of the motion produced by each sphere in the absence of the others. But this analysis is not applicable when the spheres are in contact. An important requirement in this analysis is that the fluid density should be comparable to that of sphere, so that the equations of motion can be written with the hydrodynamic forces on each sphere always balancing its weight in the fluid.

Hocking considered 'n' equal spheres and wrote the equation for the velocity of the 'i'th sphere in the presence of the others. Using this equation he determined the path of the sphere.

For three or four equal spheres released in a straight line, Hocking found the behaviour was as observed in the experiment. With three equal spheres unequally spaced, the theory and experiment agree on the sphere that is left behind, except for the range $1.2 < b/a < 2$, which is the range for which the behaviour is most sensitive to changes in b/a.

Investigating the initial stages for the formation of a regular polygon, experiment showed the spheres execute :

damped oscillations about the regular shape. Hocking considering three spheres in a horizontal isosceles triangle found that the apex sphere excecutes undamped oscillations in the horizontal plane and not that of a decreasing vertical spiral as seen in the experiment. Further, the oscillations of the base spheres cannot be predicted by theory. Since Hocking's analysis cannot explain the formation of the steady configuration for three spheres, he makes no further effort to investigate the case of more than three equal spheres in a cluster or for spheres initially placed arbitarily.

However, assuming the spheres initially placed in a regular polygon, Hocking was able to show that this configuration is stable only if $3 \leq n \leq 6$, and for $7 \leq n \leq 12$ the configuration is unstable. But Hocking was unable to show that the polygon expands at a decreasing rate, instead the polygon remains the same size and execute undamped oscillations about this position. Hocking speculated that the expansion of the regular polygon and the damped oscillations observed experimentally are due to the inertial effects which are ignored in his analysis.

Bretherton (1964) investigated this speculation by using the flow field appropiate to Oseen's flow rather than Stokes' flow. With this innovation, Bretherton was able to show that the polygon expands at a decreasing rate and the oscillations of the polygon are damped. However, the theoretical

value of the damping coefficient seems too small.

Bretherton concludes that with his analysis, which takes some account of the inertial effects, a configuration initially not too far removed from a horizontal regular polygon will relax slowly but systematically into that shape for $Re(s/r) \ll 1$ and $3 \leq n \leq 6$. But if $7 \leq n \leq 12$ this will not occur.

None of these analyses considers the case of more than 12 spheres, but as Hocking says " it is physically unlikely that the unstable configuration can change back into a stable one as the number increases".

These two theories give satisfactory qualitative agreement for the later stages of the formation of a polygon, even though the formation of the polygon in the present experiments took place mainly for higher Reynolds numbers and smaller separations than considered in these theories. But the important condition for the theoretical analyses, is that the densities of fluid and sphere should be comparable and that the spheres should move in response to the changes in the fluid velocity. In the present experiment these two conditions are satisfied. The density ratio of the sphere and that of the fluid never exceeded 1.3 and it was shown in section 2.2 B that, for at least upto Re= 4., the spheres move in response to the changes in flow.

The rotation of the spheres observed in the experiment

is again outside the theoretical considerations. Rotation is caused by the asymmetry of the flow in the two hemispheres divided by the plane parallel to the flow. This occurs only for small separations and is determined by the terms $O(r/s)^4$. For the larger separations considered in the theory, this effect is negligible.

CHAPTER 3

SEDIMENTATION OF CIRCULAR CYLINDERS.

3.1 EXPERIMENTAL ARRANGEMENT.

The experimental set up was very similar to that used with spheres. However, the dispensers had to be modified to hold the cylinder firmly. This was accomplished by using adaptors shown in fig.3.1.

These adaptors, cut from perspex rods, essentially consists of a groove on one end to hold the cylinders, and the other end shaped so as to connect securely to the tubes A and B in dispenser 1 or to the plate in dispenser 2. A hole through the axis of the adaptor connects the groove to the suction system.

The dispenser 1 modified with these adaptors could release the cylinders in any orientation, because the groove could be rotated in a vertical plane, while the tubes of the dispenser in a horizontal plane. With dispenser 2 any number of cylinders could be released but only with the axes of the cylinders restricted to a horizontal plane.

For thin cylinders heavy materials such as Duralumin (ρ_s=2.80gcm^{-3}), steel (7.84gcm^{-3}) and brass (8.31gcm^{-3}) were used. The diameters of these cylinders ranged from 0.0435 cm

FIG 3.1

Adaptor

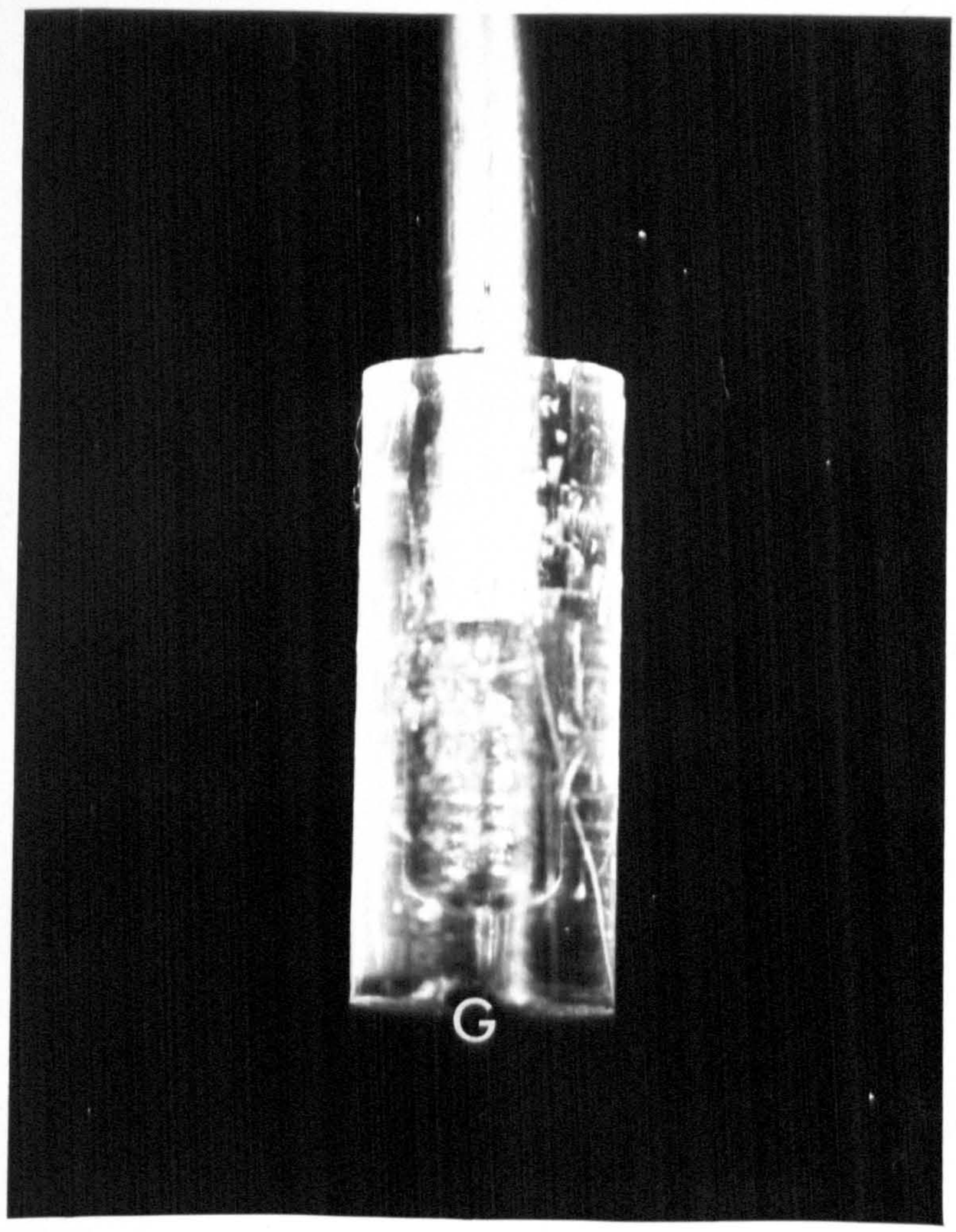

G = Groove

to 0.120 cm. With perspex or polystyrene, much higher diameters upto 0.640 cm (1/4 in.) were possible. The cylinders were cut from smooth rods of these materials and the ends were faced so as to get right circular cylinders, and made smooth by polishing.

The diameters of the cylinders were measured using a micrometer screw gauge, so that measurements could be made to three significant figures. Any cylinder with more than 0.5% variation in the diameter along the length was rejected. The length was measured either with vernier calipers or a low-power travelling microscope, so that this also could be evaluated to three significant figures. All the cylinders used have to be straight and rigid, hence the maximum permissible length was limited by the diameter and the material of the cylinder. For thin metal cylinders this length was about 8 cm, while for perspex cylinders with greater diameters, lengths as much as 15 cm were possible.

The liquids used were the same as for spheres, except that sugar solutions of concentrations as high as 49% was used. The density of this solution was 1.22 gcm^{-3} and has a kinematic viscosity of 10.2 cs at 20°C. The liquids were kept in the same tanks as mentioned in section 2.1 chapter 2. With this combination of solids and liquids, it was possible to make careful observations on cylinders ranging in Reynolds numbers defined as $Re = \frac{V_o d}{\nu}$, where V_o is the terminal velocity when falling with the long axis horizontal, d, the diameter, and ν, the kinematic

viscosity of the fluid, from less than 0.01 to about 10^3

3.2 BEHAVIOUR OF SINGLE CYLINDERS.

A Orientation and flow behind

In section 1.3 chapter 1, it was stated that for very low Reynolds numbers, a body would fall in any orientation, but as the inertial effects become prominent and depending on their geometry, bodies fall in such a way as to present the greatest resistance to motion.

For cylinders, if Re<0.01, any orientation is possible. They fall in the same attitude with which they were released, and unless the initial orientation of the axis of revolution is vertical or horizontal, the cylinders fall inclined to the vertical in the direction of this axis. With higher Reynolds numbers, the cylinders tend to orient with their axes of revolution horizontal if the diameter to length ratio d/L is less than 1, and with their axes vertical if d/L is greater than 1, and those with d/L = 1, fall in either orientation, depending upon their attitude on release. If 0.01<Re<0.1, long cylinders (L/d >5) oscillate before reaching their stable orientation, but when Re>0.1, these oscillations are heavily damped.

The type of cylinders hereafter considered in this chapter are those with L/d >5 and Re>0.01, hence the cylinders always fall with their axes of revolution horizontal.

Flow behind cylinders was observed in the same way as for spheres, and found to depend on the Reynolds number and the diameter-length ratio.

For all cylinders upto a Reynolds number of 26, no standing eddies were observed. However, as the Reynolds number increased beyond unity, the flow round the cylinder becomes increasingly asymmetrical. When the Reynolds number exceeds 26, the flow lines in the rear become reversed and give rise to two standing eddies of opposite rotation. In this case, as for spheres, the Reynolds number for which eddies are visible, is much higher than that observed or predicted by previous workers.

For a long cylinder, these two eddies rise from either side along the length of the cylinder leaving a wavy flat streak behind. Fig. 3.2 shows this wavy streak as seen from the direction along the length of the cylinder. For a shorter cylinder, the flow past the ends give rise to a three-dimensional circulation which is pyramidal rather than cylindrical in shape as shown in fig. 3.3 a and b. The flat streak behind a long cylinder becomes thinner and less wavy as the length decreases until, when the pyramidal flow occurs, a thin straight streak is formed. On further reducing the length, two separated streaks as shown in fig. 3.3b are formed. The separation between these two streaks is greater when the cylinders are short.

When the Reynolds number exceeds 50, eddies separate from the surface of the cylinder, and are shed as Karman vortex

FIG 3.2

Flow behind a long circular cylinder, $26 < Re < 50$

(Perspex, d = 1/8", L = 6.0 cm. Re = 39.5)

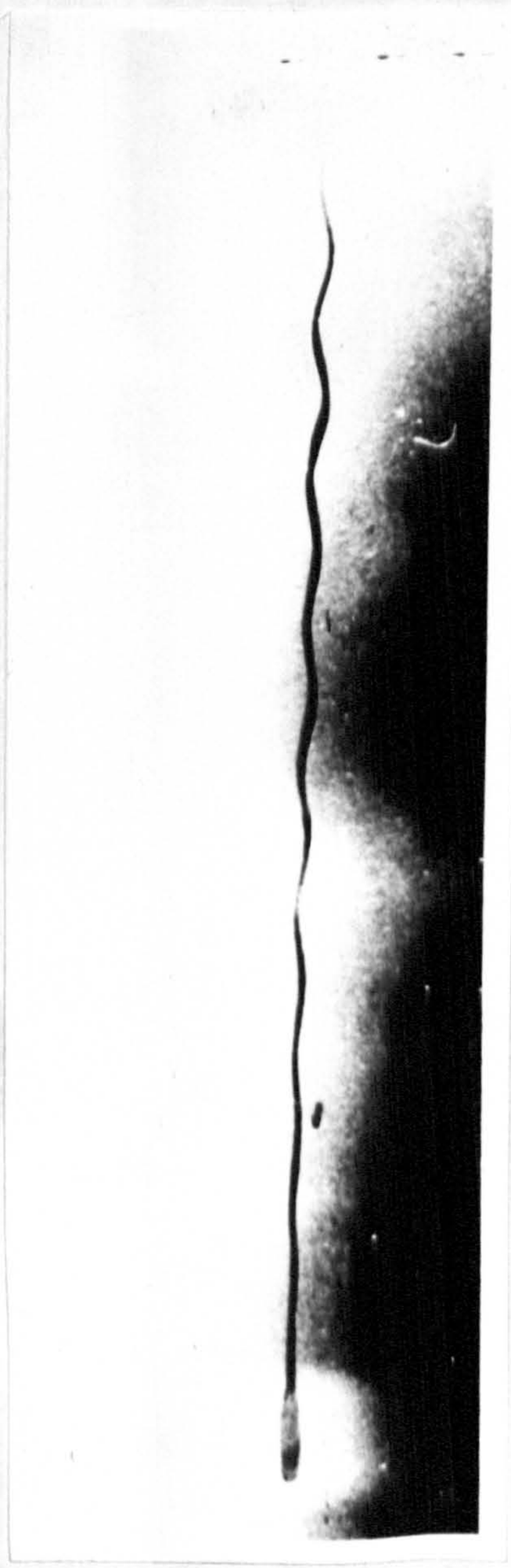

End-on view

FIG 3.3

Flow behind a short circular cylinder, $26 < Re < 50$

(Perspex, d = 1/8"; L = 2.0 cm. Re = 39.5)

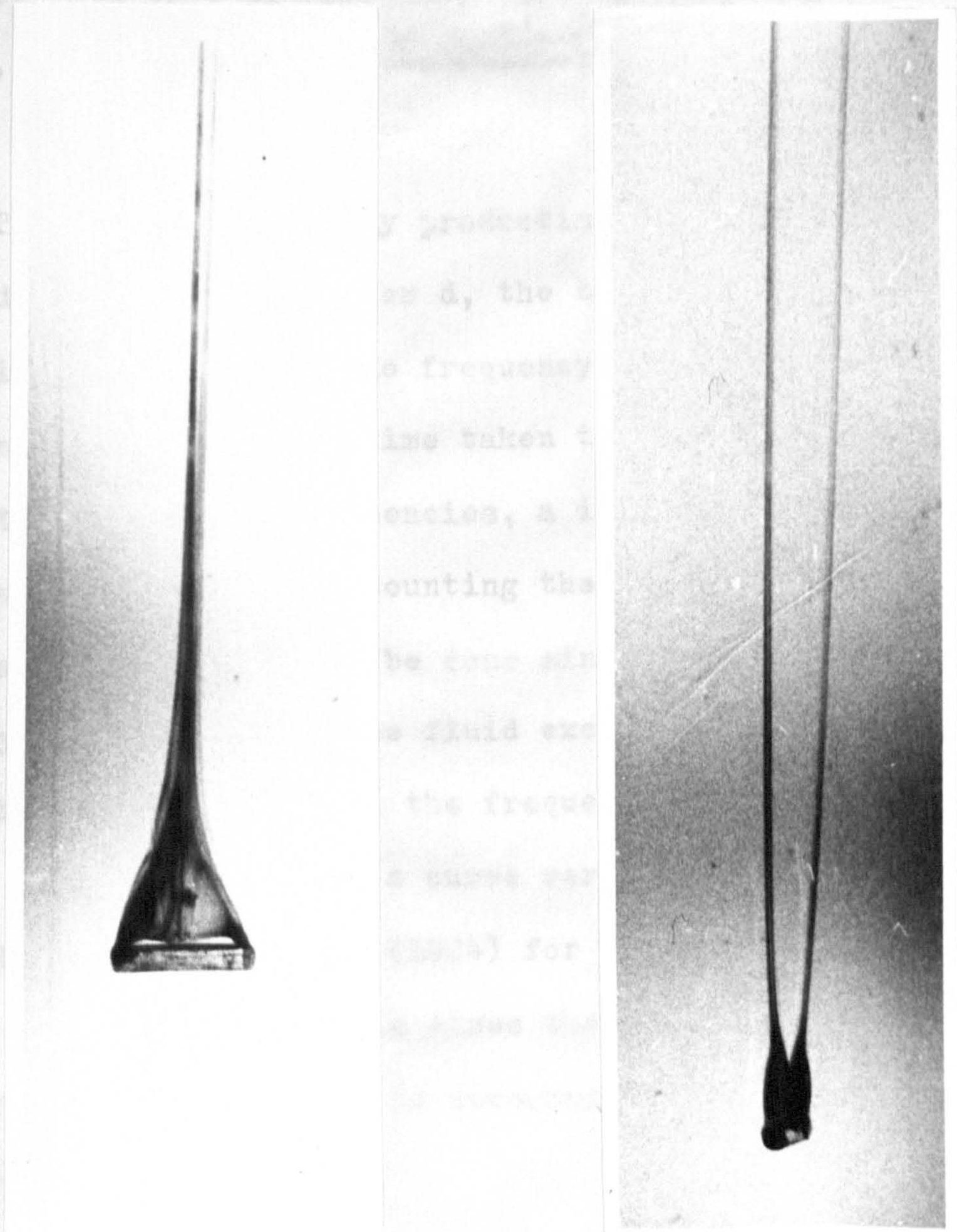

(a) Broad - side view

(b) End - on view

streets. For a long cylindor, vortices are shed regularly and alternately from the opposite sides and two sets of regularly spaced, expanding vortex rings of opposite rotation are formed along its trail as shown in fig. 3.4. This observation agrees fairly well with that of Kovasznay (1949), who using a hot wire technique, detected periodic ~~observation~~ oscillations behind a cylinder at $Re > 40$.

The frequency of eddy production was measured and found to depend on the diameter d, the terminal velocity V_o, and the Reynolds number Re. If the frequency of shedding is low, it is measured directly by the time taken to shed a given number of rings, while for higher frequencies, a indirect method of photographing the rings and counting the number in a given length, was used. This could be done since the rings remained stationary with respect to the fluid except for their expansion. Knowing the velocity of fall, the frequency could be calculated. A plot of $\frac{Nd}{V_o}$ against Re gave a curve very similar to that obtained by Relf and Simmons (1924) for ventilated stationary cylinders (see fig. 3.5). This shows that in this regime, the fall in the drag coefficient is accompanied by a rise in the vortex frequency.

/For shorter cylinders eddies of comparable strength break away from the edges as well as from the sides. This gives rise to a flutter of the cylinder about a horizontal axis through the centre and normal to its length. The amplitude of

FIG 3.4

Shedding of eddies by a circular cylinder, Re > 50

(Perspex, d = 3/16", L = 6.0 cm. Re = 73.2)

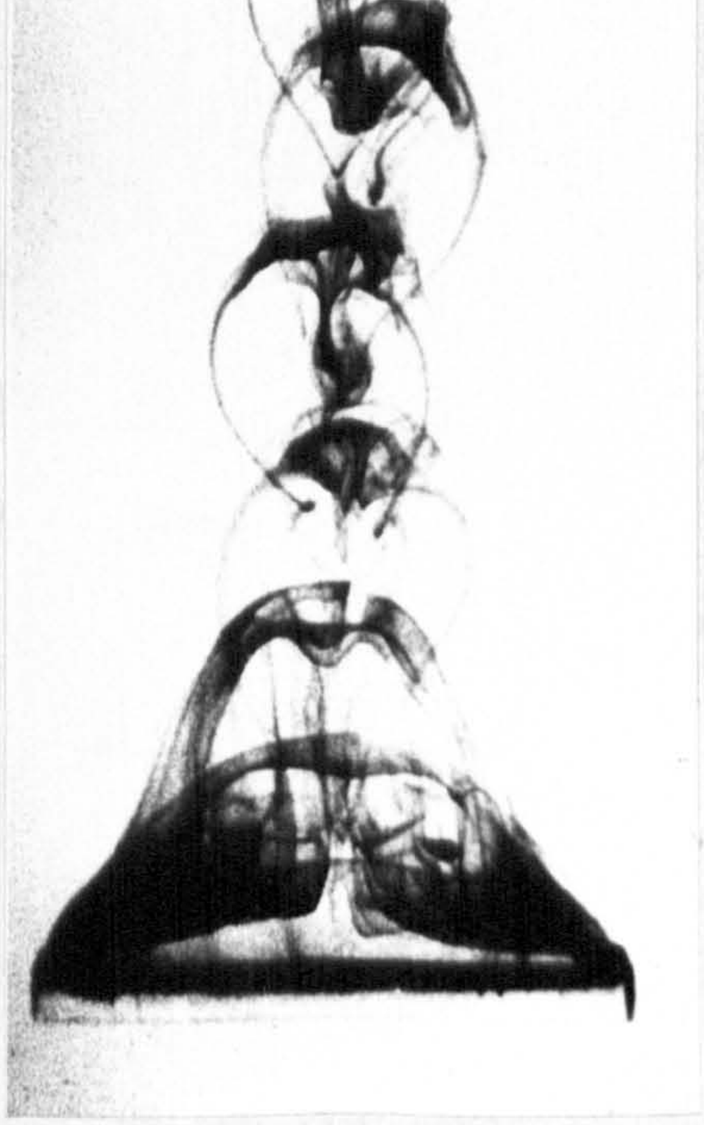

(a)

Broad - side view

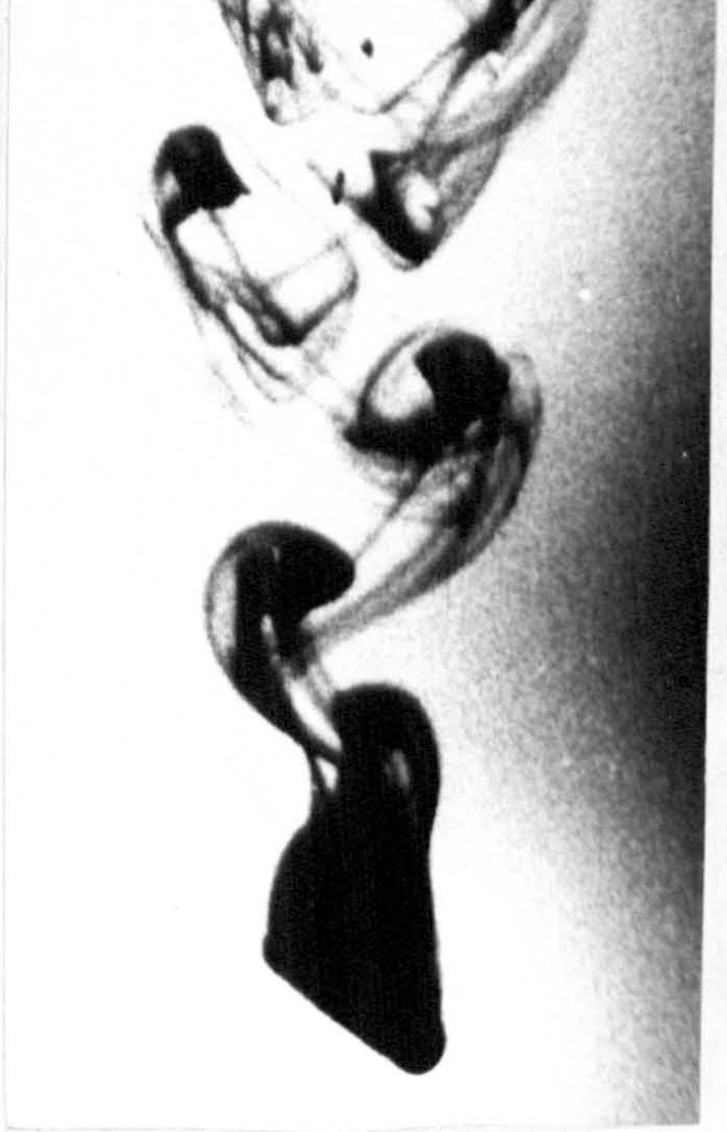

(b)

End - on view

Fig. 3.5 Rate of generation of eddies

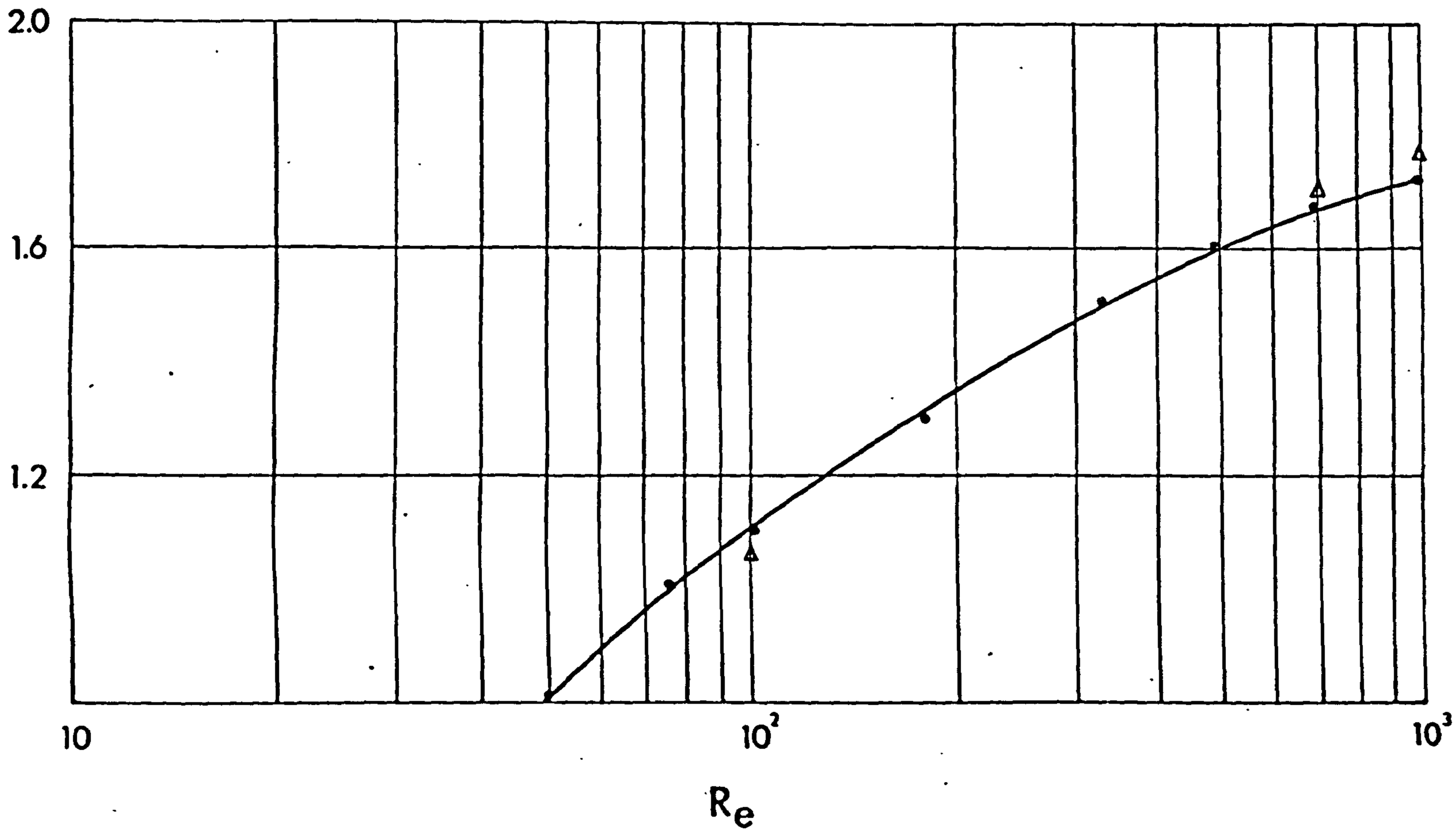

oscillations is comparatively large for shorter cylinders, but decrease progressively as the length increases, and the cylinder falls stably.

The transition from the fluttering motion to steady motion is not abrupt, the observations of fig. 3.6 allow a fairly definite boundary to be drawn between the two regimes. Different boundary curves, when d/L is plotted against Re occurs for different materials and it was not possible to find a suitable parameter to fit these different curves together. In fig. 3.6, two such curves are drawn for steel and perspex cylinders. For clarity individual observations for steady, persistant fluttering, and heavily damped fluttering are drawn only for steel. In both cases the influence of d/L for transition from steady to fluttering motion decrease as Reynolds number increases. On the lower Reynolds number side, both boundary curves are asymptotic to Re=50, the Reynolds number for which vortices are shed, and on the higher Reynolds number side, it shows that if $L > 25d$, whatever the Reynolds number, the cylinder would fall stably. Thus for lengths greater than 25 diameters, the flow round the edges has no effect on the behaviour of the cylinder for all Reynolds numbers considered.

Long cylinders with $Re > 50$, which fall stably with the long axis horizontal, showed a small oscillation about this axis due to shedding of eddies from the opposite sides of the cylinder but unlike the case of spheres, this did not cause the cylinders

Fig. 3.6 Transition from steady to unsteady motion of cylinders

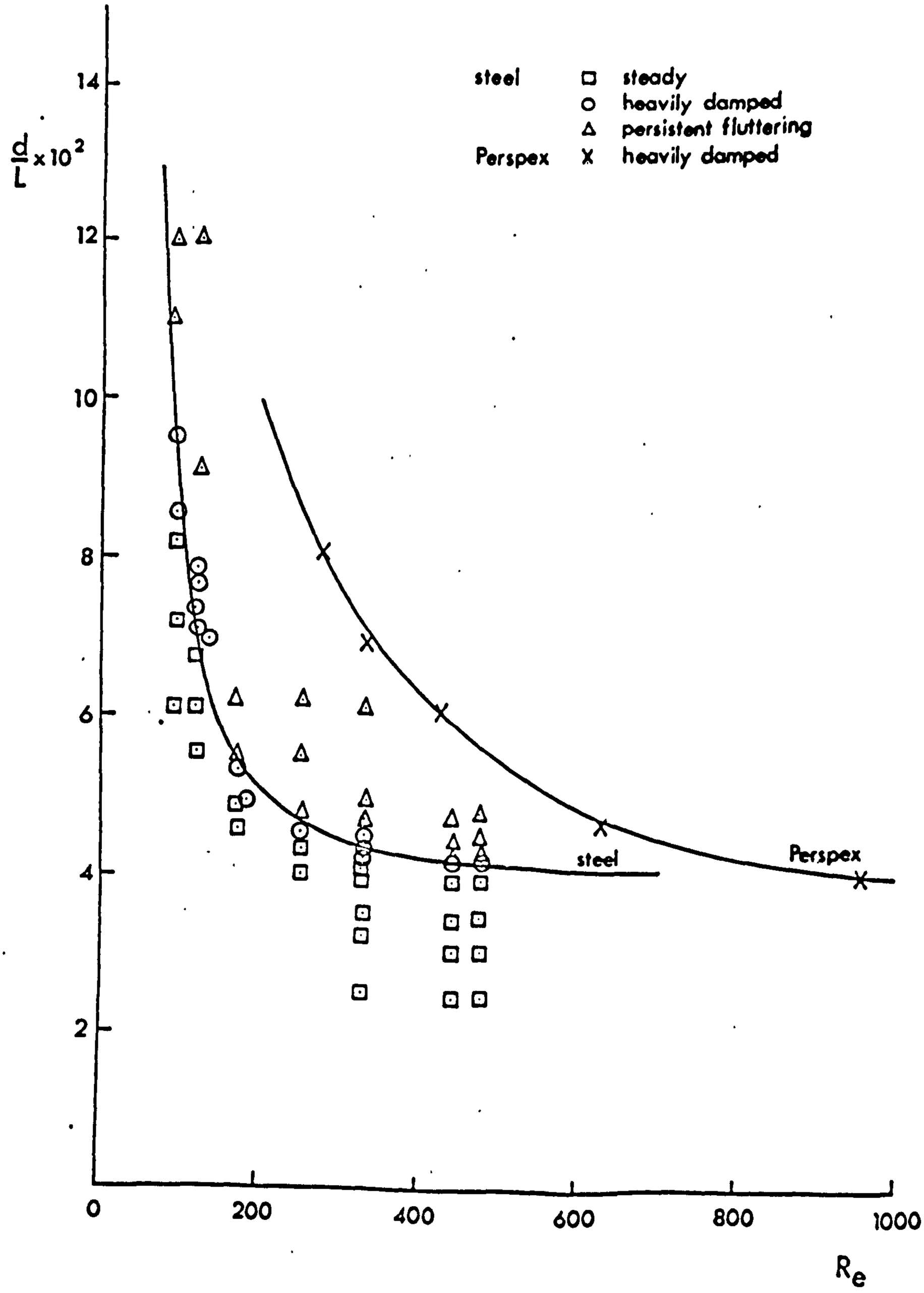

to deviate from a vertical path. Short fluttering cylinders showed a slow spin about the vertical axis (about 1/2 revolution in 40 cm fall). The spin is not smooth and the direction arbitrary. A possible cause for this spin could be the separation of the eddies from the edges.

B Terminal velocity of fall and the drag coefficients.

For a cylinder of length L, and diameter d, falling with its long axis horizontal at terminal velocity V through a viscous fluid, the drag coefficient C_D could be calculated by equating the drag forces to the net weight of the cylinder as

$$\frac{\pi d^2}{4} L (\rho_s - \rho_f) g = \frac{1}{2} C_D \rho_f V^2 dL$$

giving $$C_D = \frac{\pi}{2} \frac{d}{V^2} \frac{\rho_s - \rho_f}{\rho_f} g \qquad \ldots\ldots\ldots\ldots \quad 3.2.1$$

The terminal velocity of fall was measured for cylinders of different diameters and lengths. For a particular diameter at low Reynolds numbers, the velocity of fall in a given fluid increases smoothly with length to reach a nearly constant value at large lengths (see fig. 3.7). For $Re_{\frac{d}{L} \to 0} < 0.3$, this maximum constant value is reached for L/d ~100, corresponding to about 6 cm of the cylinders used. But as $Re_{\frac{d}{L} \to 0}$ increases, the L/d ratio to obtain this maximum velocity decreases to about 5 for Re =1.

For long cylinders, the terminal velocity is determined only by the drag per unit length of the cylinder, hence is

Fig. 3.7 Velocity as a function of length

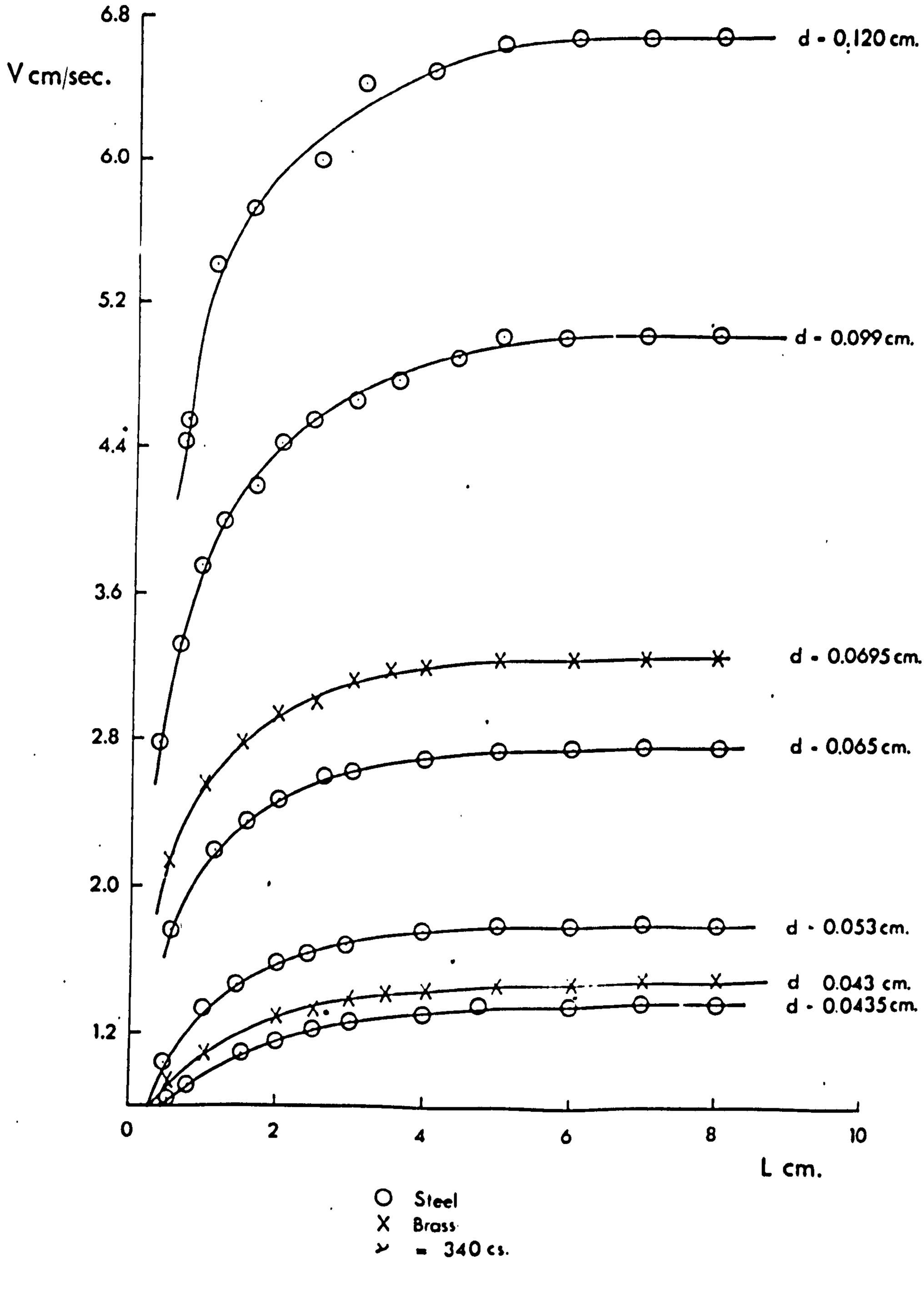

independent of length. The decrease in velocity as the length decreases can be attributed to the drag caused by the ends being comparable to the drag on the curved surface of the cylinder. The present results show that this end-effects decreases as the Reynolds number increases; but for low Re<0.3, this effect exists for lengths as large as 100 diameters.

Since the dimensions of the tank is 30 cm x 30 cm, the effect of the walls on the velocity of fall of long cylinders cannot be neglected; for when R_e<0.3 a length as much as 6 cm was necessary to attain the maximum velocity. But since the wall effects decrease with the Reynolds number and further since the maximum velocity is reached for smaller lengths, the wall effects are negligible for Re>0.5. Anyway for Re>1, even for long cylinders, the wall effects can be neglected.

The effect of walls parallel to the long axis of the moving cylinder is negligible in these experiments. Takaisi (1955) investigated this effect theoretically for an infinite cylinder with Reynolds numbers in the Lamb's regime. The ratio of the diameter of the cylinder to the distance between the walls in the present experiments never exceeded 0.005, making Takaisi's correction factor to Lamb's formula negligible.

To evaluate the correction due to the walls on the velocity of fall of a long cylinder, Brenner's (1962) theoretical expression for the effect of boundaries on the Stokes' resistance

of a particle was used. This expression mentioned in section 1.2 chapter 1, is as

$$F = \frac{F_\infty}{1 - k \frac{F_\infty}{6\pi\eta V D} + O\left(\frac{L}{D}\right)^3} \quad \ldots\ldots\ldots \quad (3.2.2)$$

where D is the distance between the walls and k=2.1

If a cylinder falls at terminal velocity V_∞ in an infinite fluid and at velocity V in a bounded fluid of the same dynamic viscosity η, the drag F is the same in both cases, being equal to the effective weight.

Thus

$$F = \frac{1}{2}\eta C_{D_\infty} Re_\infty V_\infty L = \frac{1}{2}\eta C_D Re\, VL \quad \ldots\ldots\ldots (3.2.3)$$

where the subscripts refers to an infinite fluid.

Hence

$$\frac{V_\infty}{V} = \frac{C_D\ Re}{C_{D_\infty} Re_\infty} \quad \ldots\ldots\ldots\ldots\ldots \quad (3.2.4)$$

If F_∞ is the drag on a cylinder of the same length moving in an infinite fluid with velocity V, then C_{D_∞} and Re_∞ take new values such that

$$F_\infty = \tfrac{1}{2}\eta C'_{D_\infty} R'_{e_\infty} VL \quad \ldots\ldots\ldots \quad (3.2.5)$$

Using (3.2.3), (3.25) and (3.2.2) we have

$$\frac{C_D R_e}{C'_{D_\infty} R'_{e_\infty}} = \frac{F}{F_\infty} \quad \ldots\ldots \quad (3.2.6)$$

and from (3.2.4)

$$\frac{V_\infty}{V} = \frac{C'_{D_\infty} R'_{e_\infty}}{C_D\ R_e} \cdot \frac{F}{F_\infty}$$

For small Re and since V_∞ is not very different from V Lamb's

expression

$$\left[C_{D\infty}\, Re_{\infty}\right]_{\frac{d}{L}\to 0} = \frac{8\pi}{\frac{1}{2} - \gamma - \log_e \frac{Re_\infty}{8}} \qquad \ldots\ldots\ldots (3.2.7)$$

allows us to write

$$C'_{D\infty}\, Re'_{\infty} \simeq C_{D\infty}\, Re_{\infty}$$

Hence $$\frac{V_\infty}{V} = \frac{F}{F_\infty} = \frac{1}{1 - 2.1\frac{F}{6\pi\eta V_\infty L} + O\left(\frac{L}{D}\right)^3} \qquad \ldots\ldots\ldots (3.2.3)$$

Neglecting the $O(L/D)^3$ term and substituting for F using the Lamb's expression

$$F = \frac{4\pi\eta V_\infty L}{\frac{1}{2} - \gamma - \log_e \frac{Re_\infty}{8}}$$

we get

$$\frac{V_\infty}{V} = \frac{1}{1 - \frac{2}{3}\times 2.1 \frac{1}{\frac{1}{2} - \gamma - \log_e \frac{Re_\infty}{8}}\left(\frac{L}{D}\right)} = \frac{1}{\alpha}\,(say) \ldots\ldots (3.2.9)$$

Hence the ratios of drag coefficients and the Reynolds numbers for a bounded and unbounded fluid is as

$$C_D / C_{D\infty} = 1/\alpha^2 \qquad \ldots\ldots (3.2.10)$$

and

$$Re / Re_\infty = \alpha \qquad \ldots\ldots (3.2.11)$$

For $Re < 0.3$, the experimental values for C_D and Re was corrected for wall effects on the longest cylinders, using the equations (3.2.10) and (3.2.11), and so produce their corresponding values in an infinite fluid. These corrected values for $10^{-2} < Re < 0.3$, appear in table 3.1, showing close agreement with the values calculated using Lamb's formula.

These results also appear with other values upto Re=1, in fig. 3.8, where the theoretical curve of Lamb and the experimental results of Finn (1953), Wieselsberger (1922) and

TABLE 3.1

Wall effect correction for the drag coefficient and Reynolds number for a freely falling circular cylinder, for Re < 0.3.

C_D	Re	C_{D_∞}	Re_∞	C_{D_∞} from Lamb
34 ± 1	0.24 ±0.01	28	0.27	28.5
50 ± 1	0.15 ±0.01	43.5	0.16	43.0
115 ± 3	0.053±0.005	97	0.055	95.0
195 ± 6	0.028±0.002	160	0.030	153.0
280 ± 9	0.018±0.001	236	0.019	225.0
85 ± 2	0.075±0.005	71	0.081	69.0
250 ± 8	0.022±0.001	200	0.023	195.0

Fig. 3.8 Drag coefficients for $10^{-2} < R_e < 1$

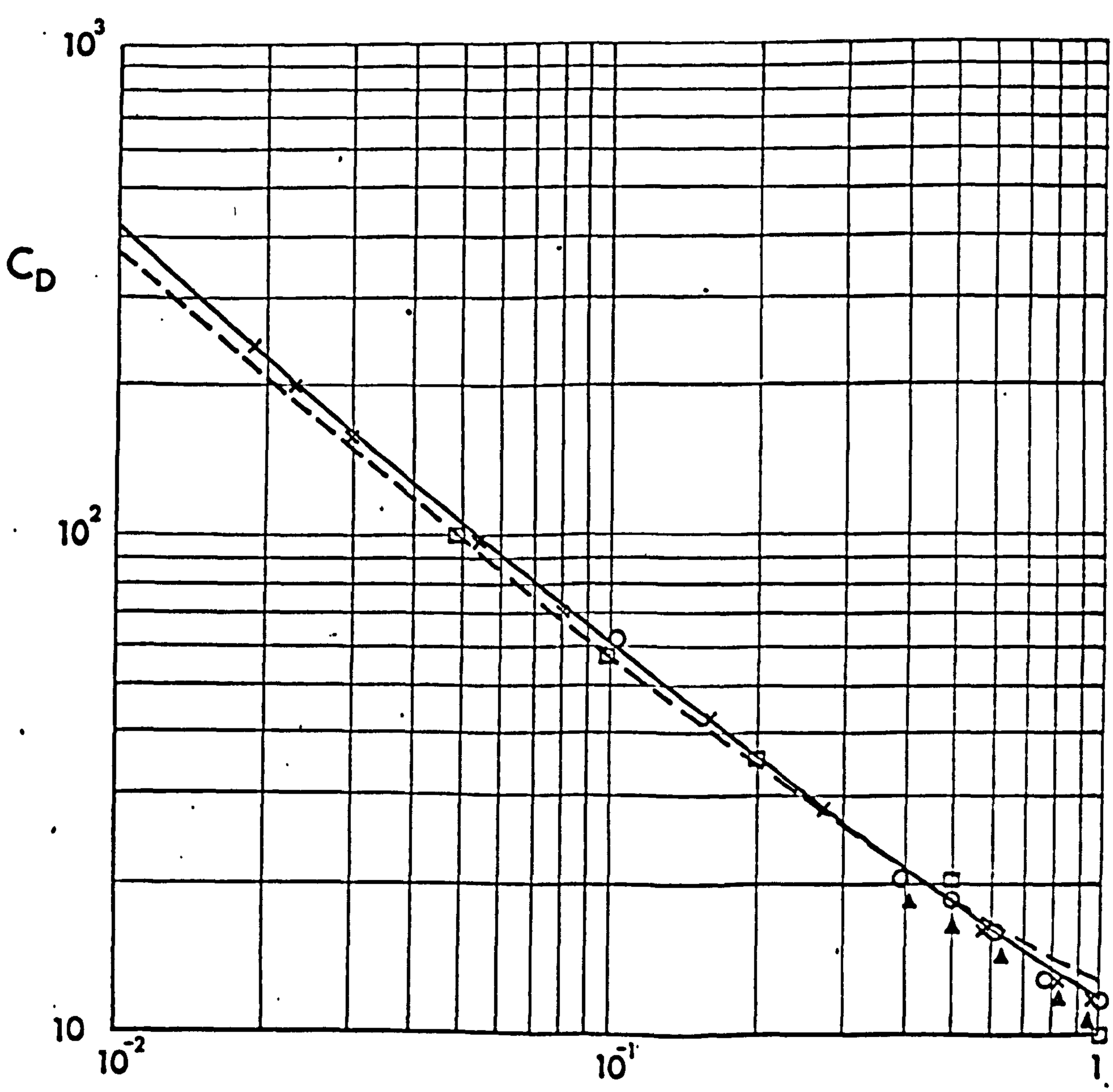

Tritton (1959) are plotted for comparison. The experimental values of the drag coefficients deviate progressively from Lamb's formula when Reynolds number increases beyond 0.4. An alternate formula derived by Burgers (1938), Davies (1947) and Broersma (1960) for the Stokes resistance for a long cylinder falling in an infinite fluid, from Gans-Oberbeck expression for a prolate ellipsoid, viz,

$$F = \frac{4\pi\eta V_\infty L}{\log_e \frac{2L}{d} + 0.5 + O(\frac{d}{L})^3} \quad \ldots\ldots\ldots (3.2.12a)$$

or

$$C_{D_\infty} R_{e_\infty} = \frac{8\pi}{\log_e \frac{2L}{d} + 0.5} \quad \ldots\ldots\ldots (3.2.12b)$$

gives much poorer agreement with the experimental results than does Lamb's formula for these Reynolds numbers. The limit for Burgers' formula could be placed at Re = 0.05 within the limits of the present experimental accuracy. However, deviation is apparent beyond Re~0.01. Indeed Burgers' formula implies that, for a fixed L/d, C_D Re = constant, and experimentally this is certainly not the case.

The discrepancies are apparent in fig. 3.9 where the two extreme curves of fig. 3.7 are compared with values computed from both the Burgers' and Lamb's formulae as corrected for wall effects from equation (3.2.2). The agreement for long thin cylinders is good in all three cases at Re=0.02, but at Re=0.24, the Burgers' formula gives velocities that are 50% too high.

In fig. 3.10, the present values of the drag coefficient for $1<Re<10^3$ are compared with those of Rolf (1913), Wieselsberger

Fig. 3.9 Velocity of fall compared with Lamb and Burgers' formulae

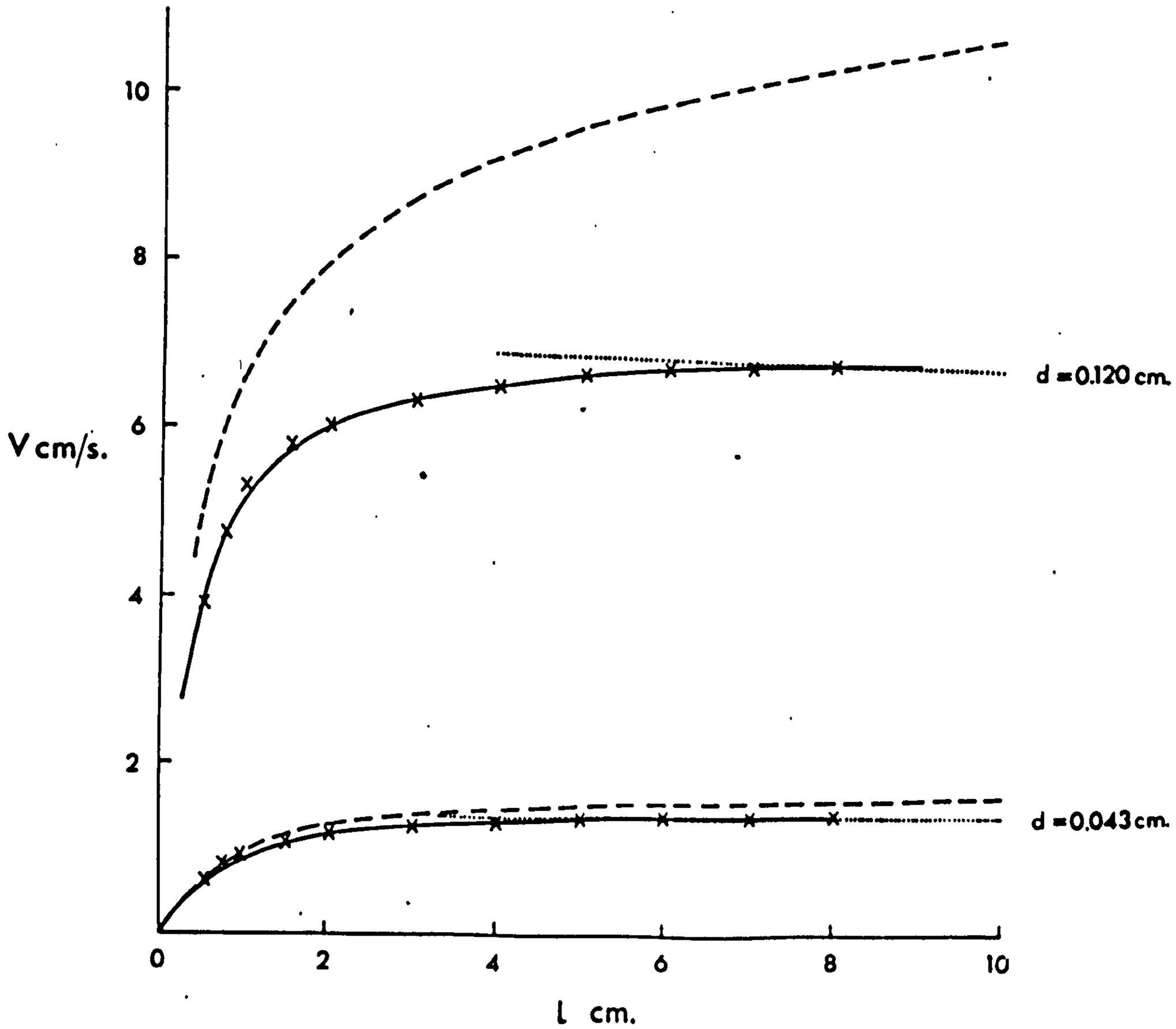

Fig. 3.10 Drag coefficients for $1 < R_e < 10^3$

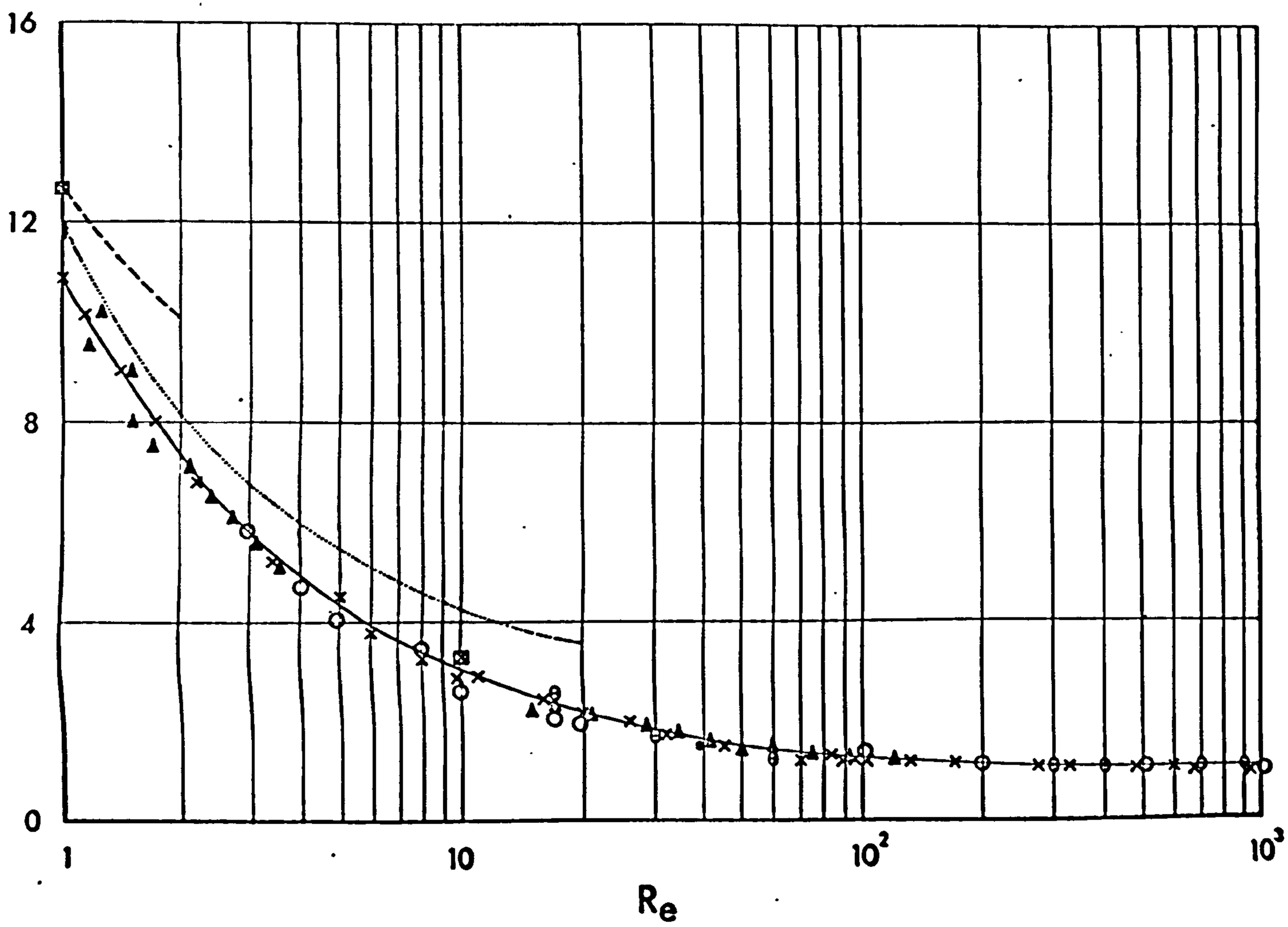

Theoretical
- ––– Lamb
- ..... Bairstow et al, Tomotika & Aoi
- ⊠ Allen & Southwell
- • Kawaguti

Experimental
- x Present values
- ▲ Tritton
- o Weiselsberger
- θ Relf

(1922) and Tritton (1959). The agreement between all these values are quite impressive but they all give values lower than the theoretical values obtained using Oseen's approximation. However good agreement exist with the values from relaxation methods of Allen and Southwell (1955) for Re=1 and 10.

The decrease of velocity as length decreases was attributed to the end effects . For Re<0.3, this effect exists for L~100d. (See fig. 3.7). No theoretical formula exist for the drag coefficient of cylinders when the length becomes comparable to the diameter. Burger's formula which takes into account this factor proves inadequate for Re>0.05.

However, with the present results, an empirical formula can be suggested to take into account the end effects when Re<0.3, of the form

$$V'_\infty = \frac{V_\infty}{1 + \frac{1.2}{Re_\infty^{0.6}} \left(\frac{d}{L}\right)} \qquad \text{.....(3.2.13)}$$

where V'_∞ refers to the velocity of a finite cylinder in an infinite fluid.

Combining this equation with equation (3.2.9), the velocity V for a finite cylinder in a bounded fluid is given by

$$V = V_\infty \frac{1 - \frac{2}{3} k \frac{1}{\frac{1}{2} - \gamma - \log_e \frac{Re_\infty}{8}} \left(\frac{L}{D}\right)}{1 + \frac{1.2}{Re_\infty^{0.6}} \left(\frac{d}{L}\right)} \qquad \text{.....(3.2.14)}$$

or in terms of $C_D Re$ this leads to

$$C_D Re = C_{D\infty} Re_\infty \frac{1 + \frac{1.2}{Re_\infty^{0.6}} \left(\frac{d}{L}\right)}{1 - \frac{2}{3} k \frac{1}{\frac{1}{2} - \gamma - \log_e \frac{Re_\infty}{8}} \left(\frac{L}{D}\right)}$$

$$= \frac{8\pi}{\frac{1}{2} - \gamma - \log_e \frac{Re_\infty}{8}} \frac{1 + \frac{1.2}{Re_\infty^{0.6}} \left(\frac{d}{L}\right)}{1 - \frac{2}{3} k \frac{1}{\frac{1}{2} - \gamma - \log_e \frac{Re_\infty}{8}} \left(\frac{L}{D}\right)}$$

for $10^{-2} < Re < 0.3$ and $\frac{L}{D} < 0.3$

The empirical formula for the velocity (3.2.14) is plotted in fig. 3.11, for comparison with the experimental results. The continuous line refers to the formula, while 'X' indicates the experimental values. The agreement is impressive for L<5 cm, but for greater lengths, the theoretical formula gives smaller velocities than the experiment. This discrepancy increases for higher Reynolds numbers of the cylinders. For Re= 0.23, a discrepancy of about 5% exists for L=6 cm. This means that at high Reynolds numbers, the end correction term does not decrease fast enough as length increases to make the end effects negligible for L>100d. For Re<0.1, this formula fits very well with the experimental values for all lengths L>5d.

The formula (3.2.14) could be used to explain the discrepancy between a set of White's (1946) experimental results and Lamb's theoretical formula (3.2.7). White found that for two identical steel cylinders, the velocities of fall in two glycerine solutions of viscocities 6 and 13 poise in identical cylindrical containers were inversely proportional to the dynamic viscocities.

Fig 3.11 Velocity of fall compared with the empirical formula.

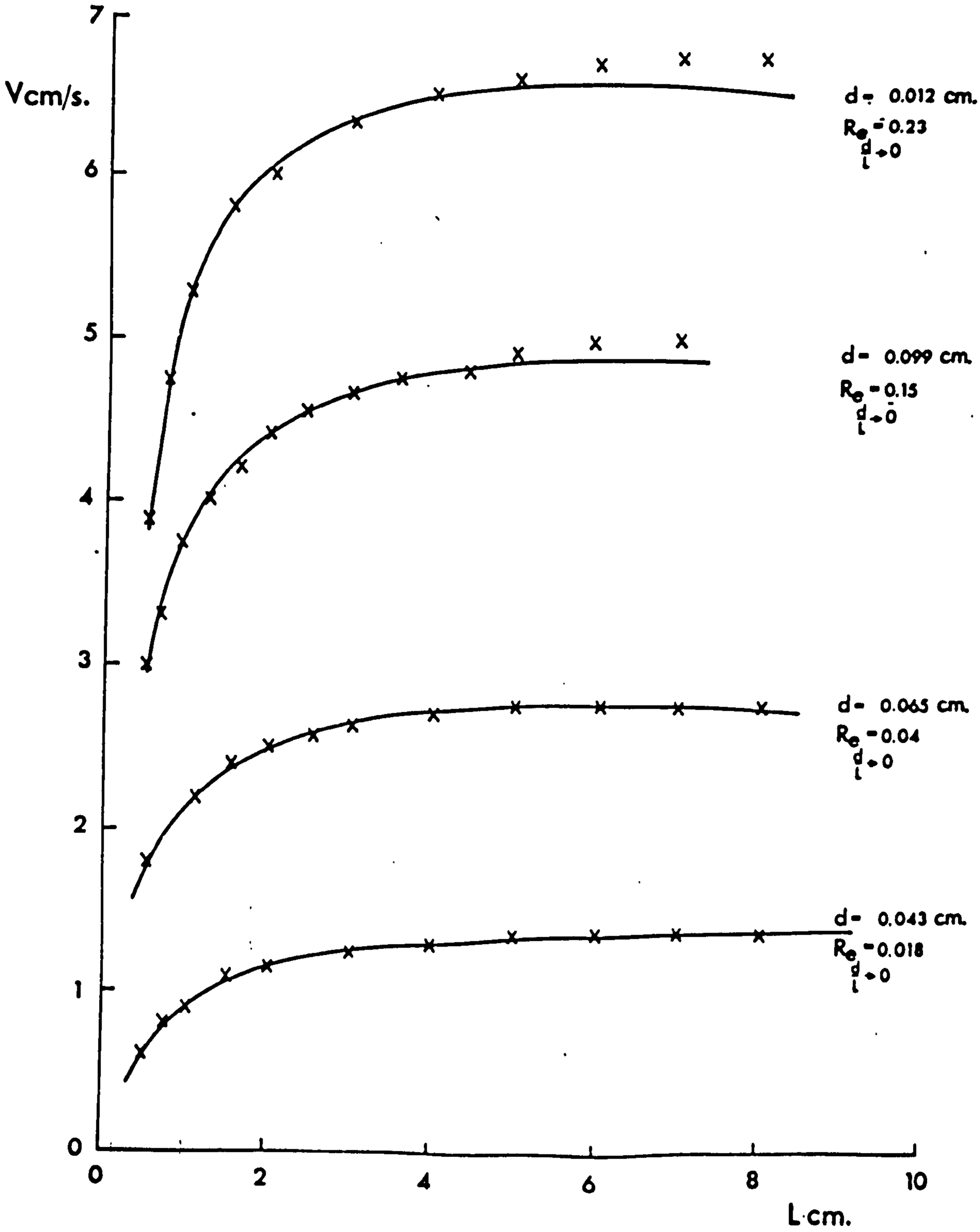

Since the product $C_D Re$ is proportional to $V\eta$, White's results show that for the two Reynolds numbers in the two cases, $C_D Re$ is the same. But White goes on further, assuming that since he used the same cylinder in identical containers the end and wall effects should be the same, to conclude that in the general case of a long cylinder falling in an infinite fluid the product $C_D Re$ is independent of the Reynolds number. Since the Reynolds numbers in White's experiments are ~ 0.1, this conclusion is in direct conflict with Lamb's formula.

The error in White's conclusion lies in his assumption that the end effects in the two cases are equal. The equation (3.2.14) was applied to White's results and it was found that the velocities in the two cases turn out to be equal within 2% , which is well within White's experimental accuracy. The end effects decrease with Re in such a way as to make the product $C_D Re$ a constant for the two cases but in no way contradicts Lamb's formula.

C Conclusion

From the present experimental results it could be concluded that for $Re < 0.3$, Lamb's formula could be used to determine the terminal velocity for long cylinders ($L > 100d$), falling freely in a viscous medium. However, if the distance between the bounding walls of the medium is comparable with the length of the cylinder, a wall correction has to be applied,

using Brenner's expression.

For higher Reynolds numbers greater than 1, the wall effects are negligible as the present results agree very well with those of previous workers.

When the diameter of the cylinder becomes comparable with the length, and if the Reynolds number is within the validity of Lamb's formula, a empirical correction factor could be introduced to Lamb's formula. This correction factor decreases with the Reynolds number, but does not decrease fast enough with length to make the end effects negligible for L>100d.

The present experimental results limits the validity of Burgess' formula ~~for~~ to Re<0.01, showing that for higher Reynolds numbers the cylinder no longer falls in a pure viscous regime. This is in agreement with the observations on orientation where for Re>0.01, the inertial forces become appreciable to make the cylinder move in a preferred orientation.

3.3 BEHAVOUR OF TWO THIN LONG IDENTICAL CYLINDERS

Two equal long cylinders interact with each other in all directions, extending upto 100 diameters when released vertically one behind the other. Their behaviour was determined largely by their relative positions on being released into the tank. But in all cases the ultimate effect is for the two cylinders either to fall separated but parallel to each other or together crossed at

the centre right angles to each other. The behaviour was found to be independent of the Reynolds number upto that in which vortex rings are shed. However detailed observations are made only for $0.01<Re<1$.

A Released simultaneously in the same horizontal plane

(a) Long axes parallel

The two cylinders rotate inwards and separate horizontally as they fall but still remain parallel to each other (See fig. 3.12 photograph 1). In this respect they behave very much like spheres (See section 2.2A chapter 2), in that the separation and rotation decrease as the separation increases. However, the maximum separation was very much larger in the case of cylinders, that they were found to separate right along the fall. Hence it was not possible to estimate the maximum separation as the influence of the walls at these separation ~~are~~ is quite appreciable.

(b) Long axes crossed

Whatever the initial position of the two axes as long as they are crossed, they slide relative to each other and attain a stable position in which they bisect each other at right angles. The two cylinders were released with angles between the axes as low as 30°, and crossing each other at various points. Photographs taken in a horizontal plane from the bottom of the tank after a 50 cm fall, showed that for all cases the two cylinders fall

FIG 3.12

Final configuration for two and three equal cylinders

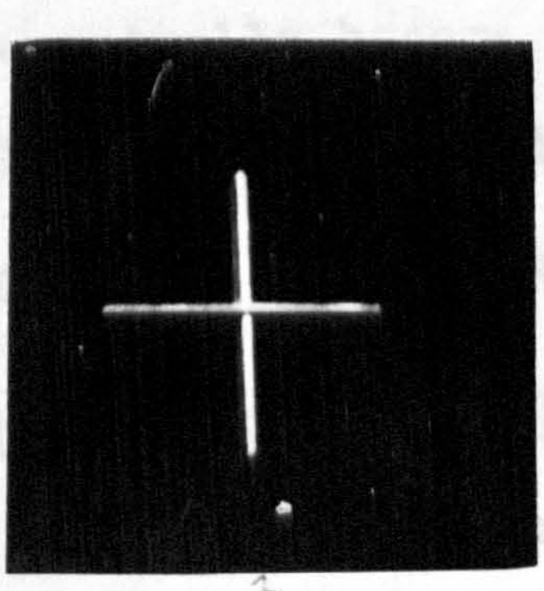

2

Steel d=1.2 mm. L=3.0 cm.

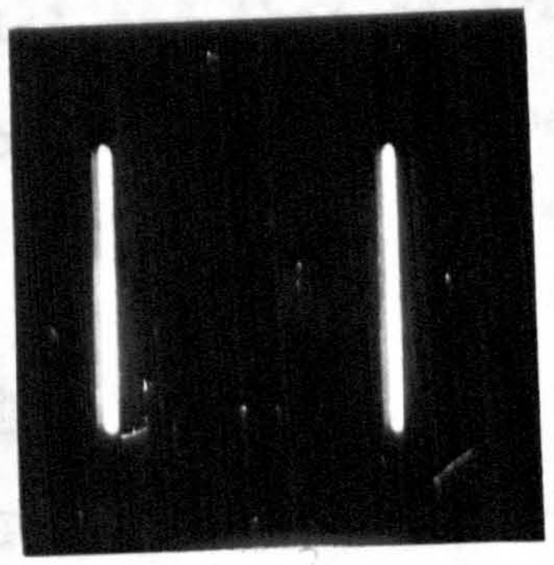

1

d=1.2 mm. L=3.0 cm.

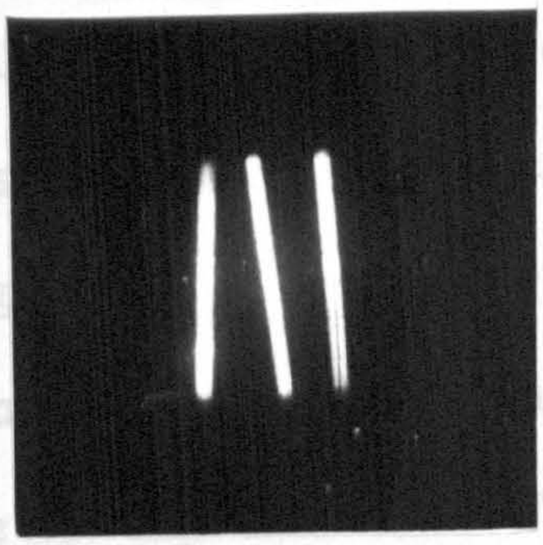

3

Steel d=1.2 mm. L=3.0 cm.

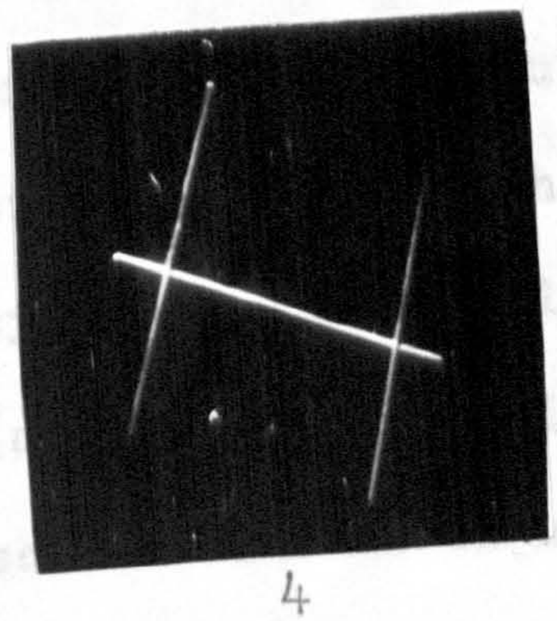

4

d=0.63 mm. L=6.0 cm.

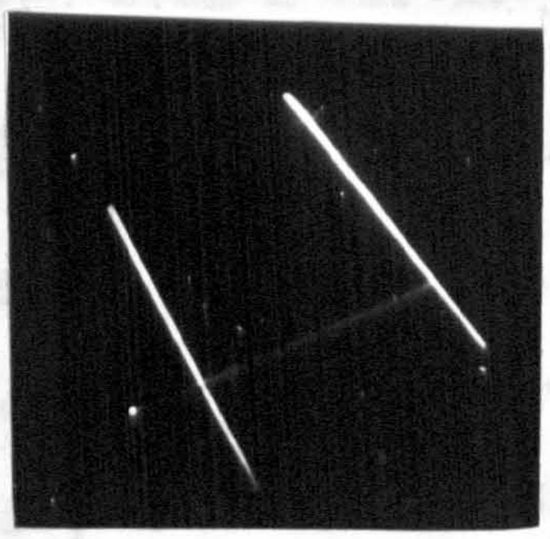

5

Steel d=0.63 mm. L=6.0 cm.

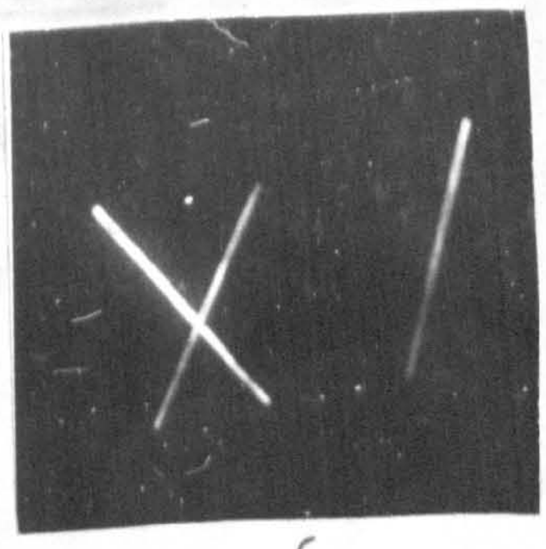

6

d=0.63 mm. L=6.0 cm.

stably and are bisected at right angles (See fig.3.12 photograph 2). This stable configuration is attained more rapidly at higher Reynolds numbers.

(c) Separated but not parallel.

The two cylinders flutter as they fall, with decreasing amplitude, and eventually become parallel and then separate as in (a) above. Simultaneous release is important in this experiment, otherwise the cylinders tend to become crossed.

(d) In line and separated along the common axis.

In this case, two distinct types of behaviour are observed. If $R_e>0.1$, the cylinders continue to separate but preserve their initial orientation. If $R_e<0.1$, the cylinders tilt in the vertical plane towards each other and flutter about a horizontal axis. The oscillations of both cylinders which are 180° out of phase, gradually decrease, the cylinders eventually become parallel and then separate as in case (a). The final position is attained more rapidly and with fewer oscillations at higher Reynolds numbers.

B Released with a vertical separation.

(a) Parallel and directly one behind the other.

As ~~Like~~ in the case of spheres wake capture exists but for much greater separations. The trailing cylinder catches the leader, rotates round it, and when the line of centres become horizontal, they separate and fall as in A(a). The two cylinders always keep

their axes parallel to each other.

The velocity of approach was calculated by measuring the separation at successive intervals of time during the fall, using the same photographic technique as for spheres. The velocity of approach thus calculated is plotted as a function of separation shown in fig.3.13. Whereas for spheres the approach velocity decreases slowly to reach zero at large separations, with cylinders it drops sharply from a maximum value at separations of about 30 diameters, to zero at about 80 diameters.

The same experiment was conducted with unequal cylinders. When the trailing cylinder is shorter and has a lower terminal velocity than the leader, it may catch the leader only if the difference in the terminal velocities is less than the maximum approach velocity for a pair of identical cylinders. Just as in the case of spheres, the trailing cylinder, in addition to its own terminal velocity, acquires the velocity of the fluid dragged by the leading cylinder. This linear superposition of the velocities of the cylinder and the fluid occurs in all cases irrespective of whether the trailing cylinder catches the leader or not.

When the trailing cylinder is longer than the leader, and if the difference in the terminal velocities could cause capture, the trailing cylinder tends to flutter before it overtakes the leader, but remain in the vertical plane common to both cylinders.

In the region swept out by the cross-sectional area of the cylinder, the flow could be regarded to be the same along any

Fig 3.13 Wake capture of two equal cylinders

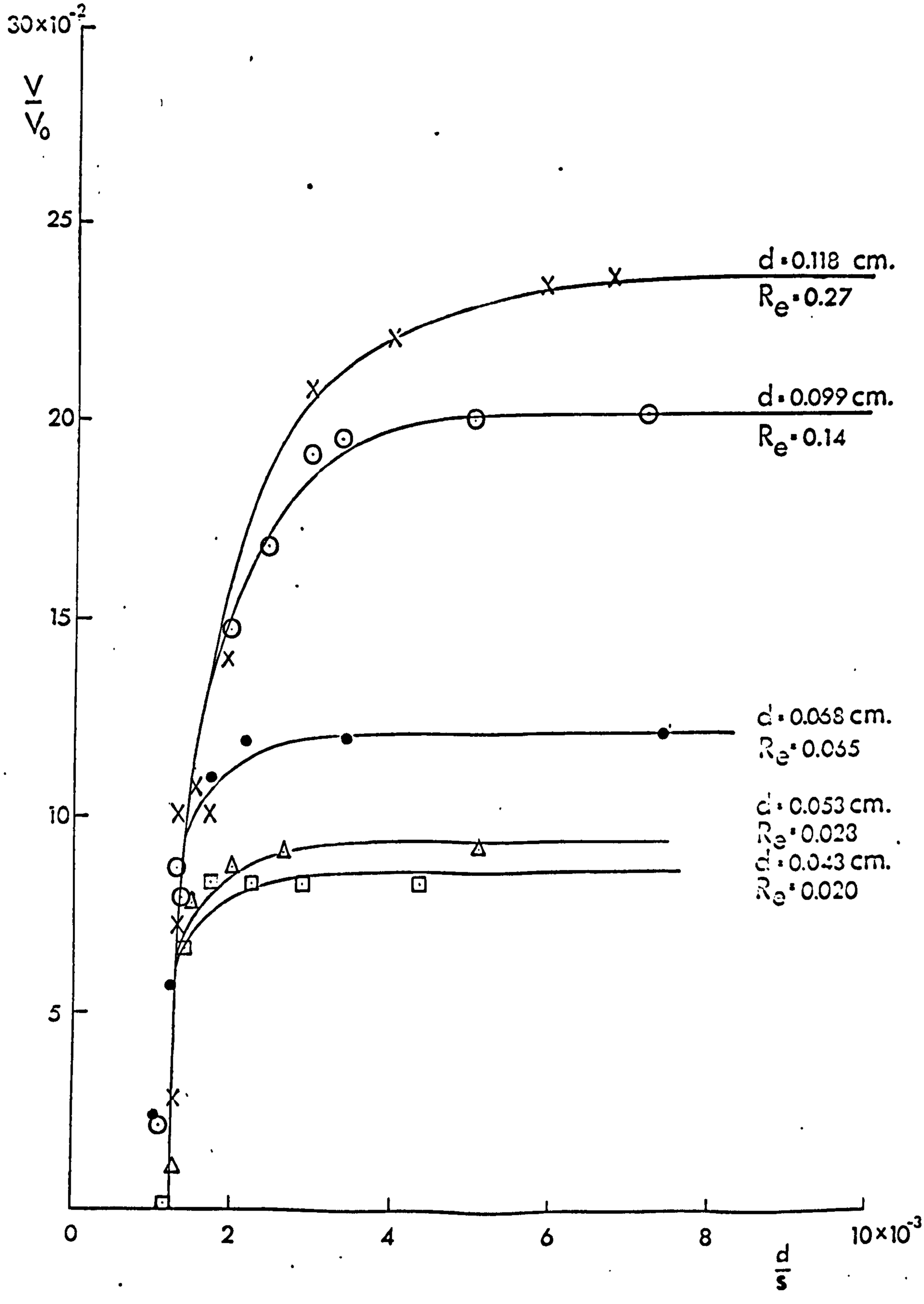

section parallel to the cylinder as long as the end-effects of the cylinder are negligible. Hence a short cylinder parallel to the leader placed vertically behind the leader would experience the same velocity along its length, but a cylinder longer than the leader would experience a faster moving fluid at the centre than at the ends. This inhomogeneity of flow along the length may be the cause ~~for~~ of longer cylinders to execut~~e~~ing oscillations in the wake of the leader.

(b) Parallel but displaced horizontally as well.

The relative motion of such a pair was determined by plotting their horizontal and vertical separations at successive intervals of time. The path of the trailer with respect to the leader placed at the origin is shown in fig.3.14. Points are separated at 1/4 sec intervals. As the cylinders approach each other, they close more rapidly in the vertical than in the horizontal direction. At a certain stage the horizontal separation remains sensibly constant while the vertical separation continues to decrease. When the cylinders are sufficiently close, the trailing cylinder moves away from the leader increasing the horizontal separation. Eventually the two cylinders maintain a constant vertical separation but separate horizontally at decreasing rate. All through the motion the two cylinders fall with their axes horizontal and parallel to each other. The path is very similar to that observed for equal spheres similarly displaced (See fig.2.11), except that the two spheres finally

Fig 3.14. Path of a cylinder relative to an equal cylinder in front

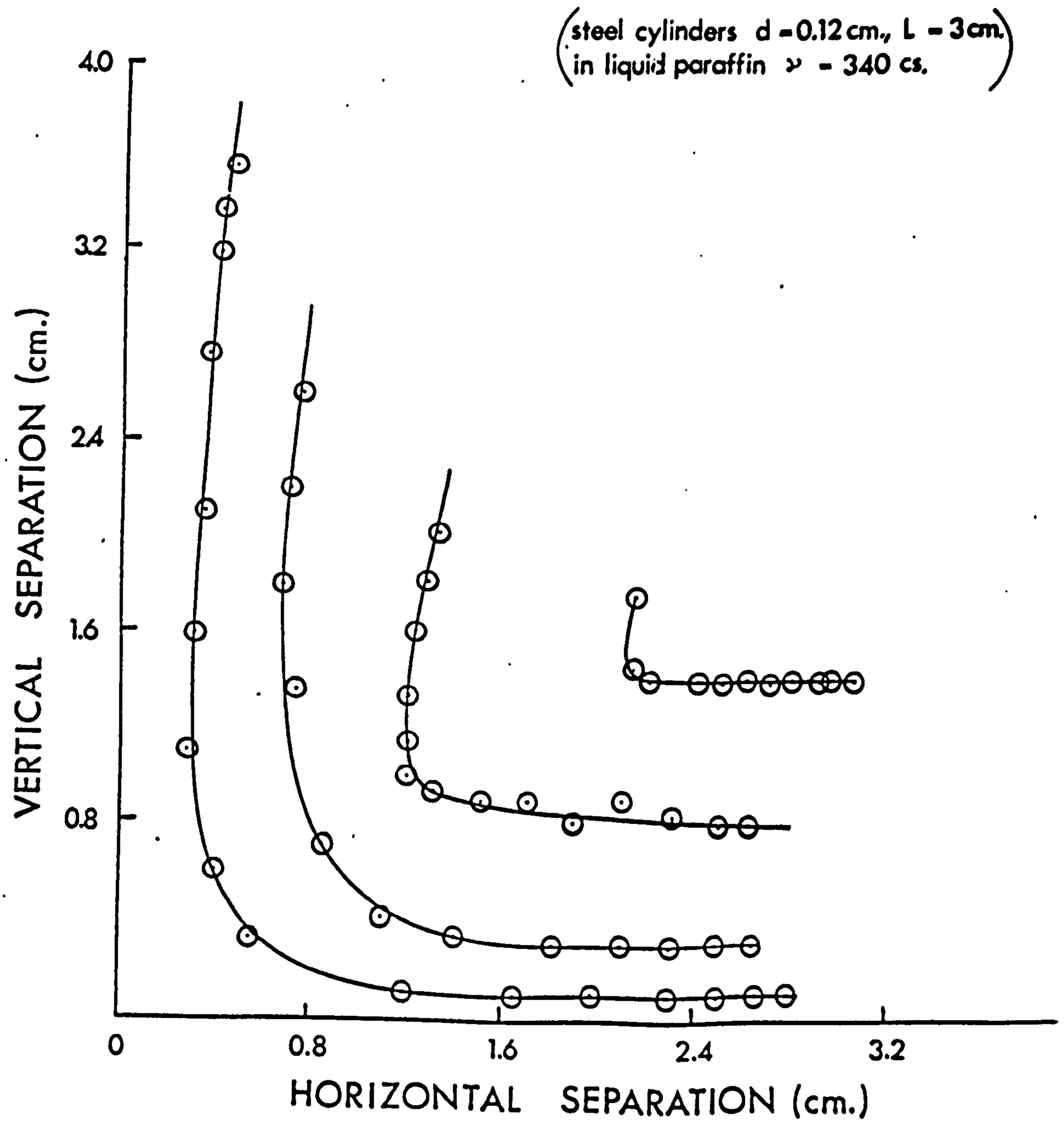

reach the same horizontal level while the cylinders separate maintaining a fixed vertical separation. In both cases fixed paths are followed determined by their initial positions.

(c) Not parallel

The trailing cylinder tilts towards the leader and slides towards it. Both cylinders now flutter before taking up a stable position in which they bisect each other at right angles.

3.4 THREE OR MORE IDENTICAL CYLINDERS

Using the dispenser 2 with the corresponding adaptors, three or more long identical cylinders were released with the axes horizontal, but with various initial configurations.

When released simultaneously all parallel to each other, the cylinders separate but maintain their axes parallel and remain in the same horizontal plane. If the axes are not parallel initially, then the cylinders tend to fall parallel to each other. Fig. 3.12 photograph 3 shows this effect.

For all other initial configurations, they may cluster to form crossed doublets or symmetrical ++ patterns. While the crossed doublet is stable, the latter is not. The two parallel members separate, remaining nearly parallel, while the upper member falls between and away from them. The two of these separating cylinders may later combine to form a symmetrical cross that falls faster than the remaining cylinder and leaves it behind. This sequence is shown in photographs 4, 5 and 6 of

fig. 3.12.

Hence if there are two or more cylinders, they either form into sets of stable pairs crossed at the centre, right angles to each other, or separate with their axes parallel.

3.5 CYLINDERS LOADED WITH SPHERES.

A needle shaped or columnar ice crystal will fall freely in air with its long axis horizontal. But if this ice crystal captures a supercooled water drop in its path, its orientation, direction and velocity of fall would be considerably affected.

To investigate this behaviour in the laboratory, a cylinder was loaded with a single sphere along its length and the motion was studied. However, the experiments could be performed only in a large water tank (2 ft x 4 ft x 6 ft), as the motion of these loaded cylinders were such that with any smaller tank, the walls would interfere with the motion. Hence the materials of the cylinders and spheres have to be restricted to either perspex or polystyrene. The Reynolds numbers were greater than about 100, with the cylinders shedding Karman vortex streets along their path.

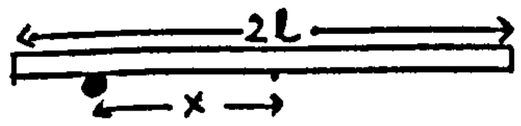

If a cylinder of mass m_r, length $2l$ and diameter d is loaded with a sphere of mass m_s and radius r at a distance x from the centre, the behaviour depends on all these parameters. The observed behaviour can be classified into three

distinctly different types according to its orientation as

motion I Long axis horizontal.

motion II Long axis inclined.

motion III Long axis vertical.

Classifying the behaviour into these three types by changing all the above mentioned parameters, it was found that the behaviour can be determined entirely by two parameters.

(1) the ratio of the weights of the sphere in water to that of the cylinder in water W_s/W_r , and

(2) the x/l ratio

In fig. 3.15, three types of motion are plotted with respect to these two parameters. Distinct boundaries divided the three zones from one another. From these three zones, the type of motion for a given combination of the two parameters W_s/W_r and x/l can be predicted.

Motion I

The cylinder remains with its axis horizontal and moves in a vertical path. If the diameter of the sphere is equal or greater than that of the cylinder, the cylinder turns so that the sphere is on the underside. For shorter cylinders which flutter when falling unloaded (see section 3.2), loading tends to stabilise this behaviour. Fluttering of a loaded cylinder occurs for much shorter lengths. However, the length below which fluttering occurs depends on the position of loading and the

Fig. 3.15 Zones of different orientations of loaded cylinders

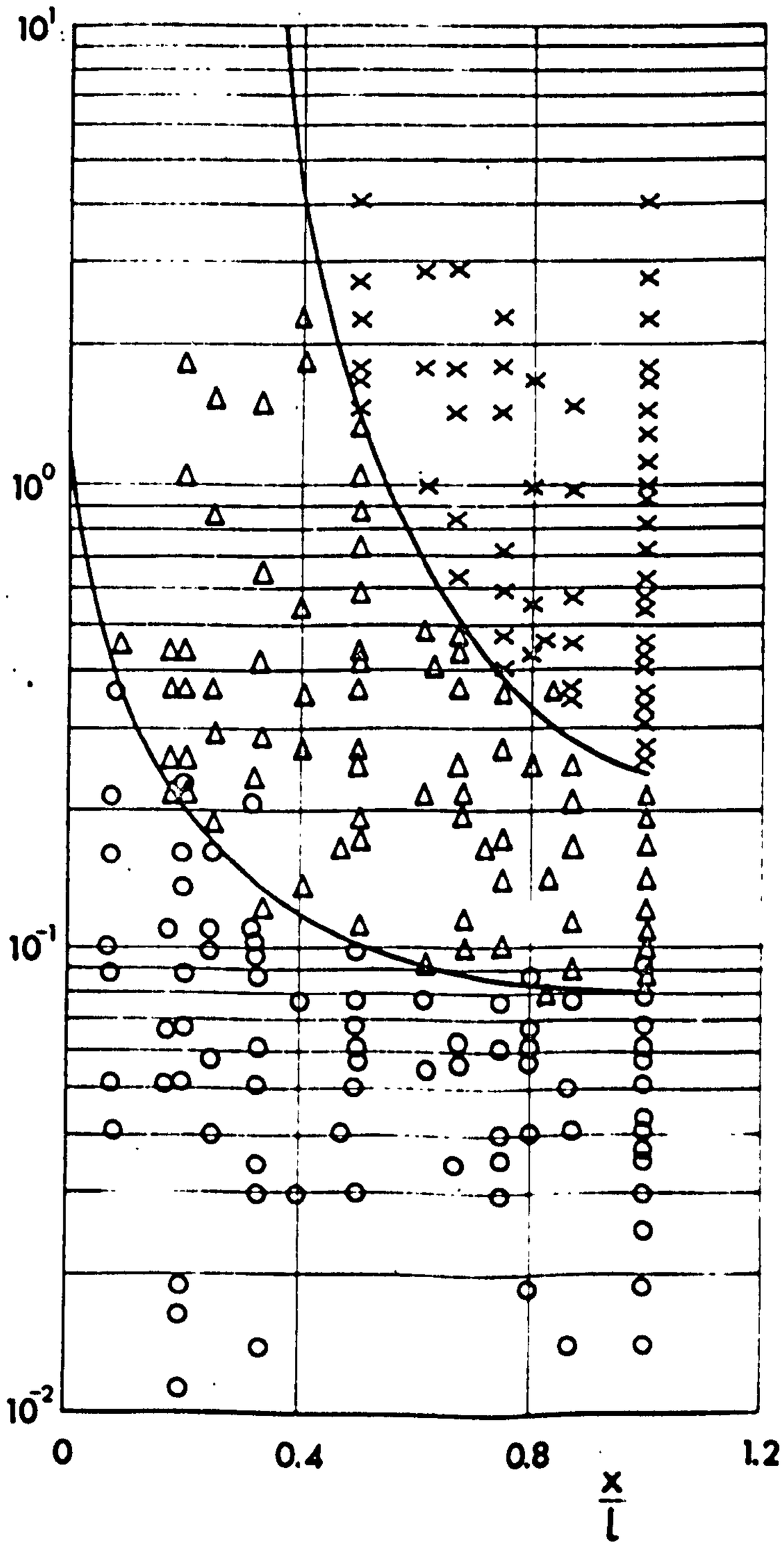

weight ratio. For smaller W_s/W_r, as the loading becomes close to the centre, the critical length for fluttering approach to that of a unloaded cylinder.

Loading of a cylinder falling with its axis horizontal, increases its terminal velocity of fall. But the velocity for a given W_s/W_r, remains independent of the position of loading as long as the cylinder falls horizontally. For example, if for a particular sphere and cylinder, the loaded cylinder falls in a horizontal position for $x=x_1$, then for all $x<x_1$ (see fig.3.15) it will remain horizontal and will fall with the same terminal velocity.

When x=0, all loaded cylinders fall vertically with the axes horizontal; with larger ratios of W_s/W_r (>0.5), the rod oscillated about its long axis, may be due to the shedding of vortex rings from the sphere, but still the combination fell vertically.

The terminal velocity V of fall for a cylinder loaded at the centre showed a steady increase with the mass of the loaded sphere. In fig. 3.16, the ratio of the terminal velocities of a cylinder loaded at the centre to that of an unloaded cylinder, V/V_o, was plotted as a function of W_s/W_r. There is a considerable scatter in the results, however, it shows a steady increase of V/V_o with W_s/W_r. It is evident from the graph that if $W_s/W_r < 0.04$, loading cannot cause a increase in the terminal velocity.

Fig 3.16 Velocity of fall of loaded cylinders

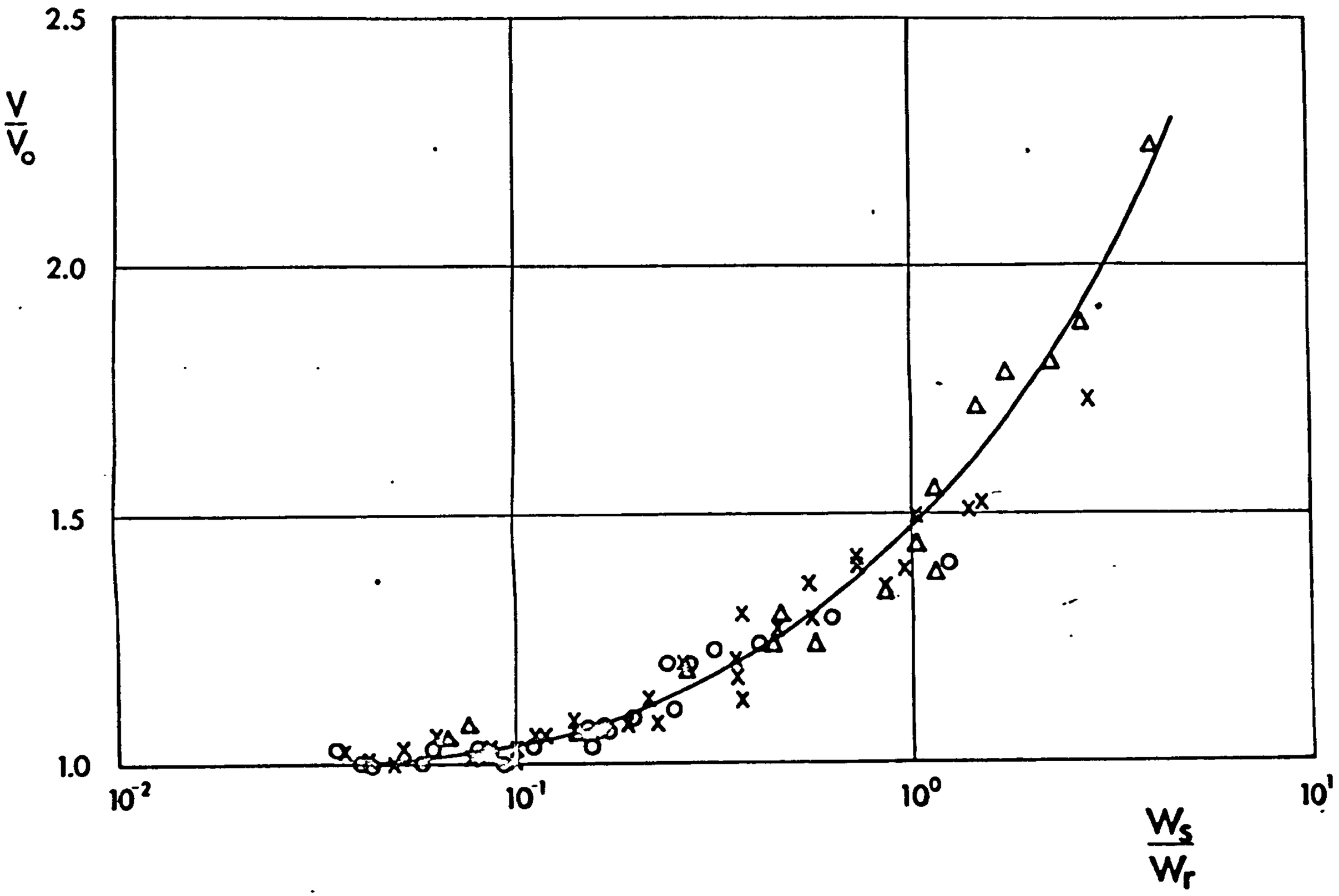

Motion II

The axis of the cylinder is inclined to the horizontal. The fall path is no longer vertical but inclined in the direction of the axis. The deviation from the vertical is a maximum when the inclination of the axis is 45°. In the initial stages of this motion, the cylinder moves with the sphere on the underside without any oscillations, but later rotary oscillations about its long axis set in. The onset of oscillations is quicker when the loaded mass is higher.

Motion III

The cylinder falls with its long axis vertical and spinning about this axis. The motion becomes less stable as the loading gets further away from the edge. The velocity of fall is very much increased as the drag for this position of fall is considerably reduced.

The flow behind the loaded cylinders did not reveal any information as to the type of behaviour. Vortices are shed from both the cylinder and sphere, which later coalesce downstream to give two sets of vortex rings.

Application to needle-shaped ice crystals.

By loading, it is possible to change the orientation of a freely falling cylinder. Since the three types of motion did not depend on the Reynolds number for $10^2 < Re < 10^3$, it may be assumed that the same applies for all Reynolds numbers. There is

no reason to consider the Reynolds number to be a significant parameter for these behaviour as the bodies considered have no geometrical similarity.

The average mass of a needle-shaped ice crystal is 0.004 mg. Usually the diameter of such needles remain sensibly constant, so that the mass depends on the length and is related by

$$m_r = 0.0029\ (2l) \quad \ldots\ldots \text{(Mason 1957. pp 169-172)}$$

where m_r is in milligram and l in mm.

For $m_r = 0.004$ mg

$2l = 1.7$ mm and $d = 60\mu$

the velocity of fall for such a needle is about 50 cm/sec (Mason 1957).

The smallest mass of water drop that will cause the needle to fall inclined is, $m_s = 0.08\ m_r$ (fig. 3.15, x=1). This corresponds to a radius of 45μ. To make the needle fall vertical the mass of the drop should be at least $0.25\ m_r$, corresponding to 65μ radius. The water drops of these sizes will fall in air at 0°C and 900 mb with velocities of 26 cm/sec and 40 cm/sec respectively. Hence the needle-shaped ice crystal may collide with such drops in its path.

Supercooled water drops in the above sizes are found in the atmosphere. Hence if a needle-shaped ice crystal collects such a drop it may get inclined and fall with a increased velocity, with the result that preferential collection may take place at the ends and eventually fall with the axis vertical.

CHAPTER 4

SEDIMENTATION OF DISCS AND CONES

4.1 BEHAVIOUR OF SINGLE DISCS

A Experimental arrangement

The behaviour of thin discs falling freely in a viscous liquid was investigated for Reynolds numbers, defined in terms of the diameter, d, and terminal velocity, V_o, when falling with the short axis vertical, ranging from 0.07 to 600. The materials for the discs and the liquids were the same as for cylinders (chapter 3), but in addition thin glass discs were used. The diameters of the discs varied from 0.475 cm. to 2.2 cm., and the thickness-diameter ratio (t/d) varied from 0.04 to 0.3 for perspex discs and from 0.007 to 0.10 for other materials.

The releasing mechanism was the same as for cylinders, except that the groove in the adaptors (fig 3.1) was unnecessary. Further the two tubes A and B of the dispenser 1 was modified to a shape as shown in fig 4.1.

B The behaviour and flow behind

Much of the present work on the behaviour of single

FIG 4.1

Dispenser 2 (modified)

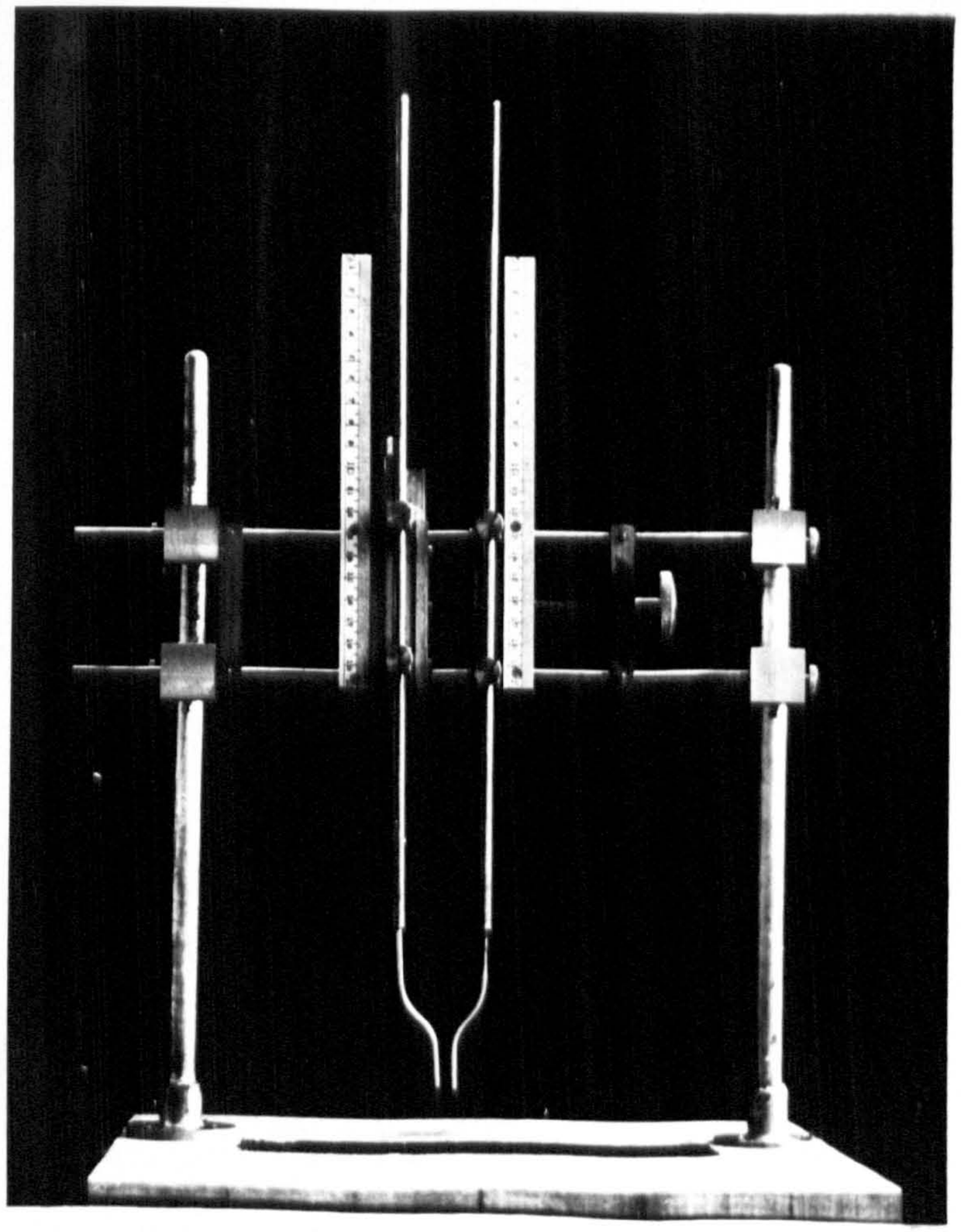

discs for Re > 1, has been anticipated in a recent paper by Willmarth, Hawk & Harvey (1964). The present experiments confirm most of their observations.

All discs in the Reynolds number range > 0.07, showed a tendency to orient themselves with their short axis vertical. Thinner discs (t/d < 0.1) attain this orientation more readily than thicker discs. However, all discs with Re > 0.2, when released with the short axis horizontal (edge-on) turned to the preferred orientation within 30 cm. of fall. This corresponds to about 1 minute of the fall time.

Detailed study of the motion of thin discs at very low Reynolds numbers (< 1) has been carried out by Schmiedel (1928) and Squires & Squires (1937), but none of these authors indicate the Reynolds number above which the discs fall with a preferred orientation. Schmiedel mentioned that at low Reynolds numbers it was difficult to orient discs with their faces horizontal as they tend to fall with their initial orientation, but gives no data of the Reynolds number in which this occurs. Squires & Squires made measurements on the drag coefficients of discs falling edge-on for Reynolds numbers upto 0.24, but only over fall distances of 17.5 cm. in which any tendency for the discs to orient would be unnoticeable. Willmarth et al (1964), did not consider Reynolds numbers of this order, but found that all discs with Re > 1, fall with the preferred orientation of

short axis vertical.

The flow behind the discs was observed using soluble dye. For Reynolds numbers as low as one, ~~two standing eddies~~ ring vortex was were visible behind the discs. Even for lower Reynolds numbers the flow is asymmetric, but no eddies were visible.

With increasing Reynolds numbers, these two eddies elongate steadily and eventually break away into a set of Karman vortex streets. Fig 4.2 shows a disc with eddies about to be separated. With the shedding of eddies, the discs flutter executing pitching motion, but the mean path remains vertical. The velocity of the discs vary from a maximum to a minimum in half-cycle of flutter, but the average velocity of fall is constant.

The Reynolds number for which the eddies separate depends on the (t/d) and (ρ_s/ρ_f) ratios. For all the discs, considered in the present experiments, if $Re < 100$, the discs fell steadily without any fluttering, while for $Re > 190$, all discs shed vortex rings executing pitching motion.

Willmarth et al investigated this transition region $100 < Re < 190$ in detail. They defined another parameter, called the "dimensionless moment of inertia, I^*," to distinguish the steady and pitching motion. I^* is defined as the ratio of the moment of inertia of a thin disc about a diameter and a quantity proportional to the moment of inertia of a rigid sphere of fluid about its diameter, d.

FIG 4.2

Disc with eddies about to be separated. Perspex in water

d = 0.635 cm.

t = 0.032 cm.

Re = 189

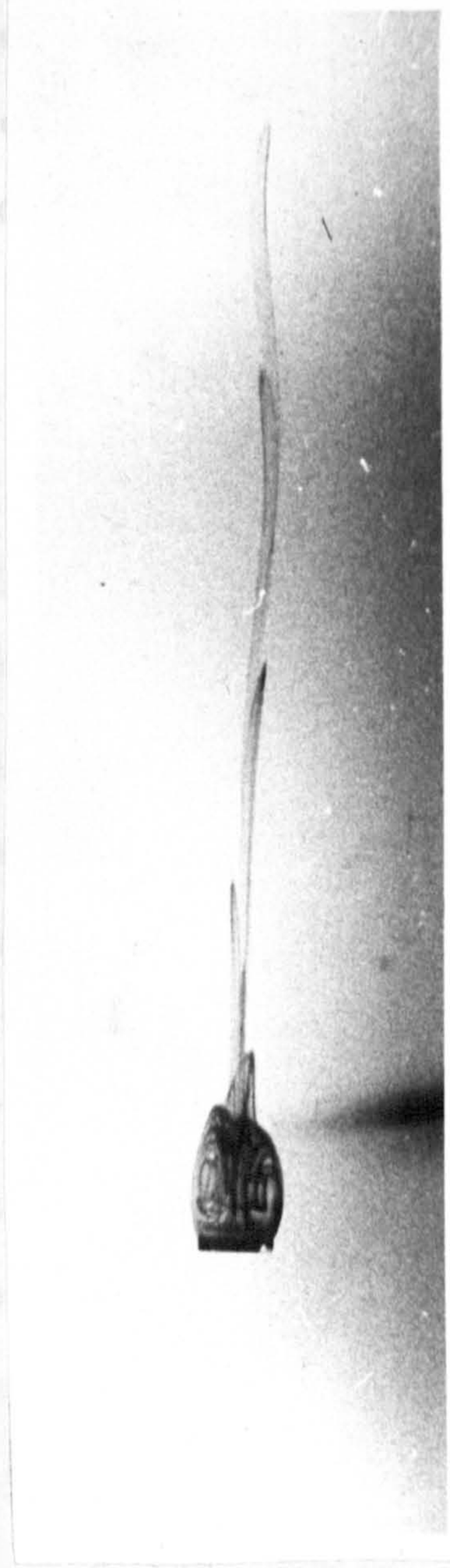

Hence

$$I^* = \frac{\pi \rho_s t}{64 \rho_f d}$$

This term displays the inertial effects of the disc and arises naturally in the inertial terms of the equations of motion for the rotation of a disc about the centre of mass.

Willmarth et al used steel discs, with t/d ratio ranging from 0.002 to 0.04, falling in glycol solutions of density 1.08 to 1.15 g cm^{-3}. The Reynolds numbers for these discs were in the transition region $90 < Re < 180$. Classifying the motion of the discs into steady and persistent pitching motion, they found a distinct boundary curve could be drawn when the Reynolds number at which instabilty occurs, is plotted against I^*. This curve is shown in fig 4.3. A disc having Re and I^* on to the left of this curve falls steadily, while on to the right of the curve executes pitching motion.

Using the boundary curve, Willmarth et al successfully explained the results of Simmons & Dewey (1930) that eddies are formed behind a ventilated stationary disc placed normal to the stream at Re = 100. A mounted disc is equivalent to a freely falling disc having a very large I^*. However, they were unable to account for the low value of Re = 80, obtained by Schmiedel (1928) for the onset of fluttering of thin discs, made from heavy materials like gold or silver, falling freely in a viscous liquid.

Fig. 4.3 Boundary separating steady and unsteady motion for discs

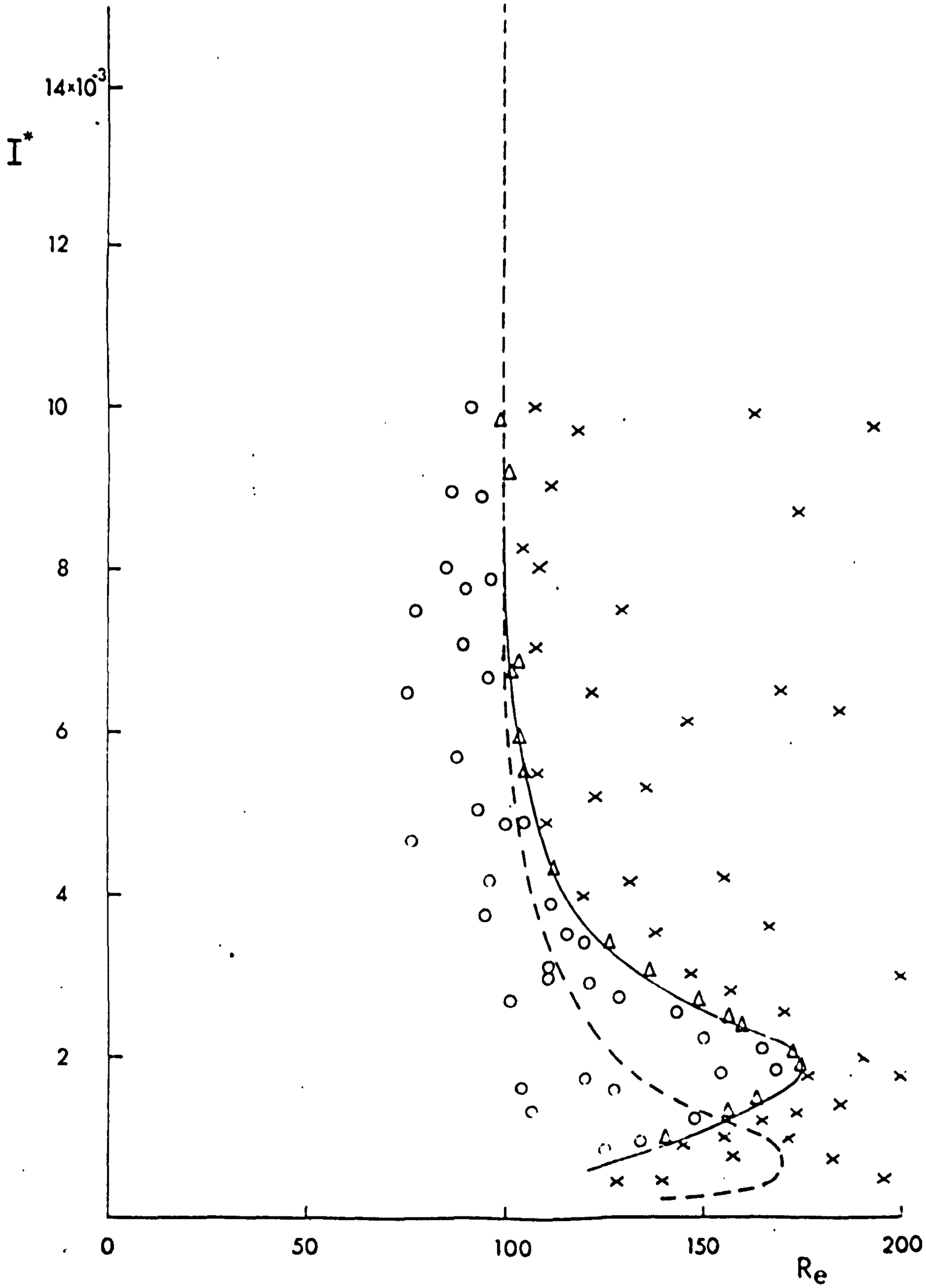

The present curves for the transition from steady to unsteady motion of steel and brass discs agree well with Willmarth et al's curve , but differs considerably for perspex and glass discs.

Since the densities of the liquids remain very nearly the same, the density ratio is mainly determined by the density of the disc. In the experiments of Willmarth et al, ρ_s/ρ_f was very nearly ~~the~~ constant at 7.5, since they used only steel discs. The present experiments were conducted with considerably different density ratios and corresponding to each, a distinctly different boundary curve was obtained. The boundary curve for steel agrees with that of Willmarth et al. But with glass and perspex discs, which have a much lower ρ_s/ρ_f , the boundary curves coincide only in the region where the Reynolds number for instability occurs at Re = 100 independent of I^*. This disagreement is illustrated in fig 4.3 and Table 4.1. In the former the boundary for glass discs is compared with that of Willmarth et al, while in the latter the values of the maximum Reynolds number for instability and the corresponding value of I^* are listed for different density ratios. This value for I^* increases with the decreasing density ratio.

Unfortunately attempts to find a suitable parameter to fit all these results were unsuccessful. A similar difficulty was encountered in the boundary between steady and unsteady motion

TABLE 4.1

The maximum Reynolds number, Re_m, for instability and the corresponding I_m^* for discs

Material of disc	ρ_s / ρ_f	Re_m	I_m^*
+ Steel	7.8	170	8×10^{-4}
+ Glass	2.5	181	2×10^{-3}
+ Perspex	1.2	189	6.5×10^{-4}
++ Steel	7.5	172	8×10^{-4}

+ Present results

++ After Willmarth, Hawk & Harvey (1964).

of cylinders (see fig 3.6). But it is evident that for a fixed density ratio, a definite boundary curve exists for steady and unsteady motion for a disc.

The frequency of eddy production increases with increasing Reynolds number and for Re > 400, the motion of the disc is very turbulent. The disc no longer fall in the same vertical plane but in a small helix with the disc spining as well as fluttering. The maximum Reynolds number in the present experiments did not exceed 600 and no tumbling of the discs was observed.

C The drag coefficients for single discs

The drag coefficient C_D for a disc falling freely with the short axis vertical could be calculated by equating the net weight of the disc in the liquid, to the drag force.

Thus

$$\frac{\pi d^2}{4} t (\rho_s - \rho_f) g = \tfrac{1}{2} \rho_f V_o^2 \frac{\pi d^2}{4} C_D$$

or

$$C_D = \frac{2 t}{V_o^2} \frac{\rho_s - \rho_f}{\rho_f} g$$

When Re < 100, a unique curve is obtained for the drag coefficient as a function of the Reynolds number (fig 4.4). These results agree well with those of Schmiedel (1928). But in the Reynolds number range (100 < Re < 190) where the transition from steady to unsteady motion occurs, the values of C_D are

Fig. 4.4 C_D – R_e curve for discs normal to flow

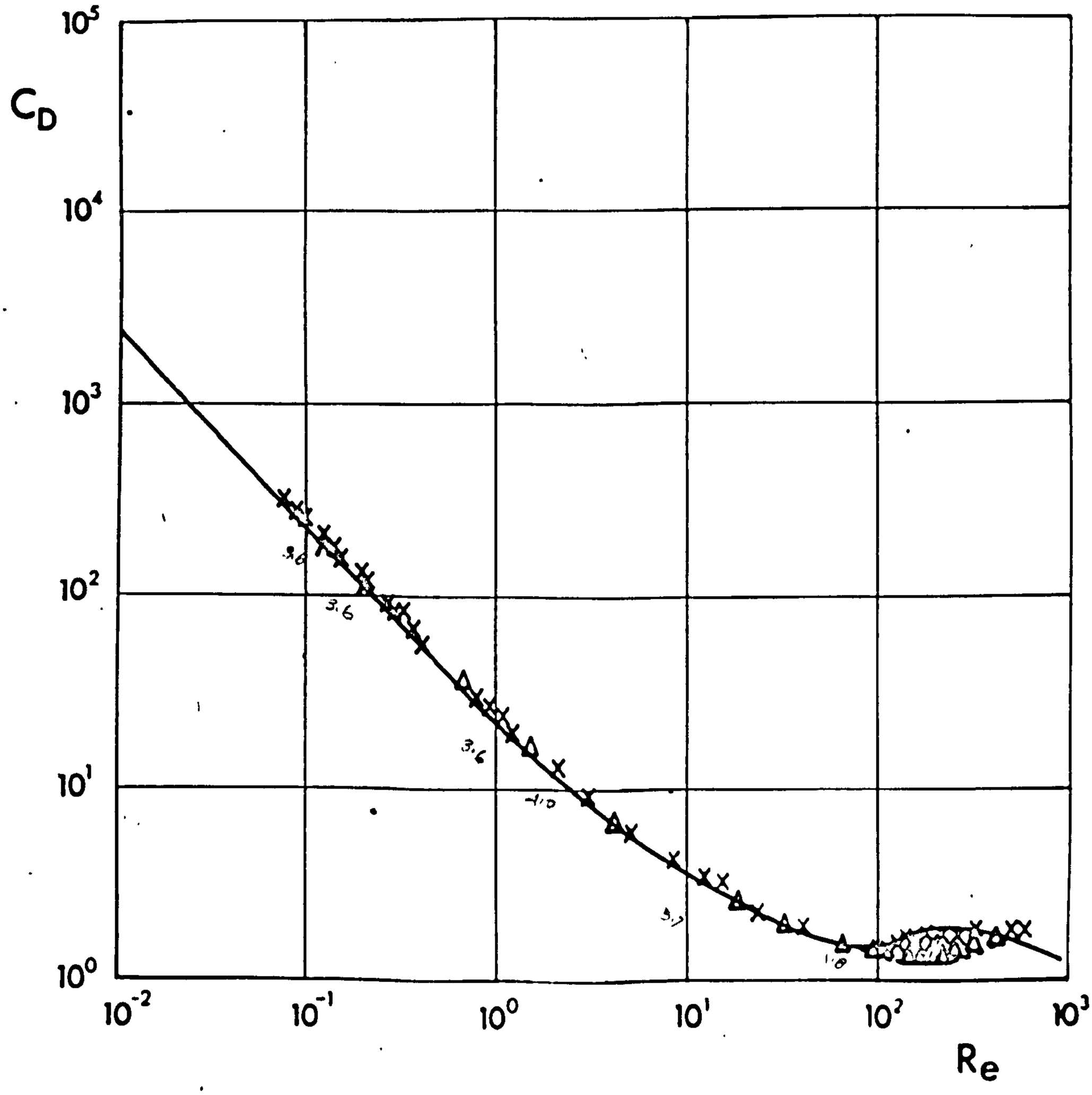

——— after Schmiedel

× Present values

Δ " " for $\frac{t}{d} \sim 0.1$ Perspex discs

scattered between 1.3 and 1.9. In this range, the drag coefficients depends very critically on the t/d and ρ_s/ρ_f ratios. Hence unless these two ratios are also matched, a unique value for C_D cannot be obtained.

For discs having the same t/d and ρ_s/ρ_f, the drag coefficient decreases smoothly with increasing Reynolds number until the fluttering occurs, when it begins to increase. The points marked -Δ- in fig 4.4 refers to one such case, where the results are for perspex discs with t/d ~ 0.1 falling in water and sugar solution. The transition for these discs occur at Re = 189. Schmiedel observed a similar curve with the transition occuring at Re = 80. In Schmiedel's experiments ρ_s/ρ_f was high (>10) and t/d was very small (<0.03) that discs of different ρ_s/ρ_f and t/d ratios should not have appreciably different hydrodynamic characteristics.

The drag coefficients for fluttering discs are calculated assuming that the disc falls with the face normal with the average velocity of fall. The increase in drag coefficients for such discs indicates that there is a decrease in the fall velocity once fluttering or unsteady motion sets in. Thus shedding of vortices is accompanied by a reduction in fall velocity of the disc.

4.2 BEHAVIOUR OF TWO OR MORE EQUAL DISCS

(a) Behaviour of two equal discs falling one behind the other.

For Re >1, attraction between two equal discs falling horizontally one behind the other is apparent at separations exceeding 40 diameters. As the rear disc is accelerated into the wake of the leader and closes to within 2 or 3 diameters it begins to oscillate and when the discs become very close they both oscillate together and fall exactly similar to each other. The two discs remain separated and never catch up completely.

When the centres of the two discs are displaced by less than a radius, the rear disc catches up and comes to rest at an angle to the leader, which remains horizontal. At higher Reynolds numbers >100, the angle between the two discs is $< 30^{\circ}$, but this inclination increases with decreasing Reynolds number and may approach 90° at Re ~ 5.

For greater horizontal displacements of the disc, wake capture does not exist, discs fall with their individual terminal velocities.

(b) Behaviour of two equal discs separated only horizontally

When Re <1, if two discs are released with their faces horizontal and the centres separated by less than two

diameters, the two discs rotate "inwards" about a horizontal axis normal to the line of centres. This rotation continues throughout but the discs do not separate. But as the Reynolds number increases the two discs separate while rotating and the number of rotations decreases, until when Re >15, the two discs tilt towards each other initially and turn back to fall unaffected by the presence of the other.

(c) Behaviour of 3 or more equal discs

Three equal discs if they cluster together form a "butterfly" configuration (fig 4.5) in which one member remains horizontal and the other two form a symmetrical 'Vee' in the rear. Such a cluster is very stable when the angle between an inclined disc and the horizontal disc is less than 30°, and falls without any fluttering, and only at high Re when the flow becomes turbulent does it tend to break up.

Even with more than three equal discs this basic "butterfly" pattern exists. The other discs may rest on this configuration. However, such clusters are not stable, the instability increases with the number of discs in the cluster.

FIG 4.5

" Butterfly " configuration for three equal discs

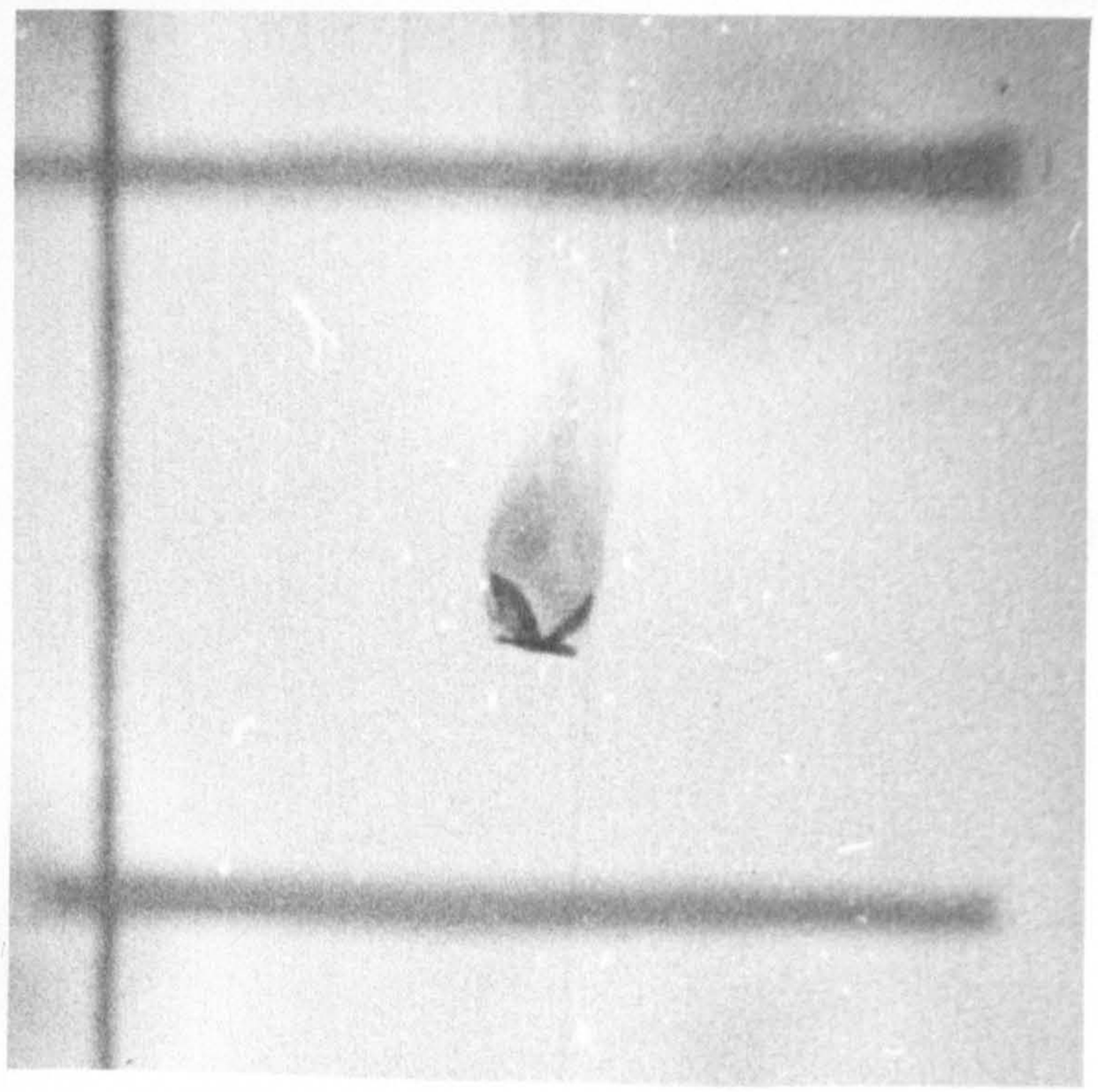

Perspex d = 1.27 cm., t = 0.032 cm. Re ≒ 280

4.3 BEHAVIOUR OF SINGLE DISCS LOADED WITH SPHERES AT THE EDGE

The effect on the motion of a single disc when loaded with one or more equal spheres at the edge was observed. The behaviour of loaded discs were such that a large tank (2'x4'x6') was required, thereby restricting the experiments to be carried out only in water, making most of the discs considered to flutter on free fall.

Since the loading was restricted to the edge, the behaviour of loaded discs depended only on the ratio of the weight in water of the loaded spheres to that of the disc,

$$k = W_s / W_d \quad .$$

In this respect this behaviour resembles that of loaded cylinder. (See section 3.5 Chapter 3)

(a) Single sphere loaded at the edge of the disc

When $k < 0.2$, the loading has hardly any effect on the motion of a disc. The pitching and fluttering motion exist as in the unloaded disc.

When $k > 0.2$, the loaded disc moves in a helix of large diameter which was 2 feet for $k \sim 0.2$ so that the disc usually hit the side of the tank. The disc continues to flutter about the diameter passing through the sphere. The disc remains very nearly horizontal and spins as it moves round the helix

in such a way that the sphere always leads. The motion is the same whether the sphere is on the underside or top side of the disc.

As k increases still further the disc becomes inclined to the horizontal and the diameter of the helix decreases. For $k \sim 0.4$, the inclination is noticeable and the diameter of the helix is about 15 cm.

Above $k = 0.6$, the disc always falls with the loaded sphere on the underside and is very heavily inclined to the horizontal. For thin discs $t/d < 0.05$, a helical motion with the disc turning round the sphere was observed.

For thicker discs ($t/d > 0.05$), the combination showed a pitching motion. The disc changing its inclination regularly about a mean inclined position, which becomes more vertical as k increases.

These two types of motion for thin and thick discs could be distinguished by the flow behind them. In the former case, the disc did <u>not</u> shed vortex rings. The thickness being insufficient to cause separation of the flow from the disc. Since the disc moves in an inclined position, the flow lines pass smoothly along the disc. The sphere on the other hand either had a single standing eddy or shed a single row of vortex rings depending on its diameter and the velocity of fall.

In the case of thicker discs, the flow separation

occurs from the edges of the discs and a double row of vortex rings are shed, the sphere shedding a single row of vortices as before. It was not possible to determine whether the rates of production of vortex rings by the sphere and the disc were the same, but from the trail, it was seen that an eddy is shed every time the disc changes the direction of pitching, and another occurs in between, possibly from the sphere.

In determining the value of k, the weights of the spheres and discs in water have to be considered. This is shown in Table 4.2, where the ratio k' of the weight in air of the sphere and disc above which the disc always fall with the sphere on the underside, are listed for different combinations of the materials of the sphere and disc. But when these ratios are transformed to the net weights in water, all values give the ratios between 0.5 or 0.55.

Summarising, these three types of motion could be classified in terms of k as

type (1)	$k < 0.2$	.....	unaffected
(2)	$0.2 < k < 0.5$	.....	falls in a large helix
(3)	$k > 0.55$	.....	sphere always on the underside

TABLE 4.2

The ratio of the weights in air of the sphere and disc, k', above which the loaded disc always falls with the sphere on the underside.

Material of disc	Material of sphere		
	Glass $\rho = 2.53 g.cm^{-3}$	Perspex $\rho = 1.19 g.cm^{-3}$	Plastacine $\rho = 1.89 g.cm^{-3}$
Glass	0.5 - 0.6	2.0 - 2.2	0.6 - 0.7
Perspex	too small	0.5 - 0.55	0.1 - 0.2

(b) <u>Two equal spheres loaded at the edge on the same side of the disc.</u>

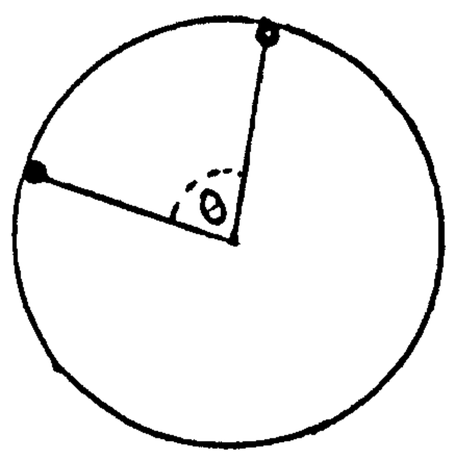

If two equal spheres are loaded at the edge subtending an angle θ at the centre, the behaviour is similar to that of a single sphere having the combined weights of the two spheres, and placed mid-way between the two spheres along the edge.

When $\theta \leq 90^{\circ}$, the values of k for the three types of motion are not much different from the case (a). But with $\theta > 90^{\circ}$, the values of k increase sharply, until when $\theta > 150^{\circ}$, loading seem to have hardly any effect on the behaviour.

$$\left(k = \frac{\text{weight of the spheres together in water}}{\text{weight of disc in water}} \right)$$

(c) <u>Two equal spheres loaded at the same position but on opposite sides</u>

For $0.2 < k < 0.4$, the behaviour is the same as for (a) above, the discs exhibiting helical motion but with the face horizontal. But for $k > 0.4$, it falls vertically with the face

along the direction of fall. The velocity of fall is very much increased as would be expected. The two sets of rings are shed, one from each sphere, and none from the disc if it is thin. With thicker discs, the flow immediately behind is complicated, but the rings later coalesce downstream to form two rows of vortex streets.

(d) More than two spheres loaded on the edge on the same side

More than two spheres, if all placed within an angle 90°, act as if a single sphere of equivalent mass was placed at the centre of mass along the periphery.

(e) Application to falling plates in the atmosphere

Assuming similar behaviour occurs when a hexagonal plate type ice crystal captures a supercooled water drop in the atmosphere, the table 4.3, gives the corresponding radii of the drops that would cause the plates to undergo motions types (2) and (3).

The drop sizes obtained are within the range of supercooled drop sizes present in the atmosphere. There is therefore a possibility that plates may capture such drops and undergo such a motion. However, due to the small difference in the terminal velocities, the drops may be captured by the plates by the wake effect. Possibility of such capture was observed in the laboratory

TABLE 4.3

Radii of supercooled water drops that effect the motion of plates in the atmosphere.

Plates (assumed as circular discs)			
Diameter (μ)	500	500	100
Thickness (μ)	50	10	10
Mass (μg)	10	2	0.08
Velocity (cm. sec^{-1}) at 900 mb. & $0^{o}C.$	50	19	6
Reynolds number	20	7	0.45
For motion in a helix			
Mass of water drop (μg) ($m_s = 0.2\ m_d$)	2	0.4	0.016
Radius (μ)	78	45	16
Velocity (cm. sec^{-1}) at 900 mb. & $0^{o}C.$	50	22	3.0
Reynolds number (of drop)	6	1.5	0.07

(continued next page)

TABLE 4.3 (continued from last page)

For motion with sphere always on the underside of the plate.

Mass of water drop (μg) ($m_s = 0.5\ m_d$)	5	1	0.04
Radius (μ)	100	60	20
Velocity (cm. sec.$^{-1}$) at 900 mb. & 0°C.	76	30	5.4
Reynolds number (of drop)	10.2	2.65	0.16

experiments with a disc and a sphere having the same terminal velocity. 1/8" perspex sphere falling in sugar solution of viscosity 2.3 cs. which has the same terminal velocity (2.7 cm. per sec.) as that of a ½" diameter, 0.062 cm. thick perspex disc falling in the same liquid, was found to be attracted by the wake of the disc for distances as much as 30 cm., when the sphere is directly behind the disc.

4.4 CYLINDERS CAPPED WITH EQUAL DISCS AT THE ENDS

Perspex cylinders of sizes as used in the experiments described in Chapter 3, were capped at each end with thin equal glass or perspex discs. These capped cylinders were released in the water tank (2'x4'x6') and their orientations in free fall, for different combinations of cylinder and disc sizes were observed.

If the capped cylinder is released with the axis of the cylinder horizontal, it remains in this position only if the length of the cylinder is greater than a particular length L_c (say). For shorter cylinders the combination turned to fall with the axis vertical.

If initially released with the axis vertical, they maintain this position for all lengths, but if released in an inclined position, fall with the axis horizontal if $L > L_c$ and vertical if $L < L_c$.

The length, L_c, has the following properties. With the rest of the parameters fixed, L_c

(1) increases with increasing diameter of the disc, d_d (fig 4.6)

(2) decreases with increasing diameter of the cylinder, d_f (fig 4.7)

The thickness and the density should have an effect on the length L_c, in that they change the mass of the disc. However, since the mass of the disc is very much smaller than that of the cylinder ($< 1/300$), changes in the thickness and density have hardly any effect on L_c.

For given diameters of cylinder and disc, if the capped cylinder is released with axis vertical, the velocity increased steadily with length, while if the axis is horizontal, the velocity* showed a small decrease at shorter lengths but attained the constant value corresponding to the velocity of a long uncapped cylinder, at large lengths. The length of the cylinder corresponding to the point of intersection of those two curves is equal to L_c. Fig 4.8 shows the set of curves for a perspex cylinder of diameter $\frac{1}{4}$" capped with glass discs of thickness 0.015 cm.

Hence when $L > L_c$, the velocity of fall with the axis horizontal is less than that with the axis vertical and vice-versa for $L < L_c$, showing that capped cylinders prefer to

---

* These mesurements could be made only if $L > L_c$.

Fig. 4.6 Variation of L_c with diameter of disc (cylinder – Perspex, disc – glass t - 0.015 cm.)

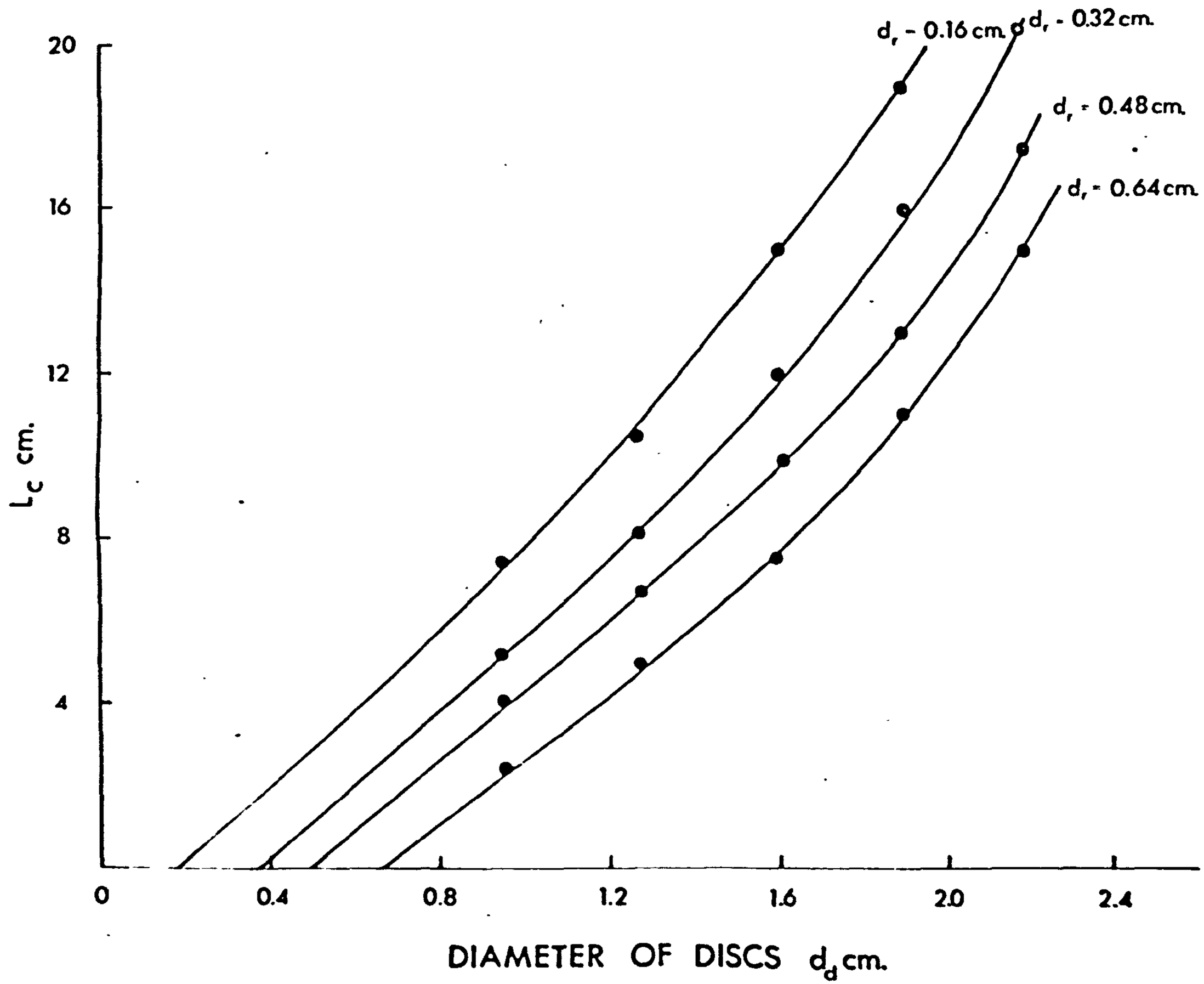

Fig. 4.7 Variation of L_c with diameter of cylinder (disc – glass $t = 0.015$ cm., cylinder – Perspex)

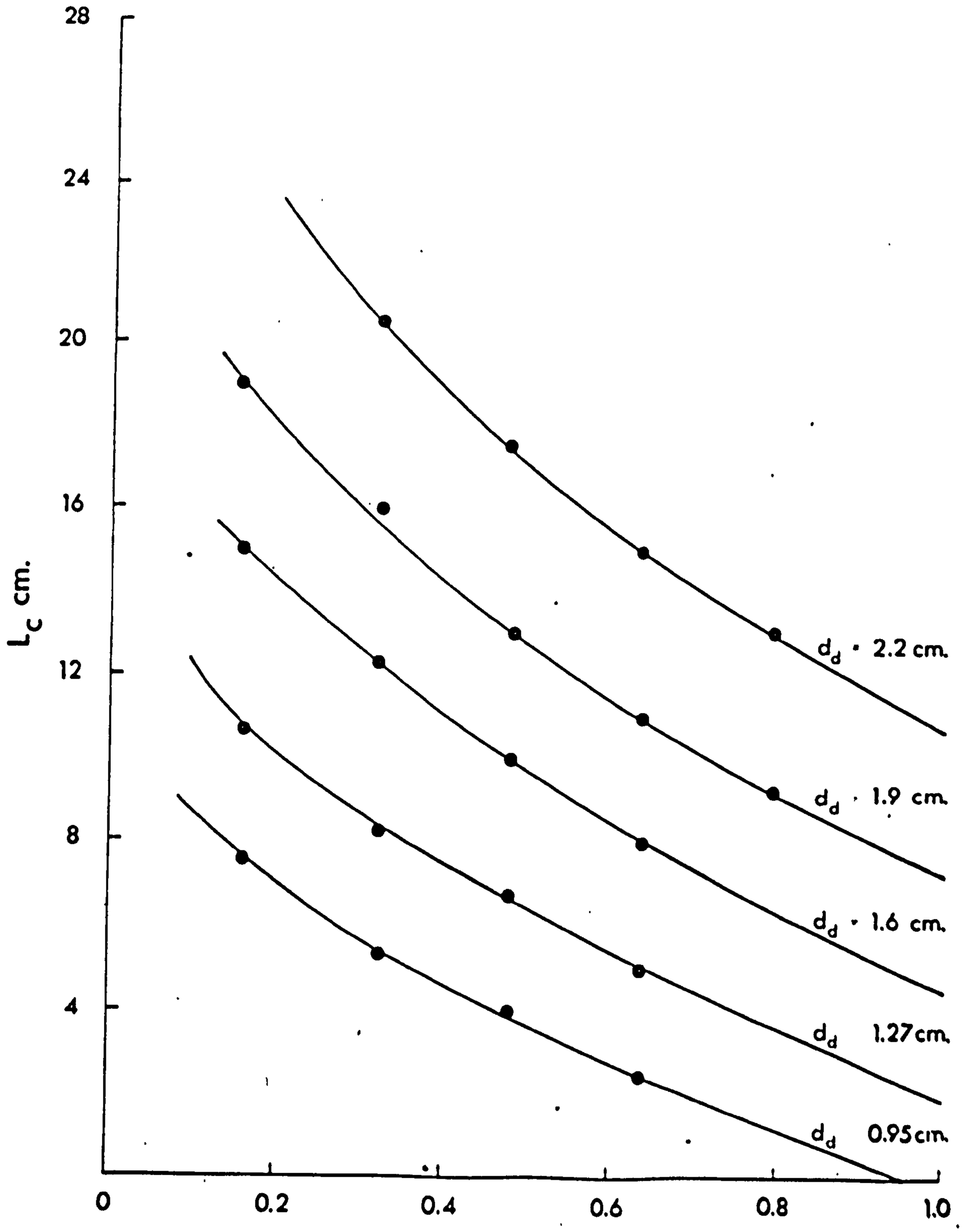

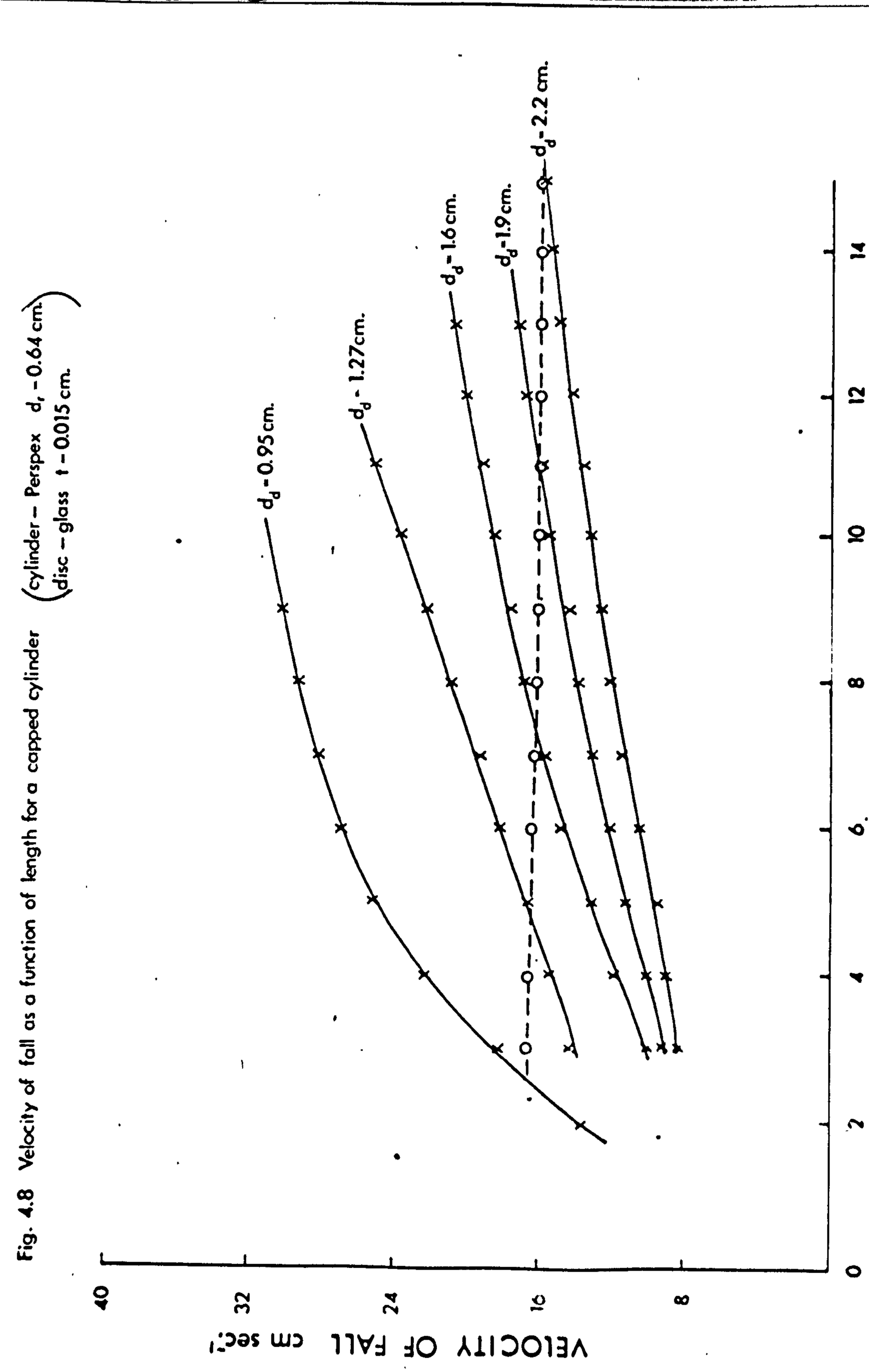

Fig. 4.8 Velocity of fall as a function of length for a capped cylinder

fall with the orientation which corresponds to the smaller velocity.

These results, while confirming that bodies fall in such a way as to present the greatest resistance to motion, also show that cylinders which usually fall with their long axis horizontal, fall with the axis vertical for lengths as much as nine times the difference between the diameters of the disc and cylinder (see Table 4.4), when capped with equal discs at either end.

Application to Cloud Physics

Prismatic columns with end plates (capped columns or collar stud) are fairly commonly occurring type of ice crystal in the atmosphere. Such crystals are formed due to the changes in the environmental conditions of the atmosphere through which they fall (Mason 1957, p177). These ice crystals sometimes have one of the plates larger than the other.

If the crystals falls with the columnar axis horizontal, then there is no reason why one of the plates should grow more than the other, but if the axis is vertical, the flux of water vapour to the leading plate is more than for the rear, hence the leading plate will grow faster than the other. For these ice crystals, the ratio of the length to the difference between the diameter of plate and column could vary from 2 to 15. Hence from the present experimental results, it could be assumed that

TABLE 4.4

Variation of L_c with ($d_d - d_f$)

($d_d - d_f$) cm.	L_c cm.	$K = \frac{L_c}{d_d - d_f}$
0.31	2.4	7.75
0.47	4.0	8.5
0.63	5.0	8.0
0.79	7.5	9.5
0.79	6.8	8.6
0.96	7.5	7.8
1.11	10.5	9.5
1.12	10.0	8.9
1.26	11.0	8.75
1.28	12.0	9.4
1.42	13.0	9.15
1.44	15.0	10.4
1.56	15.0	9.6
1.58	16.0	10.1
1.72	17.5	10.2
1.74	19.0	10.9
1.88	20.5	10.9

some of the crystals would fall with the axis vertical. For these crystals, the higher growth of the leading plate will help to maintain this position throughout the fall.

Many optical phenomena are formed by ice crystals falling with the refracting edges either vertical or horizontal. E.g. horizontal extensions of haloes are formed by crystals falling with the refracting edges vertical, while the vertical extensions are formed by crystals falling with refracting edges horizontal (Humphreys 1929).

Capped columns which could fall in either orientation, depending on the size, may give rise to most of the optical phenomena in the sky. However, other types of crystals like tabular crystals ($d/L > 1$) and columnar crystals ($d/L < 1$) may also be responsible for these phenomena. Good transmission of light through the crystals is essential for these phenomena.

4.5 BEHAVIOUR OF FREELY FALLING CONES

The behaviour of cones made of either perspex or duralloy was observed as they fall through the tanks containing either liquid paraffin or sugar solutions at room temperature. The Reynolds number, defined in terms of the base diameter, ranged from 0.5 to 1500.

Cones having a flat base and Re < 45, fall with the axis of symmetry vertical. But the orientation depends critically on the angle of the cone θ , (θ refers to the apex angle of the isoscelese triangle formed by a plane through a diameter of the base passing through the apex of the cone).

If $\theta < 45^{\circ}$, whatever the initial orientation the cones always fall with the apex upwards, while for $\theta > 45^{\circ}$, the apex downwards position is the more stable of the two. In the latter case both orientations are possible, but if the cone suffers any perturbation it falls with the apex downwards.

Cones falling with the apex upwards begin to flutter if the Reynolds number exceeds 45, while those with $60^{\circ} \leq \theta \leq 80^{\circ}$ are very steady at Reynolds numbers as high as 1500 and, even when $\theta > 80^{\circ}$, they do not flutter until the Reynolds number exceed about 100.

Double cones (fig 4.9 a) formed by cementing base to base two cones with equal base diameters with apex angles θ_1 and θ_2 (θ_2 obtuse and θ_1 acute) also fall with axes vertical at Reynolds numbers < 200. For a given θ_2, the cone always falls with the acute angled apex 'A' upwards if θ_1 is less than a critical value θ_1^* given by

$$2\theta_1^* + \theta_2 = \tfrac{3}{4}\pi$$

as shown in fig 4.10

Fig. 4.9

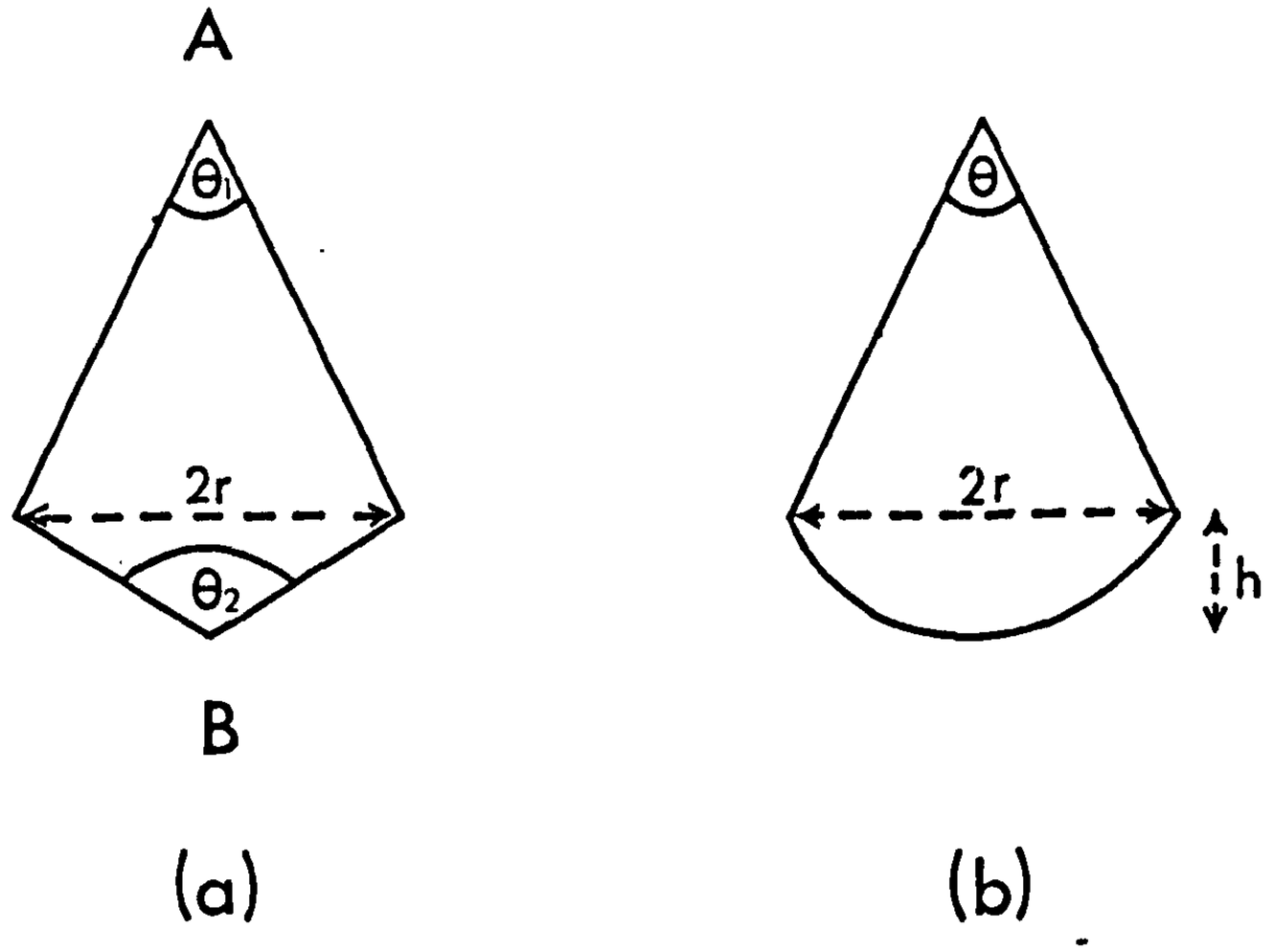

Double cone

Capped cone

Fig. 4.10 Orientation of double cones falling freely

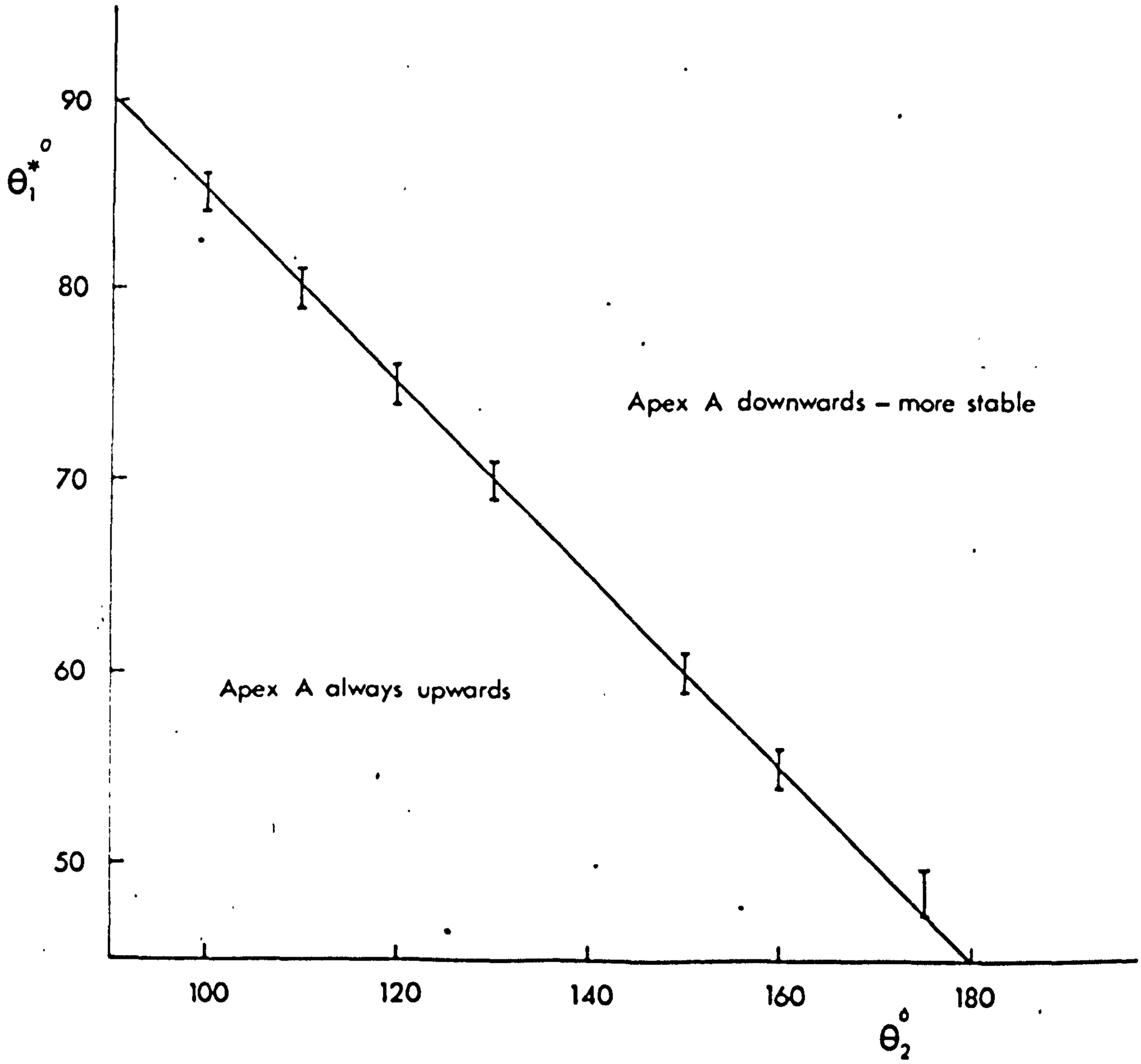

This orientation is achieved whatever the initial orientation. On the other hand if $\theta_1 > \theta_1^*$, then both orientations are possible but the more stable orientation is with the apex A downwards.

Cones with a spherical cap (fig 4.9 b) showed a similar behaviour. For a given height 'h' of the spherical cap, the cone always fall with the apex upwards if $\theta < \theta^*$ and is more stable with apex downwards if $\theta > \theta^*$ where

$$\theta^* = 0.68 \frac{h}{r} + \frac{\pi}{4}$$

This condition is observed to hold for values of h/r between 0.2 and 1.0 as shown in fig 4.11.

The fluid flow around the falling cones was observed by coating them with soluble dye. At Reynolds numbers between 5 and 200 depending upon the geometry and the orientation of the cone, separation of the flow occurs at the circle of contact and a standing eddies forms in the wake of the cone as shown in fig 4.12, above Reynolds numbers of about 200 for hemispherically-capped cones, the eddies are shed alternatively from the opposite sides of the cone which now begins to flutter - see fig 4.13. At Re $>$ 800, the flow becomes highly turbulent and erratic and the cones tumble as they fall.

Fig. 4.11 Orientation of capped cones falling freely

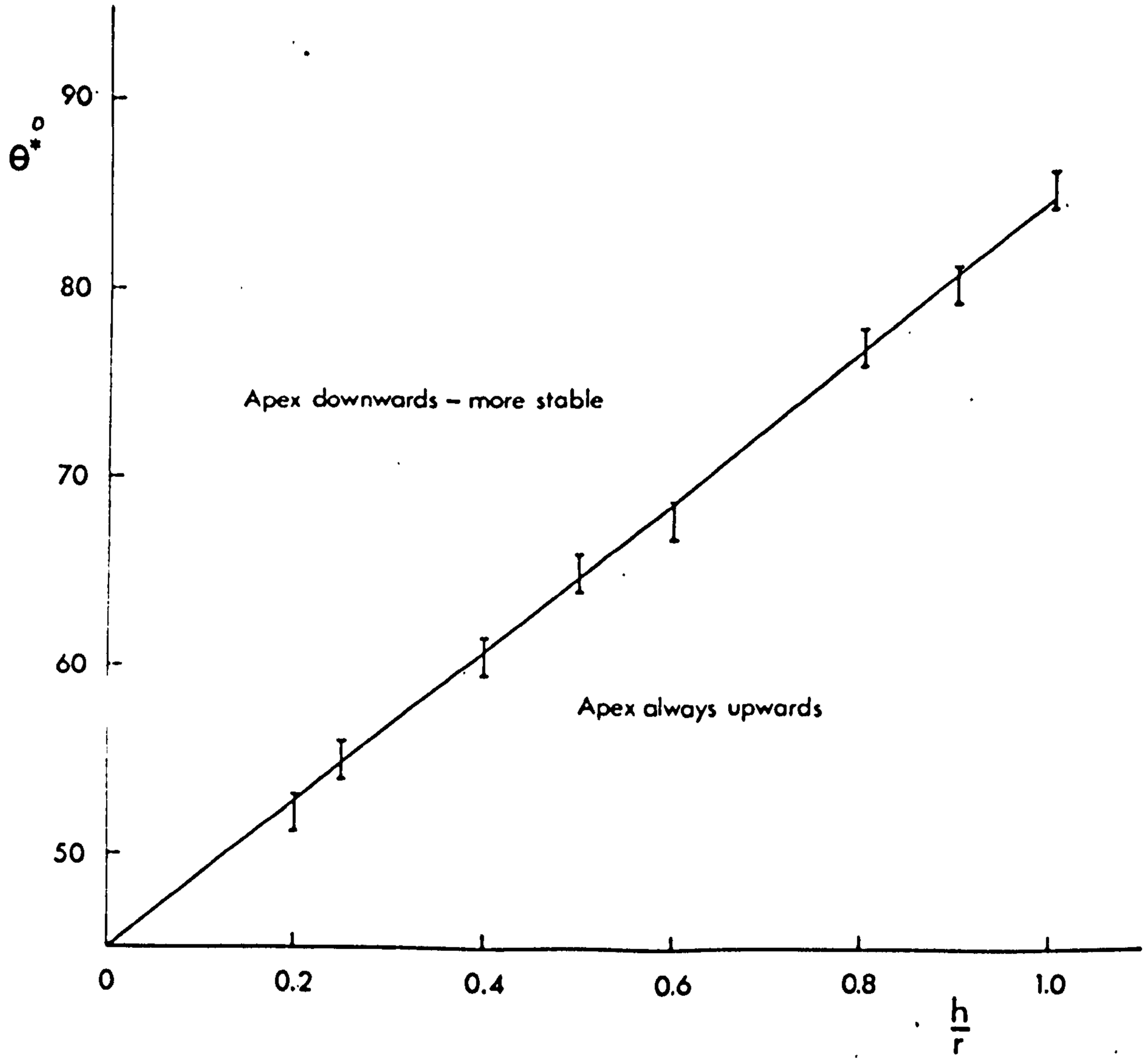

FIG 4.12

Standing eddies behind a cone

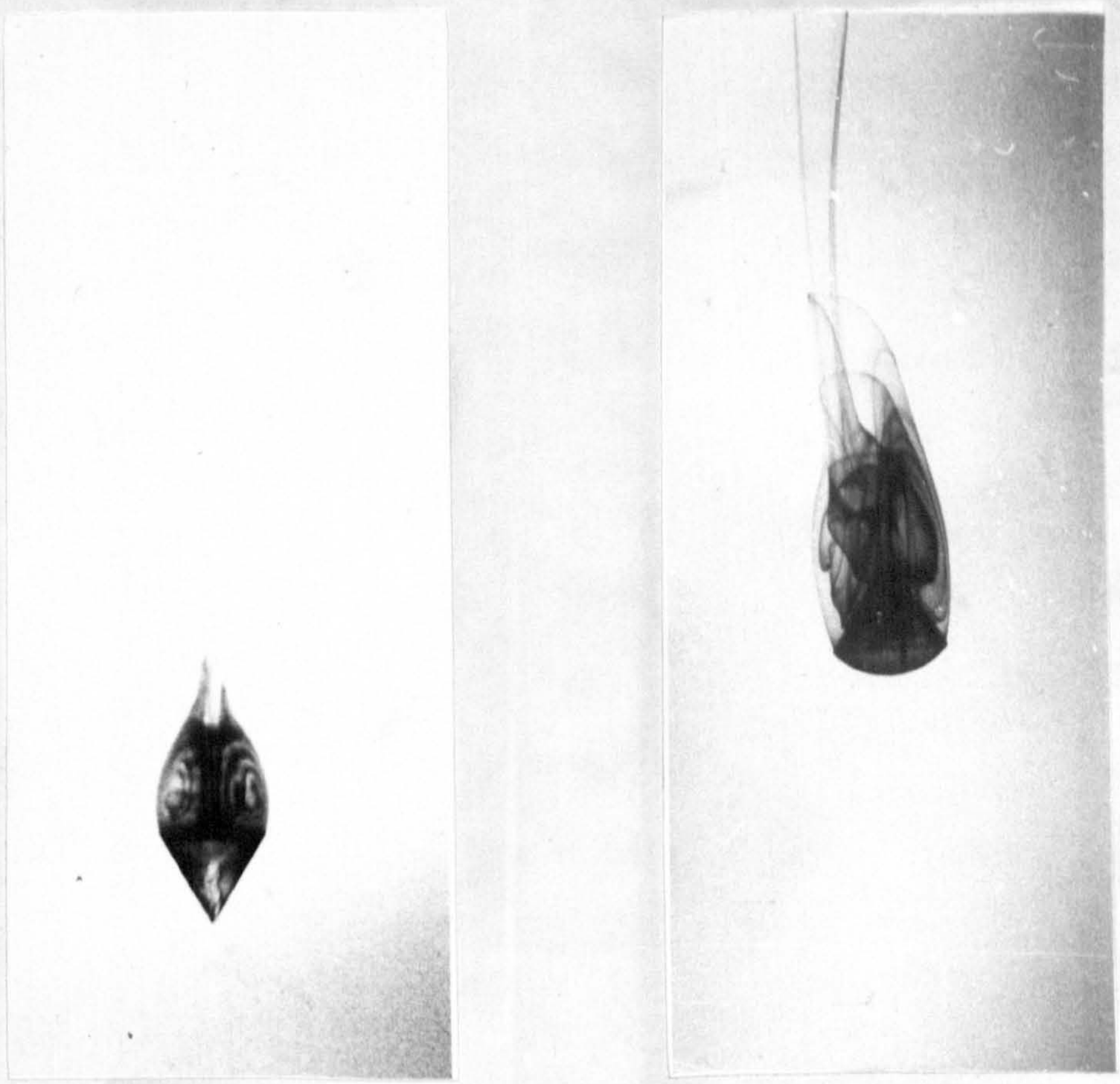

(a)

Perspex, $\frac{1}{2}$" diameter

$\theta = 60^{\circ}$

Flat base,

Re = 89

(b)

Perspex, $\frac{1}{2}$" diameter

$\theta = 60^{\circ}$

Capped, h = 1/8"

Re = 154

FIG 4.13

Shedding of eddies from a fluttering cone

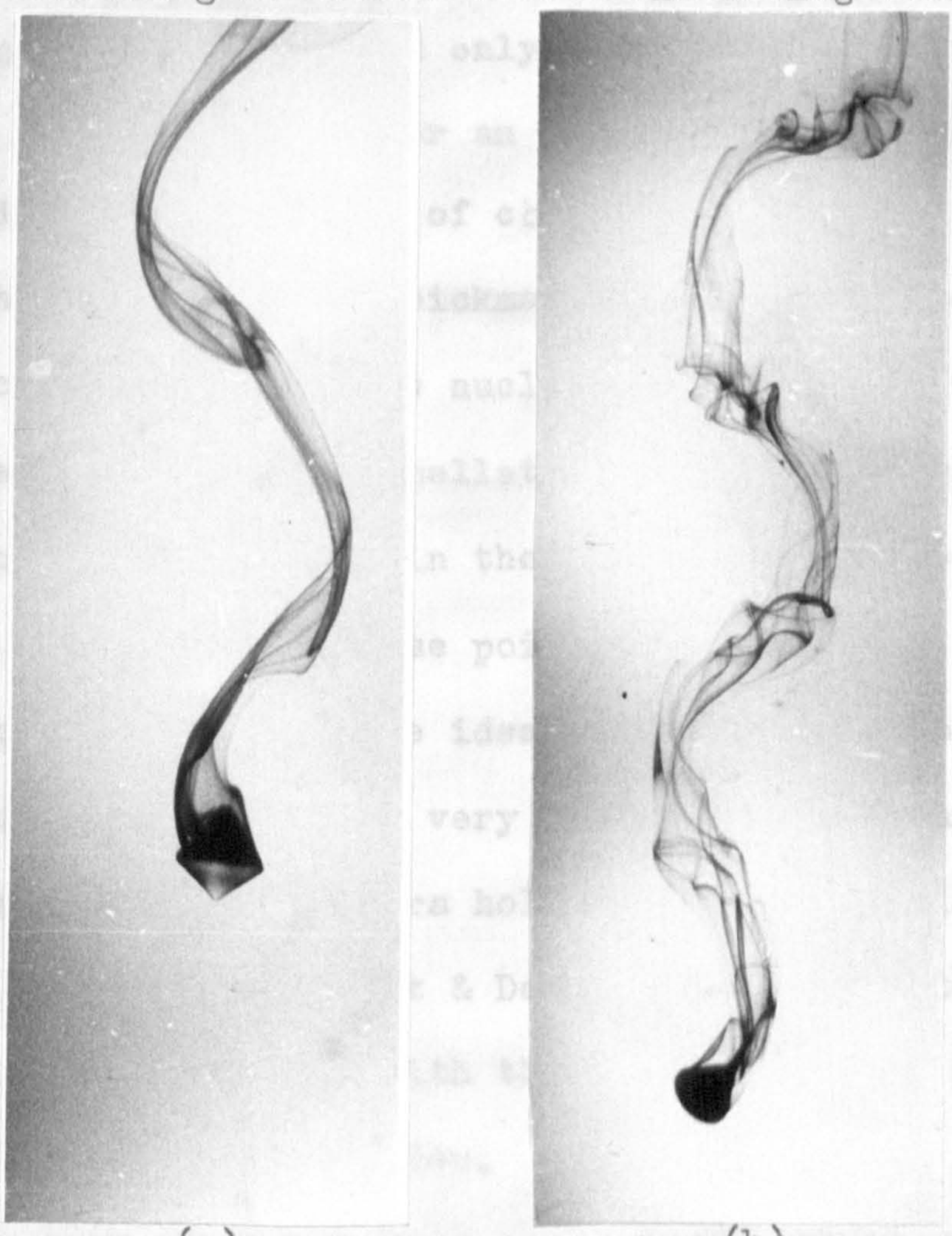

(a) Perspex, $\frac{1}{2}$" diameter Double cone,

$\theta_1 = 70^\circ$

$\theta_2 = 100^\circ$

Re = 260

(b) Perspex, $\frac{1}{2}$" diameter Capped cone,

$\theta = 70^\circ$

$h = \frac{1}{4}$"

Re = 244

Application to conical hailpellets

Most hailpellets are approximately spherical, conical or dicoidal in shape. They are formed only by accretion of supercooled droplets on to a frozen drop or an ice crystal. Of the processes that lead to the formation of conical hailstones, the most probable is that indicated by Weickmann (1956). The supercooled droplets which collide with the nucleus of the pellet will crystallize on location and the hailpellet will grow downwards in a diverging manner. The increase in the diameter of the base leads to a conical shape with the base pointing downwards.

The conical shape is the ideal form at low temperatures. Their structures and sizes have been very well documented in the literature. However, different authors hold contradictory views on the orientation of free fall. List & Davos (1959) support Buch's (1814) view, that these fall with the base downwards, while Arenberg (1941) holds the contrary view.

The results of the present experiments stress the importance of the geometry on the orientation. However, the variation of the density in the hailpellet (the bases being more dense than the tips) may exert some control on the orientation.

The usual shape of conical pellets is that of a hemispherical base with the apex angle of about 70^{o} - 90^{o}

(Arenberg 1941). Measurements on some hailpellets collected locally (on October 1964) showed that the apex angle could be even smaller $\sim 50^{\circ}$, while the bases are very nearly hemispherical or conical with angles $\sim 120^{\circ}$. The orientation of these pellets, from the present results, should be with the apex pointing upwards. Further since the apex is of a lesser density, this orientation is more likely to prevail, thus confirming the view that conical hailpellets grow in the way suggested by Weickmann.

Spherical pellets could also arise from conical pellets which tumble as they fall on reaching a Reynolds number > 800. The random collection of drops on such a pellet may lead to a spherical shape.

APPENDIX 1

FALL DISTANCE REQUIRED TO ATTAIN TERMINAL VELOCITY FROM REST

Suppose a body of mass 'm' and density 'ρ_s' fall from rest into a liquid of density 'ρ_f' and kinematic viscosity 'ν'.

Let 'V' be its velocity after it has fallen a distance 'x' in a time 't'.

If C_D is the drag coefficient corresponding to this velocity 'V' and let 'A' be the cross-sectional area of the body normal to the stream, then the equation of motion at this instant is as

$$m \frac{dV}{dt} = m \frac{\rho_s - \rho_f}{\rho_s} g - \frac{m}{2} \frac{\rho_f}{\rho_s} \frac{dV}{dt} - \frac{1}{2} \rho_f V^2 A C_D$$ (see Fuchs (1964, p70)

The first term on the right hand side is the net weight of the body in the fluid. The second term is the resistance due to the energy expended in setting the medium itself in motion, which is the resistance of an ideal fluid to the accelerated motion of a body (Fuchs 1964, p70). The third term is the drag expierienced by the body at this velocity 'V'.

Re-arranging the equation

$$m \left(1 + \tfrac{1}{2} \frac{\rho_f}{\rho_s} \right) \frac{dV}{dt} = m \frac{\rho_s - \rho_f}{\rho_s} g - \tfrac{1}{2} \rho_f V^2 A C_D$$

i.e.

$$\frac{dV}{dt} = \frac{2(\rho_s - \rho_f)}{2\rho_s + \rho_f} g - \frac{\rho_s \rho_f}{2\rho_s + \rho_f} \frac{A C_D}{m} V^2$$

$$= F^2 - k^2 V^2$$

Where

$$F^2 = \frac{2(\rho_s - \rho_f)}{2\rho_s + \rho_f} g$$

and

$$k^2 = \frac{\rho_s \rho_f}{2\rho_s + \rho_f} \frac{A}{m} C_D$$

Now C_D is a function of 'V'. But in order to solve this equation, a simplified assumption is made by making C_D a constant. As V increases from zero, C_D will decrease. Hence, if the value of C_D at the terminal velocity is used, the value for k^2 would be smaller than its actual value. As will be seen later, this will correspond to a higher estimate of the fall distance required to attain terminal velocity. If the distance as got from these calculations are allowed, then the body would definitely be falling with its terminal velocity. Hence the above assumption is justified in the context of the present problem.

Thus the equation could be written as

$$\frac{dV}{\left(\frac{F}{k}\right)^2 - V^2} = k^2 \, dt$$

~~solving for~~

solving for 'V' with the boundary condition that

at t=0, V=0

we get

$$V = C \tanh (C k^2 t) \qquad \text{where} \quad C = F/k$$

This shows that 'V' increases with t, reaching the terminal velocity V_o as $t \to \infty$

hence $C = V_o$

giving $V = V_o \tanh (V_o k^2 t)$ .....(1)

The distance 'x' traversed before attaining the velocity 'V' is

$$x = V_o \int_0^t \tanh (V_o k^2 t) \, dt$$

$$= \frac{1}{k^2} \log_e \left[\text{Cosh} (V_o k^2 t) \right] \qquad ...(2)$$

to attain 99.9% of the terminal velocity

$$V_o k^2 t = 3.8 \qquad \text{from result (1)}$$

Hence the distance traversed in this time from result (2) is

$$x_o = \frac{1}{k^2} \times 3.1$$

The largest value for x_o for a perticular liquid is estimated by choosing the parameters which gives the smallest value for k^2

For the three cases of bodies considered (1) spheres, (2) discs, (3) cylinders, the following tables give the maximum distance that has to be allowed for a body to attain 99.9% of the terminal velocity when falling in (1) water, (2) 20% sugar soulution at 20°C, and (3) liquid paraffin at 100°F.

Case 1 sphere $k^2 = \frac{3}{4} \frac{\rho_f}{2\rho_s + \rho_f} \frac{C_D}{r}$

Liquid	Max, Re	C_D	k^2	x_o cm.
Water	10^3	0.5	0.22	15
Sugar solution	150	1	0.47	6.5
Liquid paraffin	20	2.5	1.02	3.0

Case 2 discs $k^2 = \frac{\rho_f}{2\rho_s + \rho_f} \frac{C_D}{T}$ (T = thickness of disc)

Liquid	Max. Re	C_D	k^2	x_o cm.
Water	10^3	1.5	4.5	0.7
Sugar solution	300	1.5	4.5	0.7
Liquid paraffin	10	4.0	1.1	3.0*

Case 3 Cylinder $k^2 = \frac{2}{\pi} \frac{\rho_f}{2\rho_s + \rho_f} \frac{C_D}{r}$

Liquid	Max. Re	C_D	k^2	x_o cm.
Water	10^3	1.0	0.58	5.5
Sugar solution	150	1.0	0.58	5.5
Liquid paraffin	5	5.0	1.9	1.7

* High value of x_o for liquid paraffin was because much thicker discs were used with this liquid than with the other two.

REFERENCES

Allen, D.N.De G. & Southwell, R.V.	1955	Q.J. Mech. & App. Maths. 8, 129.
Allen, H.S.	1900	Phil. Mag. (5) 50, 323.
Aoi, T.	1955	J. Phy. Soc. Japan. 10, 119.
Arnold, H.D.	1911	Phil. Mag. (6) 22, 755.
Arenberg, D.L.	1941	Bull. Amer. Met. Soc. 22, 113.
Bacon, L.	1936	J. Frank. Inst. 221, 251.
Bairstow, L., Cave, B.M. & Lang, E.D.	1922	Proc. Roy. Soc. A, 100, 394.
Bairstow, L., Cave, B.M. & Lang, E.D.	1923	Phil. Trans. Roy. Soc. A, 223, 383.
Berry, A. & Swain, L.M.	1923	Proc. Roy. Soc. A, 102, 766.
Brenner, H.	1962	J. Fluid Mech. 12, 35.
Bretherton, E.P.	1964	J. Fluid Mech. 20, 401.
Bradshaw, P.	1964	" Experimental Fluid Mechanics", Pergamon.
Broersma, S.	1960	J. Chem. Phy. 32, 1632.
Burgers, J.M.	1938	Kon. Ned. Akad. Wet. Verhand (Eerste Sectre) D I, XVI, No 4. P.1

Cunningham, E.	1910	Proc. Roy. Soc. A, 83, 357.
Davies, C.N.	1945	Proc. Phy. Soc. 57, 259.
Davies, C.N.	1947	Symposium Inst. Chem. Eng. of Soc. of Chem. Eng. (Particle size analysis) p. 25.
Dryden, H.L., Murnaghan, E.P. & Bateman, H.	1956	"Hydrodynamics" Dover.
Ellis-Williams, W.	1915	Phil. Mag. (6) 29, 526.
Eveson, G.F., Hall, E.W. & Ward, S.G.	1959	Brit. J. App. Phy. 10, 43
Eveson, G.F.	1960	Brit. J. App. Phy. 11, 88.
Faxén, H.	1922	Arkiv. Mat. Astr. Fys. 17, (No 27)
Faxén, H.	1925	Arkiv. Mat. Astr. Fys. 19a, 13
Finn, R.K.	1953	J. App. Phy. 24, 771.
Fuchs, N.A.	1964	"Mechanics of Aerosols" Pergamon.
Gans, R.	1911	Silzber Akad. Munchen. 41, 197.
Gans, R.	1928	Ann. d. Physik 86, 654.

Goldstein, S.	1929	Proc. Roy. Soc. A, 123, 225.
Green, H.L. & Lane, W.R.	1964	" Particulate Clouds". 2nd ed. E.& F.N. Spon Ltd.
Harrison, W.J.	1924	Trans. Camb. Phil. Soc. 23, 71.
Happel, J. & Preffer, R.	1960	Amer. Inst. Chem. Eng. J. 6, 129.
Hawksley, P.G.W.	1951	Brit. Coal Utilisation Res. Asso. 15 (No4) 105.
Hawksley, P.G.W.	1954	Brit. J.App. Phy. 5, (Supp. 3), S 1.
Heiss, J.F. & Coull, J.	1952	Chem. Eng. Prog. 48, 133.
Hocking, L.M.	1958	Ph. D. Thesis. London University.
Hocking, L.M.	1964	J. Fluid Mech. 20, 129.
Humphreys, W.J.	1929	"Physics of Air" McGraw-Hill
Jayaweera, K.O.L.F., Mason, B.J. & Slack, G.W.	1964	J. Fluid Mech. 20, 121.
Jenson, V.G.	1959	Proc. Roy. Soc. A, 249, 346.
Kalycko, L.	1934	Heating and Ventilation No 4

Kawaguti, M.	1950	Rep. Inst. Sc. Tokyo. 4, 154.
Kawaguti, M.	1953	J. Phy. Soc. Japan. 8, 747.
Kirchoff, G.	1869	Crelles J. 71, 237.
Kovasnay, L.S.G.	1949	Proc. Roy. Soc. A, 198, 174.
Kunkel, W.	1948	J. App. Phy. 19, 1056.
Kynch, G.J.	1959	J. Fluid Mech. 5, 193.
Lamb, H.	1962	"Hydrodynamics" 6th ed. Cambridge
Landenburg, R.	1907	Ann. der Physik. 22, 287.
Langmuir, I.	1948	J. Met. 5, 175.
List, Von R. & Davos, W.	1959	Z. fur Ange. Math. und Phy. (Zamp) 10, 143.
Mason, B.J.	1957	"Physics of Clouds", Oxford.
Matthews, H.W. & Smith, F.B.	1960	Brit. J. App. Phy. 11, 87.
Miller, W. & M'Inally, T.W.	1936	J. Roy. Coll. Sc. & Tech. Glasgow, 3, 682.
Millikan, R.	1917	"The electron" Chicago, Ch. 4 & 5.
Millikan, R.	1923	Phy. Rev. 22, 1.

Mc Nown, J. & Malaika, J.	1950	Trans. Amer. Geophy. union, 31, 74.
Möller, H.	1938	Phy. Z. 39, 57.
Oberbeck, A.	1876	Crelles J. 81, 62.
Oseen, C.W.	1910	Arkiv. Math. Astron. Fysik, 6, No 29.
Oseen, C.W.	1927	"Hydrodynamik", p 205.
Pearcey, T. & McHugh, B.	1955	Phil. Mag. 46, 787.
Pettijohn, E.S. & Christiansen, E.B.	1948	Chem. Eng. Prog. 44, 157.
Prandtl, L. & Tietjens, O.G.	1957	"Applied Hydro and Aero Mechanics", Dover.
Proudman, I. & Pearson, J.R.A.	1957	J. Fluid Mech. 2, 237.
Relf, E.F.	1913	Tech. Rep. & Memo. Adv. Comm. Aero (A.R.C.) London. No 102
Relf, E.F. & Simmons, L.F.G.	1924	A.R.C. Rep. & Memo. No 917.
Rowe, P.N. & Henwood, G.A.	1961	Trans. Inst. Chem. Eng. 39, 43.
Sartor, D.	1954	J. Met. 11, 91.
Scoggins, J.R.	1964	J. Geophy. Res. 69, 591.
Schotland, R.M.	1957	J. Met. 14, 381.
Schmiedel, J.	1928	Phy. Z. 29, 593.
Schiller, L.	1932	Handbuch Expt. Physik, Leipzig, 4(2) 339.

Sidrak, S.	1950	Proc. Roy. Irish Acad. 53, 17.
Simmons, L.F.G. & Dewey, N.S.	1930	A.R.C. Rep & Memo. No 1334.
Smoluchowski, M.S.	1911	Bull. Acad. Sci. Cracow. 1a, 28.
Smoluchowski, M.S.	1912	Proc. 5th Int. Congr. Math. 2, 192.
Squires, L. & Squires, W. (Jr)	1937	Trans. Amer. Inst. Chem. Eng. 33, 1.
Stimson, M. & Jeffery, G.B.	1926	Proc. Poy. Soc. A 111, 110.
Takaisi, Y.	1955	J. Phy. Soc. Japan, 10, 685.
Thom, A.	1933	Proc. Roy. Soc. A, 141, 651.
Tomotika, S. & Aoi, T.	1950	Q.J. Mech. & App. Math. 3, 143.
Tomotika, S. & Aoi, T.	1951	Q.J. Mech. & App. Math. 4, 401.
Tritton, D.J.	1959	J. Fluid Mech. 6, 577.
Wadell, H.	1934	J. Frank. Inst. 217, 459.

White, C.M. 1946 Proc. Roy. Soc. A, 186, 472.

Weickmann, H. 1956 Thunderstorm electricity, - Byers, p 66.

Wieselsberger, C. 1921 Phy. Z. 22, 321.

Willmarth, W.W., Hawk, N.E. & Harvey, R.L. 1964 Phy. Fluids, 7, 197.

Wilton, J.A. 1915 Phil. Mag. (6) 30, 767.

Woods, J.D. & Mason, B.J. 1965 Q.J. Met. Soc. 91, 35.

Zeleny, J. & McKeehan, L. 1910 Phy. Z. 11, 78.

J. Fluid Mech. (1964), *vol.* 20, *part* 1, *pp.* 121–128
Printed in Great Britain

The behaviour of clusters of spheres falling in a viscous fluid

Part 1. Experiment

By K. O. L. F. JAYAWEERA, B. J. MASON
Physics Department, Imperial College, London
AND G. W. SLACK
Chemical Defence Experimental Establishment, Porton, Nr Salisbury, Wiltshire

(Received 17 December 1963)

The sedimentation of small clusters of uniform spheres, falling freely through a viscous liquid, has been studied with Reynolds numbers (based on diameter of the sphere and its velocity of free fall in the unbounded fluid) of individual spheres ranging from 10^{-4} to 10. The fall velocity of a cluster is, in all cases, greater than that of individual spheres, the more so when the spheres are closer together. Two spheres falling side-by-side rotate inwards and separate as they fall if $Re > 0{\cdot}05$, but no rotation nor separation is observed for $Re < 0{\cdot}03$. When equal-sized spheres of $Re > 1$ fall vertically one behind the other, the rear sphere is accelerated into the wake of the leader, rotates round it and separates from it when the line of centres is horizontal. If two spheres of unequal size but the same individual terminal velocity fall together, the smaller always travels faster than the larger. When three similar equally spaced spheres are dropped in a horizontal line, they interchange positions but do not separate when $0{\cdot}06 < Re < 0{\cdot}16$. But, if $0{\cdot}16 < Re < 3$, one sphere is always left behind; which sphere depends critically upon the initial spacings. If three to six equal spheres, of $0{\cdot}06 < Re < 7$, start falling as a compact cluster, they eventually draw level and arrange themselves in the same horizontal plane at the vertices of a regular polygon. The polygon expands at a decreasing rate during fall. When three spheres are arranged initially in a horizontal isosceles triangle, the spheres oscillate about their equilibrium positions but eventually the spheres form a stable equilateral triangle. If $Re > 7$, or the cluster contains 7 or more equal spheres, it shows no tendency to form a regular polygon but breaks up into two or more groups. A regular heptagon, and a hexagon with an additional sphere at its centre, are also unstable.

1. Introduction

The fall of single spheres and the sedimentation of a uniform suspension of many particles in a viscous medium have been studied extensively but the intermediate case of a falling cluster containing only a few spheres has apparently received little attention.

The behaviour of a pair of spheres of very low Reynolds number falling in close proximity through a viscous fluid was first treated theoretically by Smoluchowski (1911, 1912) by a method which is equivalent to superimposing the motion produced by the two spheres in isolation. He calculated the first terms in an expansion in powers of a/s, the radius of the sphere divided by the separation between centres, and his result is valid only for small values of this ratio. By introducing terms to satisfy the boundary conditions on one sphere and then on the other, the drag can be found by iteration to any degree of accuracy. This was done by Faxén (1925) who found the drag for two spheres moving along their line of centres by including terms of up to $(a/s)^5$. Stimson & Jeffery (1926) also solved this problem for two spheres falling one behind the other where there is axial symmetry. Kynch (1959) extended the analysis to include higher powers of a/s and to facilitate closer comparison with experiments for small separations. He also treated the case of unequal spheres. Hocking (1958) has expressed the drag for two spheres falling in line, either one behind the other, or side-by-side, as a series in a/s to as high a degree as required, and has evaluated the drag as a function of separation by retaining terms of up to $(a/s)^7$.

The main predictions of these workers may be summarized as follows.

(i) Pairs of spheres always fall faster under gravity than do single spheres falling alone.

(ii) This enhancement in the rate of fall is more marked when the spheres are close together.

(iii) Pairs of equal spheres falling together maintain a constant separation and orientation.

(iv) The members of a pair fall vertically only if the line joining their centres is either vertical or horizontal. Otherwise their velocity has a component in a downward sense along the line joining their centres.

(v) If two spheres of unequal size but having the same individual terminal velocity fall together, the smaller will always move faster than the larger.

Eveson, Hall & Ward (1959) claimed to have verified the first four of these predictions and also to have shown that the spheres fall without rotation but, after the publication of some observations by Matthews & Smith (1960), Eveson (1960) reported having observed a slow rotation with a pair of falling spheres.

Since the behaviour of more than two spheres falling under the influence of both viscous and inertial forces appears to defy detailed mathematical analysis, it was decided to carry out some simple experiments with spheres falling through a viscous liquid. Accordingly, observations were made with spheres having individual Reynolds numbers (based on sphere diameter and velocity of free fall) ranging from 10^{-4} to 10. The lower values allow one to test the theories based on the total neglect of inertial forces while the higher values of Re extend into régimes where both viscous and inertial terms are significant.

2. Experimental method

Experiments were conducted at Porton in a Perspex tank, 20 cm × 20 cm × 90 cm deep, containing castor oil (density 0·97 g cm^{-3} at 20 °C). The tank was surrounded by a thermostatically controlled lagged cabinet provided with glass windows and

this cabinet was itself contained in another thermostatically controlled chamber. In this way, the temperature of the liquid could be held constant to within $\pm 0{\cdot}01\,^{\circ}\mathrm{C}$ for several hours and no convection currents were ever detected. Spheres of steel (density $7{\cdot}8\,\mathrm{g\,cm^{-3}}$), aluminium ($2{\cdot}7\,\mathrm{g\,cm^{-3}}$), bakelite ($1{\cdot}3\,\mathrm{g\,cm^{-3}}$), ebonite ($1{\cdot}2\,\mathrm{g\,cm^{-3}}$) and Perspex ($1{\cdot}19\,\mathrm{g\,cm^{-3}}$) ranging in diameter from 0·03 to 12·5 cm were used. Suitable choices of sphere size and density, and of liquid density and viscosity, enabled observations to be made of spheres with Reynolds numbers ranging from about 10^{-4} to 10.

The Imperial College experiments were carried out in a glass tank 30 cm × 30 cm × 60 cm deep containing liquid paraffin (density $0{\cdot}88\,\mathrm{g\,cm^{-3}}$ at 20 °C). This tank was chosen after several tests with larger and smaller tanks showed that there were no undesirable wall effects with a tank of this convenient size. Spheres of polyethylene ($0{\cdot}98\,\mathrm{g\,cm^{-3}}$), polystyrene ($1{\cdot}05\,\mathrm{g\,cm^{-3}}$), nylon ($1{\cdot}14\,\mathrm{g\,cm^{-3}}$) and Perspex ($1{\cdot}19\,\mathrm{g\,cm^{-3}}$) ranging from $\frac{1}{8}$ in. to $\frac{3}{8}$ in. at intervals of $\frac{1}{16}$ in. were used. The Reynolds number for a constant geometry could be varied by heating or cooling the paraffin and thereby changing its kinematic viscosity which varied from 88 cS at 36 °C to 340 cS at 15 °C. With this arrangement it was possible to work with spheres of Reynolds number, defined as ud/ν, d being the diameter of the sphere, u its terminal velocity in an infinite medium and ν the kinematic viscosity of the fluid, ranging from $< 0{\cdot}01$ to 10.

Two methods of releasing a small cluster of spheres were used. The first, designed to produce a close but random arrangement of spheres, employed a $\frac{3}{4}$ in. thick aluminium disk which rotated in the horizontal plane over, and almost in contact with, a flat stationary plate over the centre of the tank. The disk contained a number of holes of various sizes and the required number of spheres was placed in whichever of the holes they most nearly filled to a height equal to its diameter. The disk was then rotated until the hole containing the spheres was brought close to the edge of a slot in the lower plate. The cluster was then released by rotating the disk rapidly through a small angle. The spheres fell about 2 cm before entering the liquid. This method greatly reduced the entrainment of air bubbles in the cluster; in any case, clusters containing bubbles were not used.

In the second method, the spheres were held by suction in holes drilled in a flat plate. The plate was suspended just below the surface of the liquid and the spheres fell away immediately the partial vacuum was released. This method enables coplanar clusters of known geometry and spacing to be produced.

3. Sedimentation of a pair of spheres

(*a*) *Equal-sized spheres falling side-by-side*

Over the whole range of Reynolds numbers, the rate of fall of both spheres is greater, in all cases, than that of either sphere falling individually, and this enhancement in speed of fall is greater when the spheres are close together.

For $Re < 0{\cdot}03$, the spheres show no tendency to separate or to rotate but for $Re > 0{\cdot}05$, each sphere rotates inwards (in the sense shown in figure 2, plate 1) about a horizontal axis through its centre and normal to the line of centres. The

rate of rotation increases with increasing Reynolds number but decreases as the spheres separate. The rotation continues until the separation reaches a maximum limiting value, which is a decreasing function of the Reynolds number as shown in figure 1, and ceases when the separation exceeds this value. Figure 2, plate 1, shows the rotation and separation of a pair of half-painted Perspex spheres ($d = \frac{3}{8}$ in., $Re \simeq 0{\cdot}1$) falling through castor oil and photographed at intervals of 2 sec.

(*b*) *Equal-sized spheres falling vertically one behind the other*

When $Re > 1$, the rear sphere becomes accelerated in the wake of the front sphere and tends to overtake it. When Re exceeds 4 this acceleration is already noticeable when the spheres are ten diameters apart. At large distances apart the

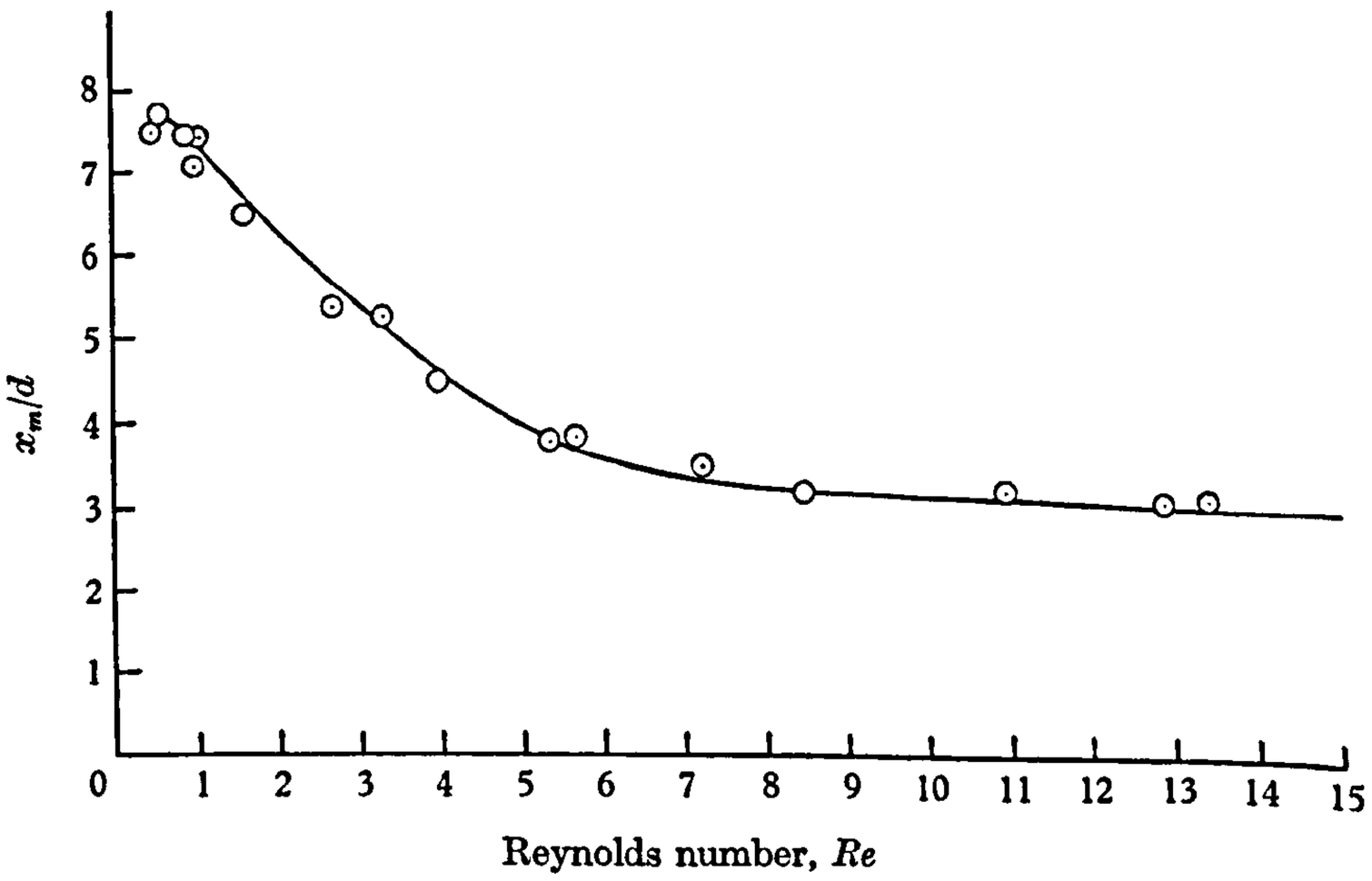

FIGURE 1. The maximum limiting separation x_m of two equal spheres falling side-by-side as a function of Reynolds number. d = diameter of sphere.

velocity of approach varies inversely as the separation as shown theoretically by Goldstein (1929) and Pearcey & McHugh (1955), but settles down to a nearly constant value at small separations—see figure 3. The relative velocity on apparent impact is about one-half the terminal velocity of an individual sphere. Until this stage neither sphere rotates but, now, the rear sphere slides round the leader and, when the line of centres becomes horizontal, the spheres separate, rotate in opposite directions, and continue to diverge laterally as they fall just as in (*a*).

(*c*) *Two equal spheres with line of centres inclined to horizontal*

A pair of equal spheres, each with $Re > 1$ and initially in different horizontal planes, appear to slide along the line of centres as well as falling vertically. They tend to occupy the same horizontal plane, and, having done so, remain like this but diverge laterally at a steadily decreasing rate.

(*d*) *Pairs composed of unequal-sized spheres having the same individual terminal velocity*

By adjusting the temperature of the castor oil an 8 mm ebonite sphere was made to fall at the same terminal velocity as a 1·58 mm steel sphere, and a 24·63 mm Perspex sphere to fall at the same velocity as a 3·97 mm steel sphere. In both cases, the smaller sphere of the pair always fell more rapidly than the larger, just as predicted by Kynch (1959), and this result was made unambiguous by adjusting the temperature of the liquid so that the larger sphere had a slightly *higher* terminal velocity.

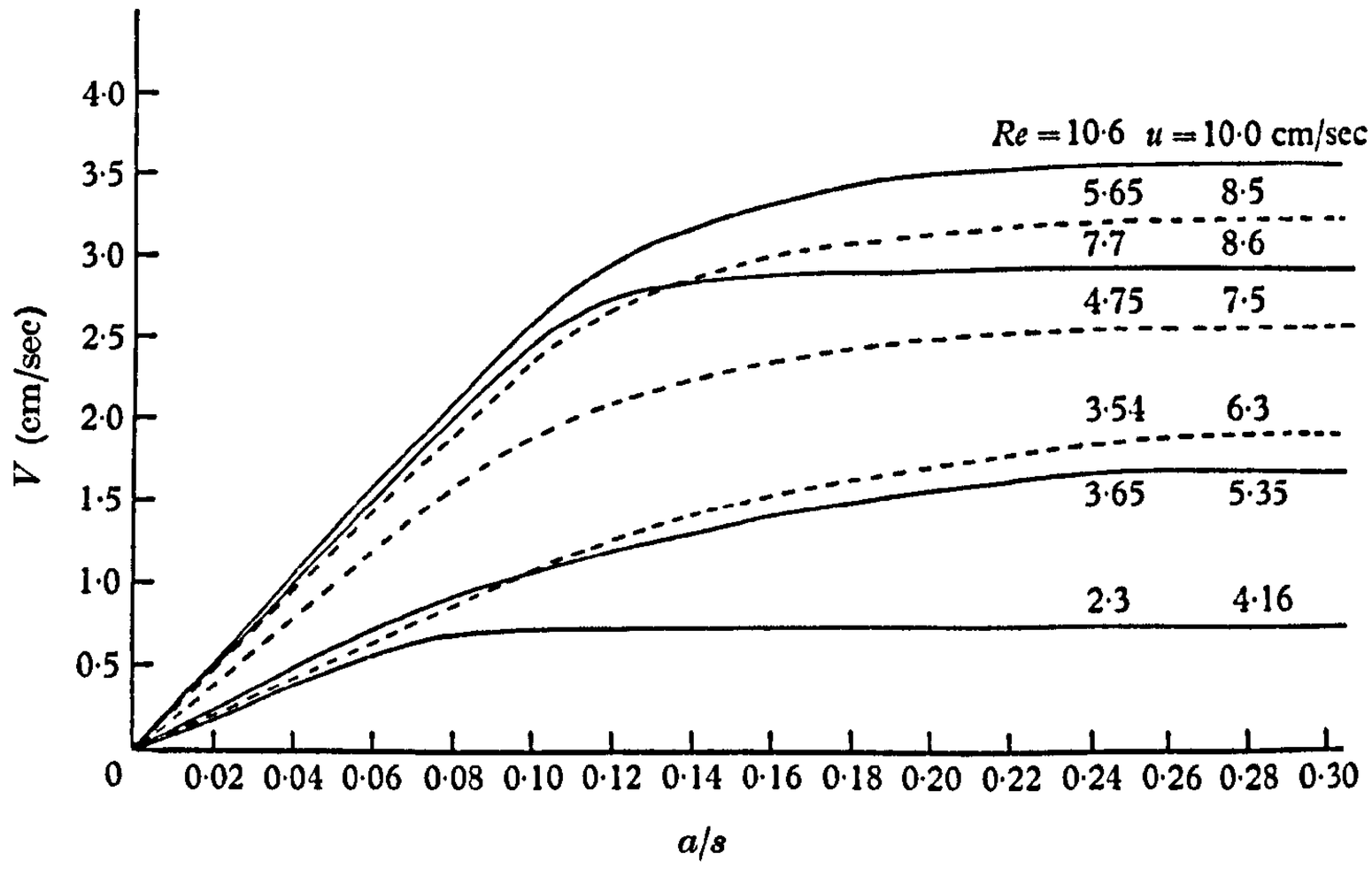

FIGURE 3. The relative velocity of approach, V, for two equal spheres falling one behind the other, plotted as a function of a/s for various values of the Reynolds number. u is the terminal velocity of an individual sphere, a its radius, and s the vertical separation of the two spheres. ——, at 88 cS; ----, at 140 cS.

The relative motion of the two spheres, with Re 0·3 and 1·8, is shown in figure 4. This shows the successive positions of the smaller sphere relative to the larger as obtained from a series of photographs taken at regular intervals. The left-hand picture shows the smaller sphere being accelerated into the wake of the larger, colliding with it, rolling round it, and then separating from it. In the right-hand picture, the smaller sphere is first attracted towards the larger but, on coming level with it, is repelled by it. Both spheres showed rotation which increased as the spheres approached each other and died away as they separated.

4. Equal-sized spheres released in a horizontal straight line

(*a*) $0{\cdot}06 < Re < 0{\cdot}16$

When three spheres, initially in contact or equally spaced within 6 diameters, are released in a horizontal straight line, the centre sphere moves slightly ahead, one of the laggards then moves between the other two, and the third (now trailing)

passes between the other two. This interchanging of positions continues throughout the fall, but the spheres keep close together and do not separate. The sphere temporarily in the lead stops rotating. If the spheres are not equally spaced initially, one sphere is always left behind. If the spheres be numbered and separated as

$$(1) \leftarrow a \rightarrow (2) \leftarrow b \rightarrow (3),$$

which sphere is left behind depends critically upon the ratio b/a as follows:

b/a	$< 1{\cdot}17$	$1{\cdot}20$–$1{\cdot}33$	$1{\cdot}33$–$1{\cdot}40$	$1{\cdot}50$	$1{\cdot}60$–$2{\cdot}0$	$> 2{\cdot}0$
sphere left behind	1	2	1	3	2	3

For $b/a < 2$, one sphere is left behind after one or two interchanges of position, but if $b/a > 2$, sphere 3 is left behind from the start.

Two slightly separated pairs initially in a horizontal straight line diverge as they fall, each pair rotating as a doublet. Ultimately the members of a pair separate. With five or six spheres the outer ones move out, re-enter the cluster from the rear, and cause it to break up.

$$(b)\ 0{\cdot}16 < Re < 3$$

If between three and six contacting spheres are released in a straight line they separate and eventually form a regular polygon, all the spheres lying in the same horizontal plane.

$$(c)\ Re > 3$$

The polygon is not regular and progressively breaks down as the Reynolds number is increased until, with $Re > 7$, the spheres appear to repel each other and separate but show no tendency to form a polygon.

5. Clusters of 3 to 6 equal spheres

$$0{\cdot}06 < Re < 7$$

When three to six equal spheres, starting as a compact cluster, fall together we observe that:

(i) Their speed of fall is greater than that of a single sphere.

(ii) This enhancement of the rate of fall is greater the more compact the cluster.

(iii) Even if the spheres are initially staggered by a few diameters they eventually draw level and ultimately arrange themselves in the same plane at the vertices of a regular polygon; see figure 5, plate 2.

(iv) The polygon expands slowly and at a decreasing rate during fall.

(v) When three spheres are arranged initially in a horizontal isosceles triangle the apex sphere oscillates in a decreasing vertical spiral relative to the other two, which execute linear oscillations along the horizontal line of centres and move apart as the apex sphere moves towards them. These oscillations gradually die out and the three spheres form a stable equilateral triangle. During the formation of 4-, 5-, or 6-sided polygons the individual spheres again oscillate about their equilibrium positions but eventually achieve a stable, regular configuration.

(vi) The final configuration is achieved more slowly with a larger number of more widely separated spheres.

(vii) During the early life of the polygon each sphere rotates inwards about a horizontal axis that is normal to a line joining the centre of the sphere to the centre of the polygon.

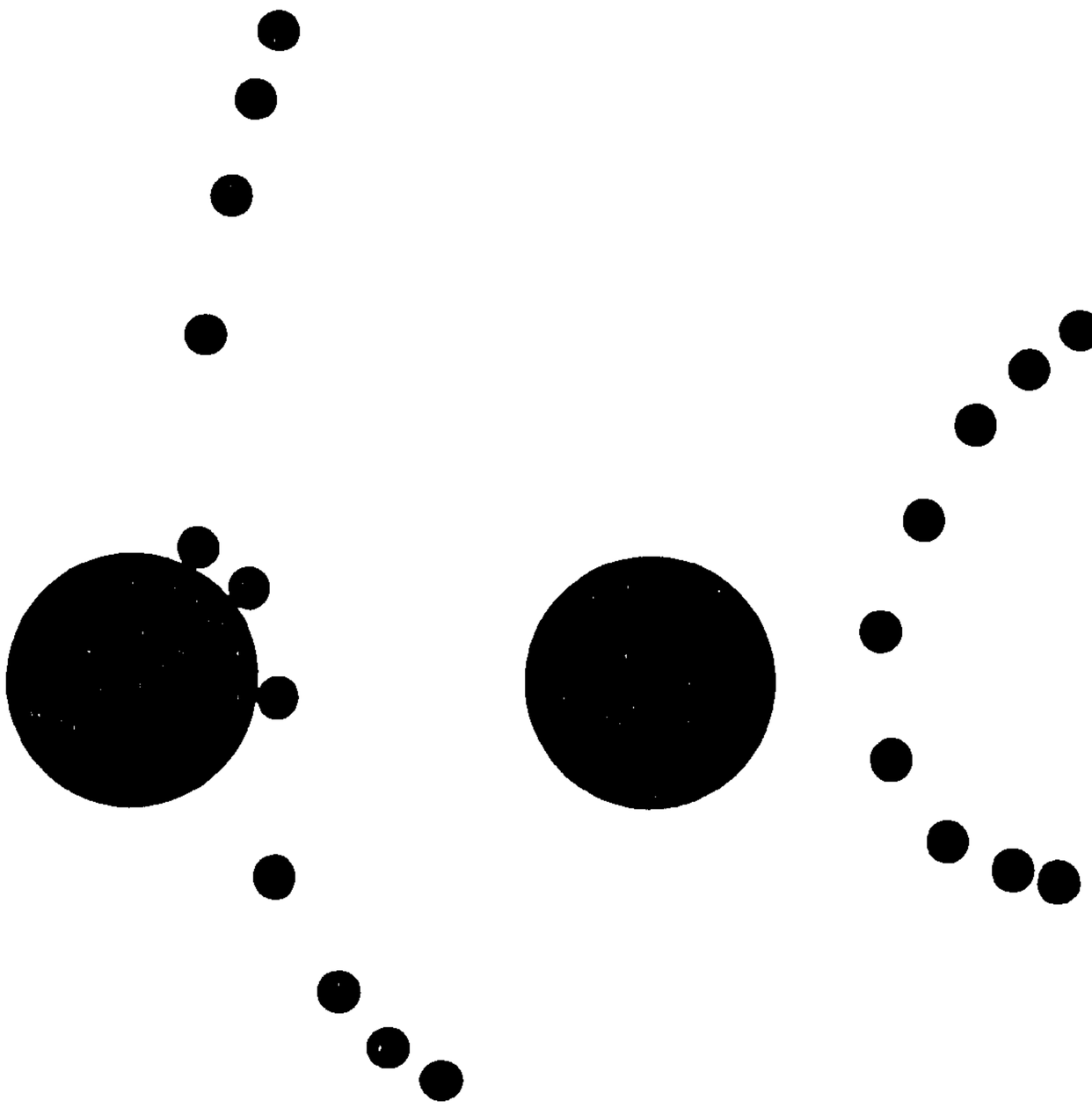

FIGURE 4. Relative motion of two unequal-sized spheres having the same terminal velocity. The diagram shows the position of the smaller sphere at equal intervals of time for two distinct cases.

(viii) When the separation of the spheres exceeds a certain value (about 6 diameters at $Re \simeq 1$ and 3 diameters at $Re \simeq 7$), rotation ceases but separation continues. Regular polygons are not formed if the *initial* separation of the spheres exceeds the critical distance.

(ix) If the spheres composing a cluster are arranged asymmetrically the densest portion of the cluster travels fastest. This causes a tilting of the cluster which then appears to slide as a whole along the line of tilt.

$$Re < 0{\cdot}06$$

The spheres tend to follow their initial configuration but fall faster than isolated spheres. They show no tendency to form a regular polygon and even if released in such a pattern they are susceptible to small perturbations.

$$Re > 7$$

The spheres of a cluster separate quickly with a sudden onset of rotation, but this soon ceases, and there is no tendency to form regular polygons.

6. Clusters containing more than six spheres

A compact cluster containing 7 or more equal spheres shows no tendency to form a regular polygon but tends to break up into two or more groups. A cluster arranged initially at the apices of a regular heptagon is unstable. For $Re < 0{\cdot}1$ the heptagon becomes distorted and for larger values of Re it breaks up during fall. If an additional sphere is placed at the centre of a regular hexagon it moves ahead and to one side. The hexagon then tilts towards this sphere which re-enters the hexagon from the rear and causes it to break up.

Figures 2 and 4 are Crown Copyright Reserved and are published by permission of H.M. Stationery Office.

REFERENCES

Eveson, G. F. 1960 *Brit. J. Appl. Phys.* **11**, 88.
Eveson, G. F., Hall, E. W. & Ward, S. G. 1959 *Brit. J. Appl. Phys.* **10**, 43.
Faxén, H. 1925 *Arkiv. Math., Astron. Fysik*, **19***a*, 13.
Goldstein, S. 1929 *Proc. Roy. Soc.* A, **123**, 216.
Hocking, L. M. 1958 Ph.D. Thesis, London University.
Kynch, G. J. 1959 *J. Fluid Mech.* **5**, 193.
Matthews, H. W. & Smith, F. B. *Brit. J. Appl. Phys.* **11**, 87.
Pearcey, T. & McHugh, B. 1955 *Phil. Mag.* **46**, 783.
Smoluchowski, M. S. 1911 *Bull. Acad. Sci. Cracow*, **1a**, 28.
Smoluchowski, M. S. 1912 *Proc. 5th Int. Congr. Math.* **2**, 192.
Stimson, M. & Jeffery, G. B. 1926 *Proc. Roy. Soc.* A, **111**, 110.

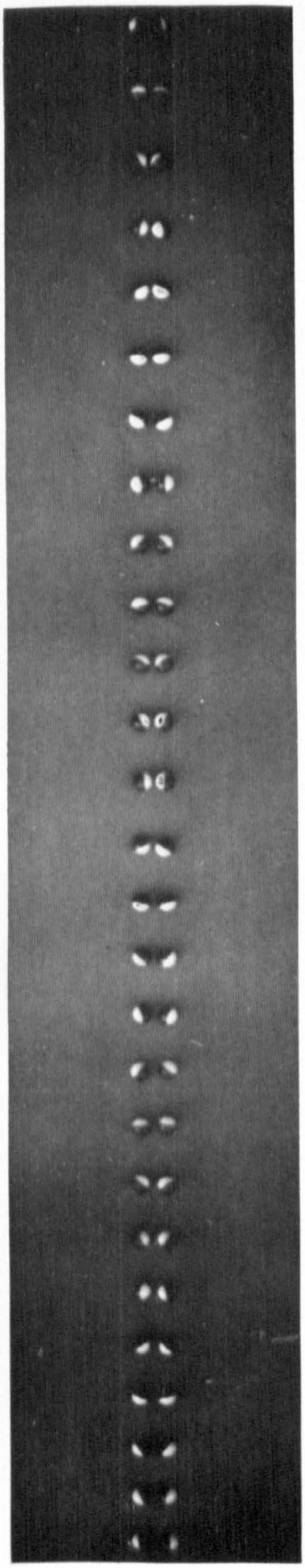

FIGURE 2. The sedimentation of a pair of half-painted, equal-size spheres, showing that they rotate and separate as they fall. Perspex spheres, $d = \frac{3}{8}$ in., $Re \simeq 0{\cdot}1$, photographed at intervals of 2 sec.

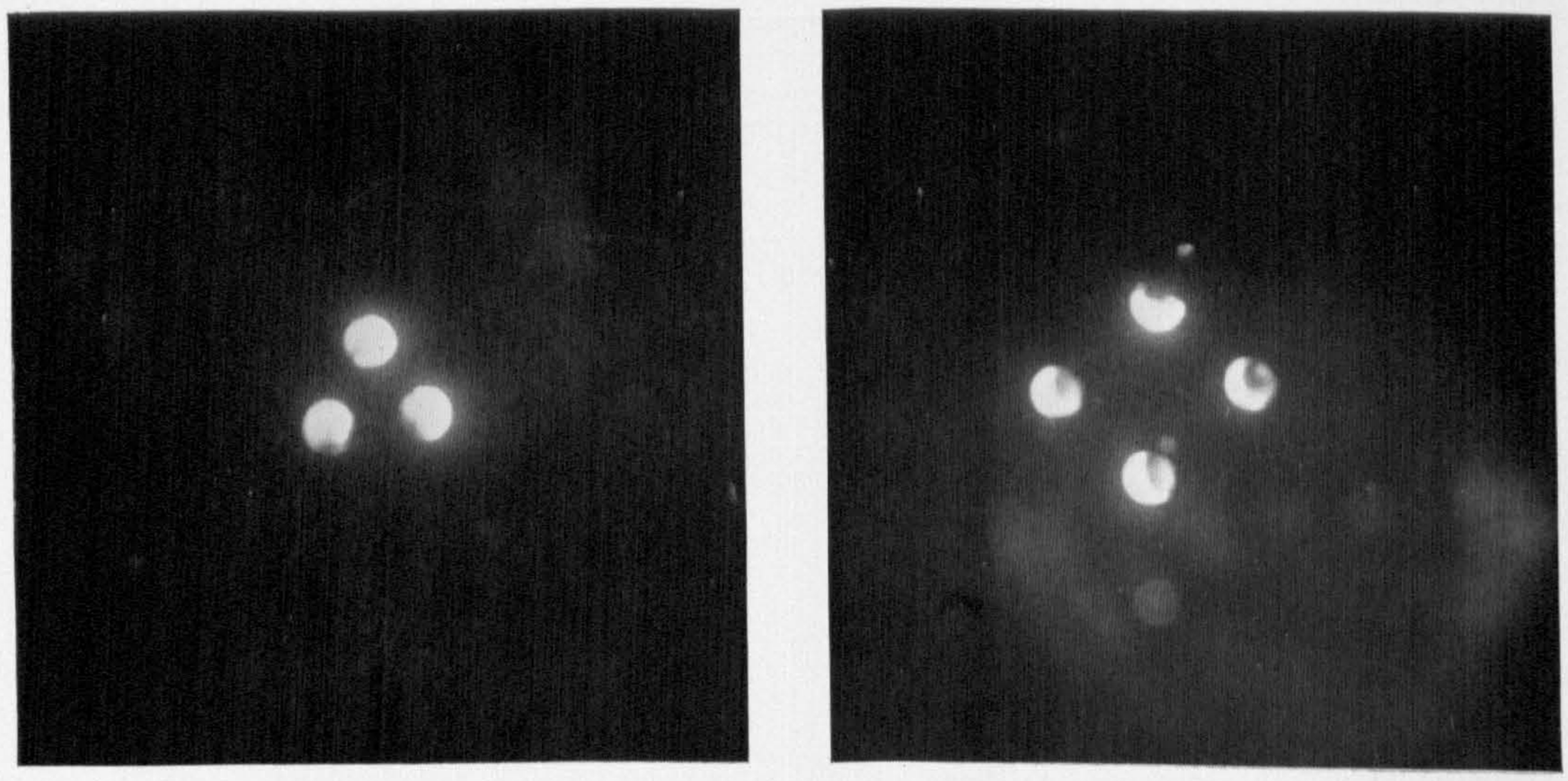

FIGURE 5. Clusters of 3 to 6 equal spheres, with $0{\cdot}06 < Re < 7$, arrange themselves in the same horizontal plane at the vertices of regular polygons. Clusters of 7 or 8 spheres fail to form regular configurations.